University of Neuchâtel

Centre of Hydrogeology

Ecole Nationale d'Ingénieurs de Tunis

Laboratoire de Modélisation en Hydraulique et Environnement

Field experimentation and modelling of salt transfer in Korba coastal plain: Impact of seawater intrusion and irrigation practices

PhD thesis presented to the Faculty of Sciences at the University of Neuchâtel to satisfy the requirements of the degree of Doctor of Philosophy in Science

by

Fairouz Slama

Thesis defence date: 3 November 2010

Prof. Rachida Bouhlila, Ecole Nationale d'Ingénieurs de Tunis
Prof. Pierre Perrochet, University of Neuchâtel
Prof. Jamila Tarhouni, Institut National Agronomique de Tunis
Prof. André Mermoud, Federal Institute of Technology, Lausanne
Dr. Ellen P. Milnes University of Neuchâtel
Ing. Général Abdelkader Hamdane, ancien Directeur Général du Génie Rural

Université de Neuchâtel

Copie certifiée conforme
UNIVERSITE DE NEUCHATEL
Faculté des Sciences
Secrétariat-décanat de la faculté

05 MAI 2011

FACULTE DES SCIENCES
Secrétariat-Décanat de la faculté
Rue Emile-Argand 11
CH-2000 Neuchâtel

IMPRIMATUR POUR LA THESE

Field experimentation and modelling of salt transfer in Korba coastal plain: Impact of seawater intrusion and irrigation practices

Fairouz SLAMA

REALISEE EN COTUTELLE AVEC

L'ECOLE NATIONALE D'INGENIEURS DE TUNIS (ENIT)

et

L' UNIVERSITE DE NEUCHATEL (CH)

FACULTE DES SCIENCES

La Faculté des sciences de l'Université de Neuchâtel,
sur le rapport des membres du jury

Prof. P. Perrochet (UniNe, directeur de thèse),
Prof. R. Bouhlila (ENIT, co-directrice de thèse),
Prof. A. Mermoud (EPF Lausanne), Prof. J. Tarhouni (INAT, Tunisie),
Dr E. Milnes (UniNe) et Ing. Gén. A. Hamdane (Tunis)

autorise l'impression de la présente thèse.

Neuchâtel, le 5 mai 2011

Le doyen :
P. Kropf

Acknowledgements The present work was entirely funded by The Swiss National Science Foundation (Joint Research Project “Gestion durable des ressources en eaux souterraines côtières - Modélisation physique et probabiliste. Application à la côte orientale du Cap Bon, Tunisie CAPBON”).

Remerciements

Au terme de ce travail, j'exprime ma profonde reconnaissance à Mme **Rachida Bouhlila**, Professeur à l'ENIT qui, en proposant ce projet de thèse, m'a non seulement offert un environnement de réalisation d'une thèse sous sa conduite, mais également donné l'occasion de faire partie d'un projet international. Par ses orientations, ses conseils et également ses encouragements continus, Mme Bouhlila a été pour moi un soutien sans faille.

J'adresse mes vifs remerciements également à M. **Pierre Perrochet**, Professeur au CHYN et co-directeur de thèse, pour avoir assuré le suivi minutieux de notre travail. Je le remercie aussi pour l'hospitalité dont nous avons fait l'objet à Neuchâtel et qui nous a permis de travailler dans de très bonnes conditions.

Je remercie aussi Mme **Jamila Tarhouni** Professeur à L'INAT, qui nous a transmis sa profonde connaissance de la problématique et sa passion pour la région. On lui doit, en outre, la riche base de données. Elle n'a pas hésité à nous appuyer afin de mener à bien les travaux de terrain et de laboratoire.

M. **Philippe Renard**, Professeur au CHYN à travers les longs échanges et discussions que nous avons eu avec lui, nous a permis de conforter nos choix méthodologiques. Il a déployé beaucoup d'efforts pour la réussite du projet. Qu'il trouve ici l'expression de ma haute considération.

Je tiens également à exprimer mes vifs remerciements à Mlle **Ellen Milnes**, maitre assistant au CHYN, qui en plus d'avoir partagé avec nous certaines missions sur terrain et de construction méthodologique, n'a ménagé aucun effort pour nous faciliter les séjours à Neuchâtel.

Je remercie **Jawher Kerrou**, collaborateur au CHYN et membre du projet JRP, pour son aide et sa collaboration scientifique. Par ses travaux, il a contribué à une meilleure connaissance du sujet et de la zone d'étude. Je le remercie également pour sa disponibilité et son soutien.

Je remercie toute l'équipe de l'INAT qui a participé au projet et en particulier Mlle **Emna Trabelsi** qui nous a beaucoup aidés et soutenus pour l'élaboration du réseau de surveillance et les analyses chimiques.

J'adresse mes remerciements aussi à M. **Abdelkader Hamdane** ancien Directeur Général de la Direction Générale du Génie Rural et Mme **Rakya Boutiti**, directeur à la DGGR, qui nous ont appuyés pour les travaux de terrain et nous ont reçus pour discuter de l'avancement du projet. Je n'oublierai pas de remercier M. **Moncef** chauffeur à la DGGR, qui a fait preuve d'une grande disponibilité afin de mener à bien les travaux sur terrain.

Je remercie aussi M. **Hédi Hamrouni** Directeur Général de la Direction des Sols ainsi que Mme **Kalthoum et M. Zidi**, ingénieurs qui nous ont toujours bien accueillis au sein de leur établissement pour effectuer les travaux d'analyse se rapportant au sol.

Je remercie également M. **Mongi Bouhlila**, Président Directeur Général de la société GETU, pour nous avoir énormément aidés et conseillés. Je remercie, M. **Msaddek** et M. **Yahia**, ingénieurs à GETU pour leur patience et leur aide ainsi que M. Naceur et M. Habib, techniciens qui nous ont fait profiter de leur longue expérience et technicité, sans lesquelles les travaux de forage n'auraient jamais réussi.

J'adresse mes remerciements aussi à la direction et à l'équipe du Commissariat Régional de Développement Agricole de Nabeul pour nous avoir facilité l'approche du terrain.

Je remercie aussi mes anciens collègues de l'INRGREF et notamment **F. Bouksila**., **H. Askri**, **O. Mahjoub**, **R. Zitouna**, **I. Mekki** et Mme **Mhedhbi**, qui n'ont pas hésité à partager leur savoir et leur matériel à maintes reprises pour nous dépanner.

J'adresse mes remerciements également aux membres du laboratoire LMHE, en commençant par M. **Mustapha Besbes**, Professeur à l'ENIT et M. **Mahmoud Moussa**, directeur du LMHE, Mme **Zoubeida Bargaoui** et M. **Jamel Chahed** Professeurs à l'ENIT, **L. Guellouz**, **M. Hafsia, M. Belakhal**, pour leur soutien et leur intérêt scientifique à notre travail. Je n'oublie pas Mme **Souad** et Mme **Fatma** assistantes du LMHE. Je remercie aussi **Hazar Bouzourra** pour son aide précieuse dans la numérisation des anciens documents. **Nesrine, Rym et Ezzeddine** qui nous ont accompagnés sur terrain.

Tous mes remerciements vont aussi aux membres du CHYN, **Antoine Bailleux**, pour son hospitalité, **Alessandro, Pascale, Xenia, Grégoire, Joanna, Barbara, Andres** pour leur amabilité et Mme **Marie-Eve Wyniger** pour son aide dans l'accomplissement des analyses chimiques.

Je remercie aussi les professeurs **Adellatif Maslouhi** et **André Mermoud** qui, lors de leur passage à l'ENIT, ont eu la gentillesse de partager avec nous de longues et fructueuses discussions sur nos travaux.

J'exprime ma profonde gratitude envers les agriculteurs qui nous ont permis de travailler sur leurs parcelles. Leur bonté et leur générosité n'ont pas d'égales, je pense particulièrement aux familles **Baní**, **Elghoul** et **Ksouri**.

Enfin, je n'oublie pas ma famille et mon mari, je n'aurai pas pu finaliser ces travaux sans leur soutien.

Abstract

Seawater intrusion and agricultural pollution are the major sources of groundwater contamination and salinization in coastal irrigated areas. The Korba coastal aquifer, located in the Cap Bon peninsula, North-East of Tunisia, has been intensively exploited since the seventies. Several studies reported the sharp piezometric drop and groundwater salinization. Seawater intrusion was presented as the major source of salinity and irrigation return flow was rarely considered.

In this study, we are proposing to identify soil and groundwater salinization sources and processes. Besides, an endeavour to quantify solute irrigation return fluxes is presented. To fulfil these objectives experimental and numerical studies were performed.

Two transects perpendicular to the shoreline and following two flow paths (the first landward and the second seaward) were selected. Soil and groundwater investigations were periodically performed along theses transects. They involved soil and groundwater sampling, piezometric measurements and Electrical Resistivity Tomography Imaging. Various geochemical methods were applied to analyse the collected data. Besides, multivariate statistical analysis techniques were performed to assess salinity sources and processes. Modelling of the seawater/freshwater mixing problem was also carried out using PHREEQC code. HYDRUS1D was used to simulate long term salt transfer towards groundwater.

The results show that seawater intrusion and agricultural pollution are the major sources of salinity. Seawater intrusion was controlled by cation exchange, carbonate weathering and redox processes. Agricultural pollution is enriching the groundwater with NO_3, Ca, SO_4, and K elements. Geochemical and multivariate statistics techniques estimated the seawater penetration length of about 4000 m.

The soil survey confirms the latter result. It shows that the soil solution gets concentrated in the dry season with possible calcite and gypsum precipitation. Rainfall, afterwards, leaches the soil and reduces its salinity.

The unsaturated modelling revealed that the solute flux considerably depended on the irrigation amounts and the vadose zone thickness. It also demonstrated the important role of stormy episode in the leaching process.

Key words: seawater intrusion, irrigation return flow, salinization, unsaturated modelling, Tunisia

Résumé

La thèse traite des transferts des sels au niveau de la plaine de Korba : impacts de l'intrusion marine et de l'irrigation. Elle s'articule autour de trois parties.

La première partie (chapitre 2 et chapitre 3) décrit les investigations entreprises au niveau de deux sections perpendiculaires à la mer et dont l'objectif est d'identifier les sources et les processus hydrogéochimiques de la salinisation des eaux de la nappe. Un réseau de surveillance comprenant 55 points a été mis en place en juin 2006 pour suivre le niveau statique, la conductivité électrique, les éléments majeurs, les nitrates et les bromures. Sept campagnes de mesures ont été réalisées. Par ailleurs trois sondes de mesure en continu de pression et de conductivité ont été installées, en décembre 2006, dans trois piézomètres réalisés lors de campagnes de forage. A l'issue des différentes campagnes, 154 échantillons d'eau ont été recueillis et analysés. Des profils de tomographie électrique ont été également réalisés pour localiser le biseau salé. D'un point de vue méthodologique, une étude géochimique classique ainsi qu'une analyse statistique multivariée (comprenant l'analyse en composante principale et la classification hiérarchique) ont été réalisées. De plus, le code libre PHREEQC a été utilisé pour simuler le mélange eau de mer eau douce. Le suivi piézométrique trimestriel ainsi que le suivi piézométrique horaire ont montré que les fluctuations de la nappe sont corrélées à la pluie et aux pompages. Il a également confirmé l'existence d'une dépression piézométrique de 5 m à 4000 m de la mer dans la première section. Dans la deuxième section la nappe s'écoule naturellement vers la mer.

L'étude géochimique a mis en évidence l'existence d'un mélange entre les eaux de la nappe et l'eau de mer, la forte contamination par des résidus d'origine agricole exprimée en de forts taux de nitrates, de bromures et de sulfates, et la possible parenté des eaux de la nappe avec des saumures mères pétrolières. La modélisation géochimique du mélange eau de mer/eau douce montre qu'au niveau de la section touchée par la dépression piézométrique, on assiste à des processus d'échange cationique directs alors qu'au niveau de la section non touchée par l'intrusion marine on assiste à des échanges cationiques inverses. Cette analyse montre également l'influence des équilibres des roches carbonatées ainsi que les processus redox sur la chimie de la nappe. Le lessivage du gypse et la dédolomitisation sont aussi des processus envisageables pouvant expliquer l'enrichissement de la nappe en calcium. L'évocation du lessivage du gypse nous renvoie également à l'hypothèse que l'irrigation contribue à

la minéralisation de la nappe via la salinisation des couches supérieures du sol et l'apport en fertilisants.

L'analyse statistique multivariée a mis en évidence qu'un nombre important de puits présente une qualité d'eau très influencée par les nitrates évoquant l'irrigation comme source de salinité. Cette analyse a également permis de localiser l'influence de la mer sur la composition chimique de la nappe à respectivement 4000 et 1500 m pour la première et la deuxième section. La pollution agricole, elle, est plutôt localisée dans les zones internes à partir de 2000 et 1500 m respectivement pour la première et la seconde section.

La deuxième partie (chapitre 4) concerne l'étude expérimentale menée au niveau de la zone non saturée. L'objectif étant de comprendre les processus qui interviennent à cette échelle sous l'effet des pratiques d'irrigation et de la pluie et leur impact sur la qualité des eaux de la nappe. Deux campagnes de forage ont été réalisées (Août-septembre 2006 et avril 2007). Au cours de ces campagnes, 9 forages destructifs à sec ont été réalisés au niveau de six parcelles irriguées à partir des eaux de la nappe. Les profondeurs de ces forages, varient entre 4 et 20 m en fonction du niveau de la nappe sur des intervalles d'échantillonnage allant de 20 à 50 cm. Le nombre d'échantillons recueillis est égal à 254. L'extrait de la pâte saturée a été effectué pour la détermination de la conductivité électrique, du pH, des éléments majeurs (Na, K, Ca, Mg, Cl, SO4, HCO3), et des nitrates. Les fractions granulométriques ont également été déterminées et ont été exploitées pour la détermination des paramètres hydrodynamiques du sol. Une quinzaine d'échantillons ont été passés à la diffraction aux Rayons X, pour l'analyse des principaux minéraux. Les mesures effectuées montrent une importante accumulation de sels, après la fin des irrigations, au niveau des horizons supérieurs du sol où la conductivité des eaux atteint les 17.5 mS/cm, la concentration en chlore atteint les 8.6 g/l. Ces concentrations diminuent considérablement au cours de la deuxième campagne d'échantillonnage, qui correspond à la saison humide, pour atteindre les 2.7 mS/cm et une concentration en chlore de 250 mg/l. Cette diminution de salinité est due au lessivage des pluies. L'analyse en composante principale a été appliquée aux échantillons de sols recueillis dans la première section. Nous avons procédé à une analyse séparée pour chaque saison. Les résultats montrent que la salinisation par concentration de solutés ainsi que la contamination par les nitrates, notamment dans les horizons contenant une importante fraction d'argile et de limons, contrôlent la composition chimiques des solutions du sol. Par ailleurs Le principe de l'alcalinité

résiduelle généralisée a été testé pour les échantillons de la première section. Il montre que sous l'effet de l'évaporation, la calcite poursuivi du gypse précipitent. Ce résultat est conforme aux calculs et à l'évolution des indices de saturation de la calcite et du gypse. Ce principe montre également que la solution du sol évolue vers la voie saline neutre.

La troisième partie (chapitre 5) concerne la modélisation des transferts de solutés en zone non saturée. La modélisation de l'écoulement et du transport a essentiellement été réalisée sur des profils unidimensionnels, dont la profondeur varie de 4 à 25 m. Nous avons retenu les deux codes de calculs HYDRUS1D 4ème version développé par Šimůnek (2008) et GEODENS développé par Bouhlila (1999). Les conditions aux limites supérieures correspondent aux conditions « atmosphériques » qui prennent en compte l'évaporation, la transpiration, les précipitations et les irrigations. L'évapotranspiration potentielle de référence a été estimée en se basant sur les données climatiques horaires de la station d'Oued Souhil situé à 30 km de la zone d'étude. Les précipitations sont celles mesurées au niveau de cette même station. Les paramètres hydrodynamiques du sol ont été déduits à partir des analyses granulométriques effectuées sur les échantillons de sol prélevés sur toute la colonne non saturée, jusqu'à la nappe. HYDRUS1D a été calé sur la saison humide en ne prenant en compte que les forçages climatiques. Il a reproduit le lessivage des premières couches du sol lors des périodes pluvieuses. Par ailleurs trois scenarii de prédiction on été testés. Le premier stipule que les quantités d'irrigation demeurent les mêmes durant dix ans de calcul, le second propose une diminution de 30% des quantités d'irrigation durant dix ans et le dernier propose l'abandon de l'irrigation durant 20 ans. Des séries temporelles de 30 ans (de 1970 à 2000) de données climatiques journalières (pluie, humidité relative de l'air, température, durée d'insolation et vitesse du vent) ont été moyennées pour servir de données d'entrée au modèle. Les simulations ont montré que le flux de solutés dépendait de la profondeur du profil. Ces flux simulés sont sous-estimés et négligeables à cause d'une forte accumulation de sels dans les profils. Cette sous-estimation est due essentiellement au fait que les pluies moyennées ont été lissées (le maximum journalier est à 10 mm) et ne présentaient plus de valeurs extrêmes, connues pour leurs pouvoir de lessivage. De plus l'évapotranspiration moyennée a été plus importante que celle mesurée à Oued Souhil. La recharge directe de la nappe par les pluies variait entre 0.7 et 6.2% de la pluie annuelle. Les simulations effectuées en utilisant GEODENS ont mis en évidence la précipitation du gypse au niveau des horizons supérieurs.

Comme perspectives à ce travail, nous proposons les axes suivants :

- Modéliser les processus géochimiques le long de la ligne d'écoulement en utilisant NETPATH ou PHREEQC
- Améliorer la conversion des résistivités électriques en teneur en eau. Une expérimentation basée sur celle décrite par Montoroi et al. (1997) et adaptée de Rhoades est en cours de montage.
- Améliorer les données climatiques d'entrée en utilisant des méthodes et modèles statistiques plus poussés.
- Réaliser un échantillonnage adéquat pour les croûtes de sels à la surface du sol et les faire analyser aux RX pour confirmer la présence de calcite et de gypse. Réaliser l'expérience de l'irrigation avec des eaux salées et sous évaporation à l'échelle du laboratoire.
- Réaliser une modélisation stochastique de l'hétérogénéité et étudier son effet sur le transport des sels en zone non saturée. Notons que la littérature manque sur ce sujet à cause du nombre important de paramètres à traiter

Table of contents

Chapter 1. Introduction

1. Salinization, an environmental hazard

Water and land resources misuse in ancient civilisations of Mesopotamia (Artzy and Hillel, 1988) and Mesoamerica has contributed to their progressive decline. Furthermore, it is interesting to notice that historians are now defending the theory of ecological failure and the irrigation infrastructure breakdown to explain the sudden end of the Khmer Empire (from the IXth to the XIIIth century) (Kummu, 2009). The misuse of water resources was also associated to the occurrence of soil and groundwater salinization. This phenomenon has been identified from the antiquity as a source of civilizational threat. It was reported that, by the end of the Punic wars (146 B.J.C.), the roman army, has spread salt on the farm fields of Carthage to sterilize their land as an ultimate form of punishment (Slim et al., 2006).

Nowadays, salinization is identified as an environmental hazard that is furthermore considered as a desertification indicator (Kosmas et al., 2006). In fact, it is classified as the third cause of desertification. It affects soil, groundwater and surface water resources and is characterised, in some cases, by its irreversible state.

The Mediterranean basin is particularly affected by this phenomenon (FAO, 1997). Indeed, in arid and semi arid regions, the annual water balance is highly disturbed by the increasing water demand (Chahed et al., 2008). Therefore, an important percentage of water resources is no longer renewed through natural recharge inducing water quality degradation as a result of solute accumulation and concentration. Note that the spread of salinization is mainly correlated to the irrigation expansion (Smedema and Shiati, 2002). Irrigation induces salinization through three principle processes: mobilization of salts, already present in the root zone, brackish shallow groundwater rise and salts accumulation in the topsoil due to irrigation with saline water combined with high evapotranspiration rates. Thus, adequate irrigation practices have to be adopted to manage irrigation-induced salinization (Hillel, 2000). Postel (1999) (Postel, 1999) discussed the durability of irrigation systems.

Irrigated coastal areas are vulnerable to salinization. In fact, in these areas, several sources of salinization can be identified: natural or primary salinity (Baba et al., 2006), seawater

intrusion (eg. Custodio and Bruggeman, 1987) and irrigation return flow (eg. Ben Moussa et al., 2010; Causapé et al., 2004a).

1.1. Seawater intrusion

Seawater intrusion occurs when heavy pumping withdraws fresh water at a faster rate than it can be renewed. The seawater/freshwater interface is thus displaced inducing the fresh groundwater contamination with salt water. Seawater intrusion is considered among the most hazardous and widespread coastal aquifer contamination mechanisms (Bear et al., 1999; Custodio and Bruggeman, 1987; Steyl and Dennis, 2009).

In Tunisia, several coastal aquifers are reported to be affected by seawater intrusion. Indeed, a study performed in the sixties, for the ministry of agriculture, detected that Korba coastal aquifer, located in the Cap Bon peninsula (North-East of Tunisia), was already contaminated by seawater intrusion (D.G.R.E, 1964). Since that date, several studies reporting other cases of seawater affected aquifers have been cited in the literature. Tarhouni et al. (1996) continued the survey in Korba coastal plain. Rekaya (1997), presented an overview about the national expand of the problem. He reported that yearly extractions from coastal aquifers already exceeded the natural recharge and moreover presented 50 % of the total extracted groundwater from all the phreatic aquifers. He also stated that protection measurements were decided by the government, yet their application was limited. Fedrogini et al. (2001) and Trabelsi et al. (2007) analysed the mineralization sources in Jebenia coastal aquifer (South of Tunisia) and classified seawater as the third major source of salinity. Bouri and Ben Dhia (2010) presented the case study of Teboulba aquifer (Tunisian Sahel) affected by seawater since the seventies. They assessed the thirty-year artificial recharge experiment through surface wells and found the technique was successful in improving both piezometry and groudwater quality. Ben Hamouda et al. (2009) set up an important isotopic and geochemical database of both Korba and Haouaria aquifers.

Several techniques to monitor and assess seawater intrusion are cited in the literature. Among these techniques, the most used are: geochemical analysis and modelling (eg. Park et al., 2003; Post, 2002), hydrodynamic modelling and assessment (eg. Kerrou and Renard, 2010) and geophysical investigations (Martínez et al., 2009; Melloul and Goldenberg, 1997)

1.2. Irrigation-induced Salinization and Irrigation return flows

Besides seawater intrusion, soil salinization and alkalinization are the other side effects of the irrigation expansion. In fact, the high rates of evapotranspiration, recorded in arid and semi arid regions, induce salt accumulation on the topsoil. These salts are then leached, under rainfall, towards groundwater. This situation made some aquifers trapped in a closed salinization cycle. This phenomenon is referred to as the solute recycling. Milnes et Renard (2004) proposed a mathematical formulation describing solute recycling. Besides, their formulation was applied and tested in the case of the Kiti aquifer in Cyprus. They have found that considering solute recycling improved the results of the aquifer numerical model.

In the last decades, the scientific community became aware about the importance of studying the impact of land use on the groundwater (Cardona et al., 2004; Kim et al., 2003), surface water and seawater's quality (Andersen et al., 2007). Indeed, in the fifties and sixties, soil scientists were rather concerned with leaching salts below the root zone. Hence, the vadose zone was assimilated to the root zone that did not exceed 150 cm depth. Moreover, even in recent literature we can read "*However for the most part, in humid regions salt affected soils are not a problem because rainfall is sufficient to leach excess salts out of the soil, into groundwater and eventually into the sea*" (Sparks, 2003). Inversely, solute transport and fate in the vadose zone is well studied in the literature. Most of these studies are in general conducted without consideration to the groundwater (Rajmohan and Elango, 2007). Therefore irrigation return flow mechanisms and quantification are poorly cited in literature.

Irrigation return flow can be assessed by using numerical or conceptual models. Conceptual models based on the salt and water balances are widely used to give a quantitative evaluation of salt transfer at different scales (Aragüés et al., 1985; Askri et al.; Causapé et al., 2004b; Marlet et al., 2009)

In Tunisia, the salinity management in irrigated areas has been studied since the early sixties in the context of the Research Centre for the Utilization of Saline Waters for Irrigation (*CRUESI*) established in 1962 with the collaboration of the Special Fund of the United Nations and UNESCO. Hachicha (2007) presented an overview of the Tunisian situation with regard to soil salinization. He reported that salt-affected soils cover about 1.5 million hectares, representing a ratio of 10% of the total surface of the country.

2. Motivations, aims and structure of the thesis

The present work deals with the study of salt transfer in the Korba irrigated coastal plain reported to be highly affected by both piezometric drop and increasing salinity.

Korba aquifer has been widely and thoroughly studied since the sixties (D.G.R.E, 1964; Ennabli, 1980; Kerrou et al., 2010; Lecca et al., 1999; Paniconi et al., 2001; Tarhouni et al., 1996). Nevertheless, experimental and modelling studies concerning the vadose zone are lacking. In fact, cultivated soils in the Korba plain are classified as light textured and thus not threatened by salinization hazards. Therefore, the analysis and quantification of irrigation return flow has to be deepened. Besides, groundwater hydrogeochemical investigations and analysis along important flow paths were not performed. Indeed, studying hydrochemical processes along flow paths enhances their identification and comprehension (Andersen et al., 2005). Moreover, the seawater/freshwater mixing problem was modelled by Kouzana et al. (2009) using PHREEQC (Parkhurst, 1995), yet the results were not discussed with regards to groundwater flow.

The present work aims at identifying sources of salinity affecting soil and groundwater, to analyse the salinization processes of both soil and groundwater in a coastal plain and finally to study and quantify the irrigation return water and solute flows. The expected results can be useful to decision makers, for sustainable management of soil and groundwater resources.

The present thesis is divided into four principle chapters presented in international conferences and submitted to peer-reviewed journals. In the second chapter, we present an endeavour to identify the salinity sources in the Korba aquifer using multivariate statistical analysis, conventional geochemical methods and electrical tomography imaging. Experimental data was collected during a three year survey along two transects.

In the third chapter we are proposing to use geochemical processes occurring at the seawater/freshwater interface as indicators of temporal and spatial seawater intrusion evolution. A modelling of seawater and groundwater mixing problem is presented.

The fourth chapter deals with an experimental study of soil and groundwater salinization under irrigation with brackish water.

The fifth and last chapter is a presentation of the unsaturated modelling of the long term transfer of salts movement in the vadose zone. The objective is to quantify salt quantities at the profile scale moving towards the groundwater. Geochemical modelling is also proposed in this chapter.

The sixth and last chapter summarizes and discusses the principal results. In this conclusion we are also proposing a perspective of eventual future fields of research to carry on as a continuation of the present work.

References

Andersen, M.S., Baron, L., Gudbjerg, J., Gregersen, J., Chapellier, D., Jakobsen, R. and Postma, Andersen, M.S., Baron, L., Gudbjerg, J., Gregersen, J., Chapellier, D., Jakobsen, R. and Postma, D., 2007. Discharge of nitrate-containing groundwater into a coastal marine environment. Journal of hydrology, 336: 98- 114.

Andersen, M.S., Nyvang, V., Jakobsen, R. and Postma, D., 2005. Geochemical processes and solute transport at the seawater/freshwater interface of a sandy aquifer. Geochimica et Cosmochimica Acta 69(16): 3979-3994.

Aragüés, R., Tanji, K.K., Quílez, D., Alberto, F., Faci, J., Machín, J. and Arrué, J., L., 1985. Calibration and verification of an irrigation return flow hydrosalinity model Irrigation science, 6(2): 85-94.

Artzy, M. and Hillel, D., 1988. Defense of the theory of progressive soil salinization in ancient southern Mesopotamia. Geoarcheology, 3 (3): 235 - 238.

Askri, B., Bouhlila, R. and Job, J.O., Development and application of a conceptual hydrologic model to predict soil salinity within modern Tunisian oases. Journal of Hydrology, 380(1-2): 45-61.

Baba, A., Howard, K., Gunduz, O. and Chambel, A., 2006. Groundwater in semi-arid mediterranean areas: desertification, soil salinization and ecosystems, Groundwater and Ecosystems. Springer Netherlands, pp. 47-58.

Bear, J., Cheng, A.H.D., Sorek, S., Ouazar, D. and Herrera , I., 1999. Seawater Intrusion in Coastal Aquifers - Concepts, Methods and Practices. Kluwer Academic Publishers, Dordrecht.

Ben Hamouda, M.F., Leduc, C., Tarhouni, J. and Zouari, K., 2009. Origine de la minéralisation dans l'aquifère plio-quaternaire de la côte orientale du cap Bon (Tunisie). Sècheresse, 20 (1): 78-86.

Ben Moussa, A., Bel Haj Salem, S., Zouari, K., Marc, V. and Jlassi, F., 2010. Investigation of groundwater mineralization in the Hammamet–Nabeul unconfined aquifer, north-eastern Tunisia: geochemical and isotopic approach. Environmental earth sciences, DOI 10.1007/s12665-010-0616-1.

Bouri, S. and Ben Dhia, H., 2010. A thirty-year artificial recharge experiment in a coastal aquifer in an arid zone: The Teboulba aquifer system (Tunisian Sahel) C.R. Acad. Sci. Paris, Sciences de la Terre et des Planètes, 342(1): 60-74.

Cardona, A., Carrillo-Rivera, J., Huizar-Alvarez, R. and Garniel-Castro, E., 2004. Salinization in coastal aquifers of arid zones: an example from Santo Domingo, Baja California Sur, Mexico. Environmental Geology, 45: 350-366.

Causapé, J., Auqué, L., Gimeno, M., J., Mandado, J., Quilez, D. and Aragüe´s, R., 2004a. Irrigation effects on the salinity of the Arba and Riguel Rivers (Spain): present diagnosis and expected evolution using geochemical models. Environmental Geology 45: 703-715.

Causapé, J., Quılez, D. and Araqüés, R., 2004b. Assessment of irrigation and environmental quality at the hydrological basin level II. Salt and nitrate loads in irrigation return flows. Agricultural Water Management, 70 211-228.

Chahed, J., Hamdane, A. and Besbes, M., 2008. A comprehensive water balance of Tunisia: blue water, green water and virtual water. Water International, 33(4): 415 - 424.

Custodio, E. and Bruggeman, K.A., 1987. Groundwater Problems in Coastal Areas UNESCO, Paris.

D.G.R.E, 1964. Etude hydrogeologique de la nappe de Korba, Direction Générale des Ressources en Eau, Tunis, Tunisia.

Ennabli, M., 1980. Etude hydrogéologique des aquifères du nord-est de la Tunisie pour une gestion intégrée des ressources en eau. Doctorat d'Etat Thesis, Ministère de l'agriculture. République Tunisienne.

FAO, 1997. Seawater intrusion in coastal aquifers, guidelines for study, monitoring and control. Water Reports no. 11. FAO Land and Water Development Div., Rome, Italy, 161 pp.

Fedrigoni, L., Krimissa, M., Zouari, K., Maliki, A. and Zuppi, G.M., 2001. Origine de la minéralisation et comportement hydrogéochinique d'une nappe phréatique soumise à des contraintes naturelles et anthropiques sévères : exemple de la nappe de Djerbeniana (Tunisie). C.R. Acad. Sci. Paris, Sciences de la Terre et des Planètes, 332: 665-671.

Hachicha, M., 2007. Les sols salés et leur mise en valeur en Tunisie. Sècheresse, 18(1): 45-50.

Hillel, D., 2000. Salinity Management for Sustainable Irrigation: Integrating Science, Environment, and Economics (Environmentally and Socially Sustainable Development. Rural Development). World Bank, 92 pp.

Kerrou, J. and Renard, P., 2010. A numerical analysis of dimensionality and heterogeneity effects

on advective dispersive seawater intrusion processes. Hydrogeology Journal.

Kerrou, J., Renard, P. and Tarhouni, J., 2010. Status of the Korba groundwater resources (Tunisia): observations and three-dimensional modelling of seawater intrusion. Hydrogeology Journal, DOI 10.1007/s10040-010-0573-5.

Kim, J., H., , Kim, R., H., , Lee, J. and Chang, H., W., , 2003. Hydrogeochemical characterization of major factors affecting the quality of shallow groundwater in the coastal area at Kimje in South Korea. Environmental Geology, 44: 478-489.

Kosmas, C., Tsara, M., Moustakas, N., Kosma, D. and Yassoglou, N., 2006. Environmentally sensitive areas and indicators of desertification In: W. Kepner, G.,, J.L. Rubio, A. David and M. Pedrazzini (Editors), NATO Security through Science Series. Desertification in the Mediterranean Region. A Security Issue, pp. 527-547

Kouzana, L., Mammou, A.B. and Felfoul, M.S., 2009. Seawater intrusion and associated processes: Case of the Korba aquifer (Cap-Bon, Tunisia). Comptes Rendus Geosciences, 341(1): 21-35.

Kummu, M., 2009. Water management in Angkor: Human impacts on hydrology and sediment transportation. Journal of Environmental Management, 90(3): 1413-1421.

Lecca et al., 1999. A modular approach to the Korba aquifer sea-water intrusion study, 2, Simulation, data manipulation, and visualization for the 3D model. Natuur-en Geneeskundige Vennootschap, Gand, BELGIQUE, 309 pp.

Marlet, S., Bouksila, F. and Bahri, A., 2009. Water and salt balance at irrigation scheme scale: A comprehensive approach for salinity assessment in a Saharan oasis. Agricultural Water Management, 96(9): 1311-1322.

Martínez, J., Benavente, J., García-Aróstegui, J.L., Hidalgo, M.C. and Rey, J., 2009. Contribution of electrical resistivity tomography to the study of detrital aquifers affected by seawater intrusion-extrusion effects: The river Vélez delta (Vélez-Málaga, southern Spain). Engineering Geology, 108(3-4): 161-168.

Melloul, A.J. and Goldenberg, L.C., 1997. Monitoring of Seawater Intrusion in Coastal Aquifers: Basics and Local Concerns. Journal of Environmental Management, 51(1): 73-86.

Milnes, E. and Renard, P., 2004. The problem of salt recycling and seawater intrusion in coastal irrigated plains: an example from the Kiti aquifer (Southern Cyprus). Journal of Hydrology, 288: 327-343.

Paniconi, C., Khalifi, I., Lecca, G., Giacomelli, A. and Tarhouni, J., 2001. Modeling and analysis of seawater intrusion in the coastal aquifer of Eastern Cap-Bon, Tunisia. Transport in Porous Media, 43: 3-28.

Park, S.-C., , et al., 2003. Regional hydrochemical study on salinization of coastal aquifers, western coastal area of South Korea. Journal of Hydrology, 2005(313): 182–194.

Parkhurst, D., 1995. User's guide to PHREEQC: a computer program for speciation, rreaction-path, advective-transport and inverse geochemical calculations, US Geol Surv Water-Res.

Post, V.E.A., 2002. Chemistry for modellers aqueous geochemistry in coastal areas, 17th Salt Water Intrusion Meeting, Delft, The Netherlands.

Postel, S., 1999. Pillar of Sand. Can the Irrigation Miracle Last? WW Norton & Company and World Watch Institute, New York, 320 pp.

Rajmohan, N. and Elango, L., 2007. Mobility of major ions and nutrients in the unsaturated zone during paddy cultivation: a field study and solute transport modelling approach. Hydrological Processes, 21(20): 2698-2712.

Rekaya, M., 1997. Tunisian experience of seawater intrusion control. In: FAO (Editor), Seawater intrusion in coastal aquifers. Guidelines for study, monitoring and control. Water Reports, Rome.

Slim, H., Mahjoubi, A., Belkhoja, K. and Ennabli, A., 2006. Histoire générale de la Tunisie, tome 1 : L'antiquité. Sud éditions, Tunis, 460 pp.

Smedema, L., K., and Shiati, K., 2002. Irrigation and salinity: a perspective review of the salinity hazards of irrigation development in the arid zone. Irrigation and Drainage Systems, 16: 161-174.

Sparks, D., L., 2003. Environmental Soil Chemistry. Academic Press, 350 pp.

Steyl, G. and Dennis, I., 2009. Review of coastal-area aquifers in Africa. Hydrogeology Journal, 18: 217–225.

Tarhouni, J., Jemai, S., Walraevens, K. and Rekaya, M., 1996. Caracterisation de l'aquifere cotier de Korba au Cap Bon (Tunisie). Progress report 95-96 for AVI-73 EC Project.

Trabelsi, R., Zairi, M. and Dhia, H.B., 2007. Groundwater salinization of the Sfax superficial aquifer, Tunisia. Hydrogeology journal, 15: 1341-1355

Chapter 2. Hydrochemical and hydrodynamical identification of superimposed salinization processes in a coastal irrigated plain, Korba (Tunisia)

Abstract

Groundwater investigations were carried out along two transects (S1 and S2) perpendicular to the shoreline in Korba coastal aquifer. They involved groundwater sampling, piezometric measurements and Electrical Resistvity Tomography imaging. The objective was to identify the potential origins of groundwater salinization and to study the associated processes. Historical data, set up since 1962, were also collected and analysed to evaluate time and space evolution of the salinization spread. Ionic ratios and deltas, conventional diagrams and geochemical modelling using PHREEQC were also used. Besides, multivariate statistics techniques, Principal Component Analysis (PCA) and Hierarchical Cluster Analysis (HCA) were performed. The piezometric survey confirmed the inversion of the groundwater flow in transect S1 where a piezometric depression of 5 m was observed at 4000 m from the shoreline. PCA reveals that two main processes are contributing to groundwater mineralization and thus salinization: seawater intrusion and agricultural contamination mainly through N-fertilizers. The geochemical impact area of seawater intrusion was estimated to 4000 and 1500 m respectively for transect S1 and transect S2. Inversely, agricultural contamination is rather acting in internal areas beginning at 2000 m and 1500 m from the shoreline for respectively S1 and S2.

1. Introduction

Salinization forms one of the most widespread and threatening groundwater contamination forms (Richter and Kreitler, 1991). Coastal aquifers are in general more vulnerable to quality degradation due to natural salinization processes and recent agricultural activities expansion and intensification (Smedema and Shiati, 2002). The latter causes seawater intrusion characterized by groundwater flow inversion due to intensive pumping. This situation is more critical in semi arid and arid areas like the Mediterranean and Near-East regions (FAO, 1997).

Custodio and Bruggeman (1987) reported that brackish groundwater is naturally common in arid regions because of climatic reasons. The other aggravating factor is that extracted groundwater is no more renewed through natural recharge processes because annual rainfall does not exceed, in some cases, 200 mm. If we consider climate change hazards, it is clear that Mediterranean countries are facing real fresh water scarcity problems. Moreover, agricultural activities are loading diverse contaminants principally issued from fertilizers and pesticides that are transferred towards groundwater. This phenomenon, known as the solute recycling through irrigation return flow, is also contributing to groundwater salinization (Milnes and Renard, 2004).

Besides seawater intrusion and irrigation return flow, case and regional studies cite fossil seawater (Vengosh and Benzvi, 1994), dissolution of evaporites (Trabelsi et al., 2007), deep brines and other anthropogenic sources (Ben Moussa et al., 2008) as possible sources of salinization. Post (2004) focuses on the relationship between geological history and salinity origins. In many cases, different sources of salinization are superimposed. This makes it difficult to identify these sources and to evaluate the contribution of each of them.

Several geochemical (Richter and Kreitler, 1991; Vengosh and Rosenthal, 1994), geophysical (Martínez et al., 2009) and hydrodynamic techniques have been developed to assess salinity sources and to study different processes accompanying groundwater salinization. Multivariate statistics techniques (Papatheodorou et al., 2007) as well as numerical modelling are contributing to the knowledge and prediction of these phenomena. Nevertheless, the reliability and applicability of these techniques remain limited, in some cases, because of the superposition and interference of different sources and processes affecting groundwater. Ghabayen (2006) used the Bayesian Belief Network (BBN's), a probabilistic expert systems, to distinguish between different sources of salinization.

Geochemical processes accompanying groundwater salinization are closely linked to the respective salinity source. For instance, seawater intrusion is mostly characterized by

cation exchange, carbonate dissolution/precipitation (Bouhlila and Laabidi, 2008) and sulphate reduction (Gomis-Yagües et al., 2000). Salinization issued from agricultural pollution is likely to be enhanced by evapotranspiration and leaching processes leading to precipitation/dissolution of minerals (Cardona et al., 2004).

Irrigation return flow is less reported in literature and is rather difficult to quantify. Indeed, most of these processes are taking place in the unsaturated zone, and need soil sampling and studies. In semi arid conditions, evapotranspiration and winter rainfall seem to act as the major motors of these processes. During the irrigation season, evapotranspiration causes minerals to precipitate and makes the upper soil layer become concentrated in solutes. This situation is aggravated each time the applied irrigation water is already saline. The precipitated minerals are then leached under rainfall action. At a long term scale, these minerals would reach the groundwater. In the case of shallow groundwater, the irrigation water can instantly recharge the groundwater. The major fingerprint of irrigation return flow is the increase of NO_3, Cl and SO_4 (Koh et al., 2007; Kumar et al., 2009).

Korba aquifer is an example of the contaminated coastal aquifers in the Mediterranean region. Surveys, experimental and modelling studies have been set up since the sixties to assess the threatening intrusion of seawater into the continental groundwater, originally suitable for agriculture. In most of these studies, seawater intrusion is presented as the major cause and origin of groundwater quality degradation. In this study, we are exploring other sources of salinity beyond the evident seawater intrusion. The main objective is to identify the sources of salinity, especially the ones originating from agricultural return flow. Besides, we will discuss the geochemical processes accompanying seawater intrusion and agricultural pollution with regards to the hydrodynamic evolution.

2. Hydrogeological settings

The Korba plain is located in the north-eastern Cap-Bon peninsula of Tunisia. The Korba aquifer is known to be a part of the regional aquifer delimited by the city of Maamoura in the south, the city of Kélibia in the north, the Mediterranean Sea in the east and the Djebel Abderrahman in the west (

Fig. 1) (Lecca, 1999). The aquifer is alluvial and phreatic and it covers about 438 km². Two principal geological units form this aquifer (Ben Hamouda, 2009). The first unit was formed during the Pliocene and Quaternary ages by deposition of eroded products from the Djebel Sidi AbedErrahmen anticline and the Dakhla syncline. The Pliocene formation is sandstone with alternating marl units and having a mean thickness of 85 m. The

Quaternary alluvium is composed of detrital sediments (sand, gravel, and silt) with thin clay lenses and has a thickness that varies between 20 m and 25 m.

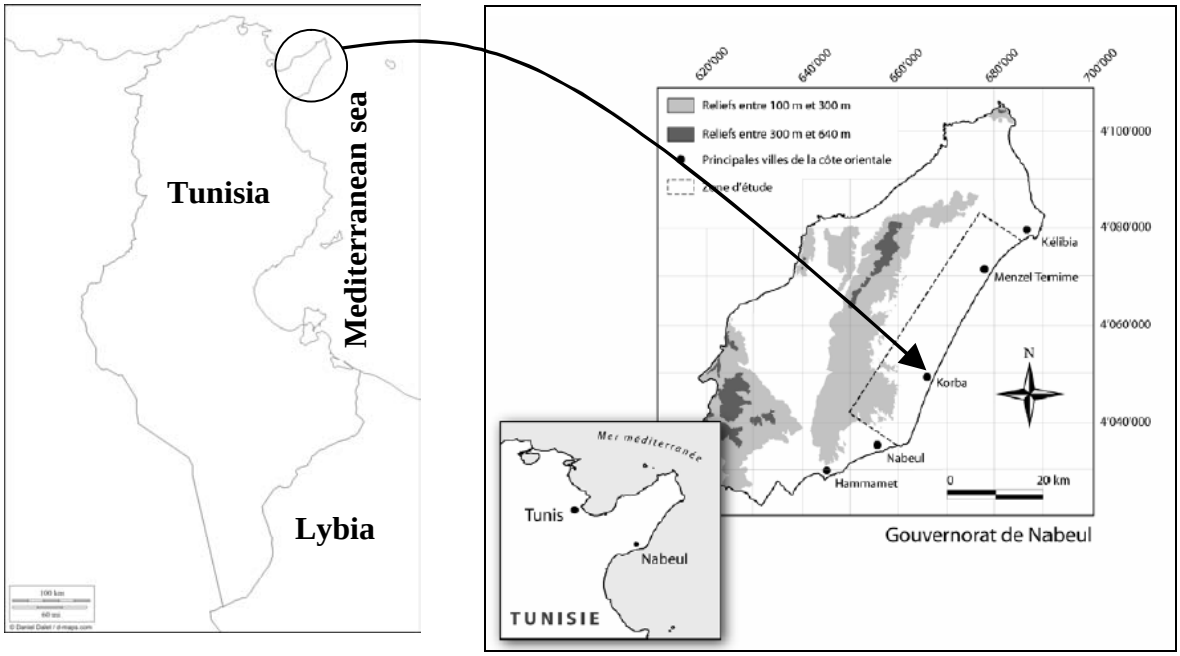

Fig. 1. Location of Korba coastal aquifer

The second unit is constituted of a Miocene marl formation underlying the first unit (Paniconi et al., 2001). Transmissivities in the Korba aquifer range from 5.10^{-5} to 10^{-2} m^2/s (Ennabli, 1980). The Korba plain has a semi-arid climate with a Mediterranean influence. The annual mean precipitation is 450 mm while mean annual evapotranspiration reaches 1100 mm. Ennabli (1980) estimated the real recharge in the range of 5-8 % of the average annual precipitation (21-34 mm/year). Recently, Kerrou et al. (2010) found that the annual recharge rate can reach 20%. This aquifer is being intensively exploited, mainly for agricultural purposes, since the sixties. More than 9000 wells equipped with motor-driven pumps and extracting about 54 Mm^3/year were registered (Ben Hamouda, 2009). This situation caused groundwater level to decline steadily leading to the creation of a wide depression between Diar El Hojjej and Tafelloun villages where the measured hydraulic head reached 12 m below the mean sea level in 2004 (Kerrou et al., 2010). Alongside with piezometric depression, groundwater salinity has been increasing since the seventies (Fig. 2). It reaches in some regions 15g/L.

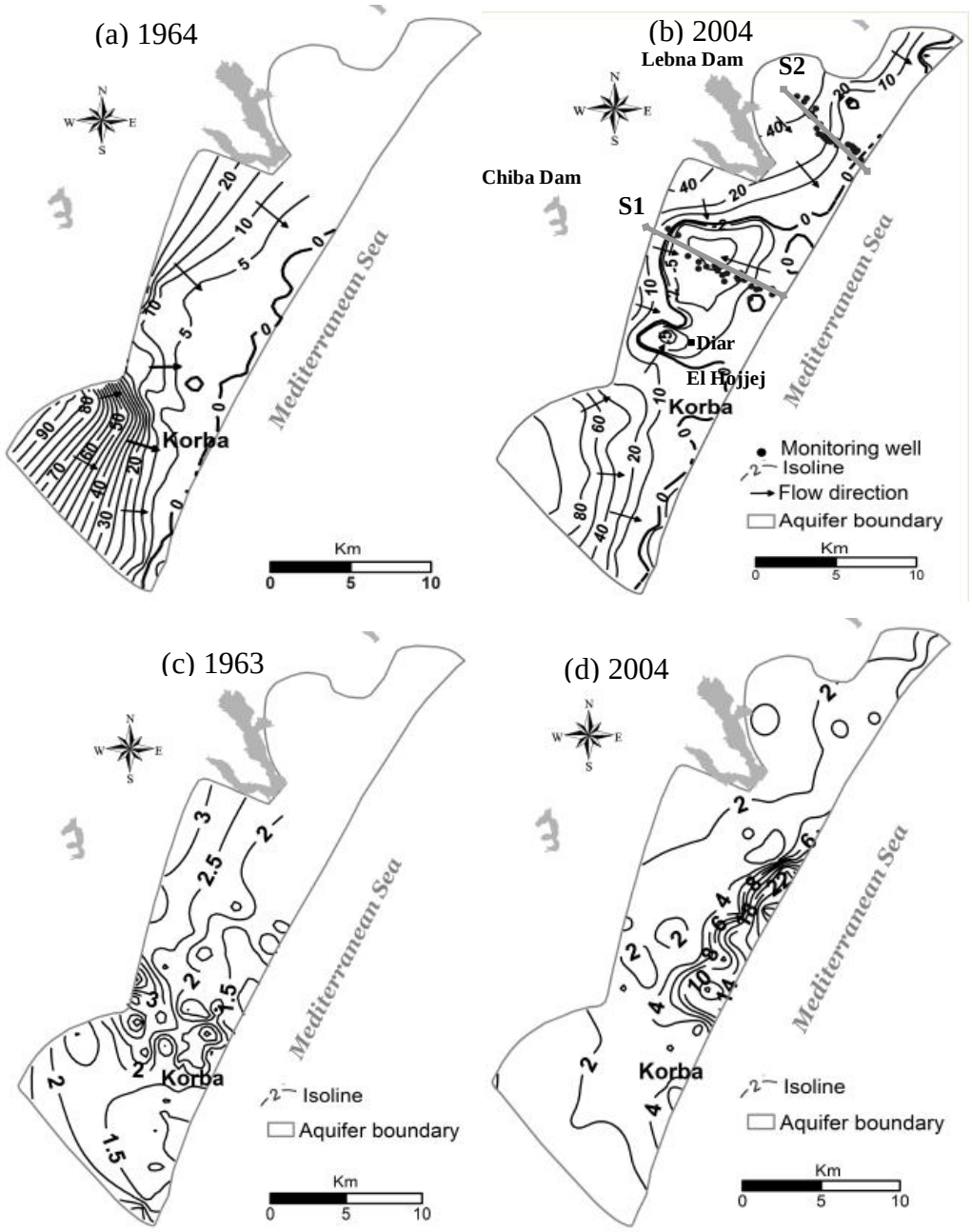

Fig. 2 Time evolution of the groundwater hydraulic heads (a) 1963 (DGRE, 1964), (b) 2004 (Kerrou et al., 2010) and the salinity expressed in TDS (mg/l) (c) 1963 (DGRE, 1964) and ,(d) 2004 (Kerrou et al., 2010) in the Korba aquifer. The location of transects S1 and S2 is also indicated.

To cope with seawater intrusion, a protection perimeter located in Diar El Hojjej irrigated area was defined in 1998. This area receives surface water from the Northern dams of Tunisia (via Mejerda Cap Bon Canal) for irrigation and artificial recharge purposes. Moreover, the ministry of agriculture decided to plan artificial groundwater recharge sites with treated wastewater.

3. Materials and methods

3.1. Historical data

Hydrodynamic and quality data have been collected through a network, set up since the sixties by the Regional Office of agricultural development (CRDA Nabeul), and covering an important part of the aquifer (DGRE, 1964). The resulting database is partially available but is discontinuous regarding time and space scales. The analysis of this database is though crucial for the comprehension of time and space evolution of the salinization processes and origins. In this work, we have exploited the results of a sampling campaign carried out in 1964 where major elements (Na, Ca, Mg, Cl and SO4) and Total Dissolved Salts (TDS) were measured (DGRE, 1964). Besides, we have plotted pizometric and TDS maps measured respectively in 1963 (DGRE, 1964) and 2004 (Kerrou et al., 2010) (Fig. 2).

3.2. Groundwater investigations along two transects

Two transects, perpendicular to the seashore and following a flow path (S1 and S2) were selected to carry out different groundwater investigations (Fig. 2). The methodology based on investigations along flow paths is proposed in some case studies (Andersen et al., 2005; De Montety et al., 2008; Yakirevich et al., 1998). It allows the comprehension of geochemical response to different hydrodynamic processes. The selection of these two transects was based first on the piezometric map and secondly on the seawater intrusion and salinization state. The first transect S1 is located in an area characterized by the inversion of the groundwater flow landward and the high salinity. The second transect is located at about ten kilometres north from the first one and is globally not affected by seawater intrusion (Fig. 2).

In each transect, a monitoring network composed of piezometers, exploited and abandoned wells was set up (Fig. 2 and Appendix A). Besides, in transect S1, three piezometers (set up for the purposes of the present study) were equipped with automatic data loggers measuring hourly the pressure head, the electrical conductivity and the temperature. Water sampling and piezometric measurements were performed in June, August, December 2006, March, June, November 2007 and March 2008. Rainfall was measured in Oued Souhil Climatic station (INRGREF[1]) located at 30 km south from the first transect S1.

Temperature, pH and electrical conductivity were measured in situ. Major elements (Na, K, Ca, Mg, Cl, SO_4) and nitrate were analysed in the CHYN Laboratory with ionic

[1] Institut National de Recherche en Génie Rural Eaux et Forêts

chromatography after the samples were filtered (0.45 µm). Bicarbonates ions (HCO_3^- and $CO3^{2-}$) were analysed using titration and bromide with a spectrophotometer. The ionic balance error was calculated to evaluate the analytical precision of the measurements. Most of the samples presented an acceptable error, i.e. below 5%.

3.3. Geochemical methods

Several geochemical techniques are proposed in literature to identify the salinity origin in groundwater. Among these techniques, we can cite ionic ratios and stable and non-stable isotopes. Shoeler (1996) first proposed the use of ionic ratios rather than ionic concentrations. This method is now widely recommended and used the literature (Ghabayen et al., 2006; Richter and Kreitler, 1991; Vengosh and Rosenthal, 1994). In this paper, we will use Br/Cl (Andreasen and Fleck, 1997; Hsissou et al., 1999), Na/C1, Mg/Ca, HCO_3/ Cl, Ca/(SO_4+HCO_3) (Vengosh and Rosenthal, 1994) and SO_4/Cl (Pulido-Leboeuf et al., 2003) as the most significant ratios indicating the salinity origins.

In general, groundwater under natural conditions does not contain high nitrate concentrations. If so, nitrate pollution indicates contamination through agricultural effluents. Thus nitrate can be used to distinguish salinization induced by irrigation return effluents from that related to other sources (Cardona et al., 2004).

Water types were determined, for each transect, using the conventional Piper diagram (Appelo and Postma, 2005). Besides, Hounslow diagram (Hounslow, 1995), for the identification of brine origins, was applied to samples issued from the present study as well as those collected in 1964.

3.4. Multivariate statistical analysis

When studying multiple quality variables measured in different observation wells at different seasons, the multivariate statistics techniques present a useful tool to differentiate the role of each variable in the final chemical composition of the groundwater. They also allow the classification of the different observation wells into groups (Morell et al., 1996). Among the multivariate statistics techniques, we can cite Principal Component Analysis (PCA) and Hierarchical Cluster Analysis (HCA). These two techniques have been widely applied in case studies of groundwater quality (Hussein, 2003; Melloul and Collin, 1992). Physical and chemical variables describing groundwater quality, usually present different units and an important variety in variances and means regarding space and time. Therefore, a data transformation is processed prior to the application of a multivariate statistics technique (Melloul and Collin, 1992). Moreover, this procedure makes the data

dimensionless. The data transformation is based on the standardization technique: for each variable *i*, and for each observation well *j*, we subtract the mean $\overline{X}_i$ from the value to standardize X_j and then divide it by the standard deviation S_i to obtain the standardized value Y_{ij} as follows:

$$Y_{ij} = \frac{X_{ij} - \overline{X_i}}{S_i}$$

The PCA and HCA techniques were applied separately for each transect considering sampled wells at the dry season performed in august 2006. This survey was selected because it is the most complete one regarding space and time. The number of samples was then 20 for transect S1 and 21 for transect S2. The considered variables for both techniques and both transects are the following: Na, K, Ca, Mg, Cl, SO4, HCO_3, NO_3 and EC

For the HCA, we applied Ward's method with Euclidian distance as a measure of similarity (Hussain et al., 2008).

3.5. Electrical Resistivity Tomography (ERT) imaging

Electrical Resistivity Tomography imaging (ERT imaging) is one of the electrical geophysical techniques that are used in the assessment of sweater intrusion mainly to study the freshwater/seawater interface and soil salinization (Bear et al., 1999; De Franco et al., 2009; Yaouti et al., 2009). In the present work, a Campus Tiger resistivimeter was used to perform two profiles (T1 and T2) in two plots of transect S1 located respectively at 600 and 1200 m from the shoreline. The profiles were oriented orthogonal to the shoreline. The Wenner protocol was applied with a number of electrodes varying from 32 to 64 spaced of 5 m leading to an investigation depth ranging from 6 to 40 m. The profile T1 was repeated with higher resolution using an electrode spacing of 1 m. Inversions were computed using RES2DINV software (Geotomo Software, 2010).

4. Results and discussion

4.1. Hydrodynamic assessment and ERT imaging

The hydraulic heads, plotted along transect S1, show the inversion of the flow, from the sea landward, and confirm seawater intrusion. Inversely, in transect S1 the groundwater flows seaward. Fig. 3 reveals that piezometry is correlated to rainfall and pumping and that it does not react to any instant recharge from irrigation return flow. This situation can be explained by the big thickness of the unsaturated zone (ranging in transect S1 from 3.5 to

24 m). Indeed, in shallow groundwater systems, with low initial water table, groundwater is instantly recharged through irrigation return flow (Slama et al., 2004).

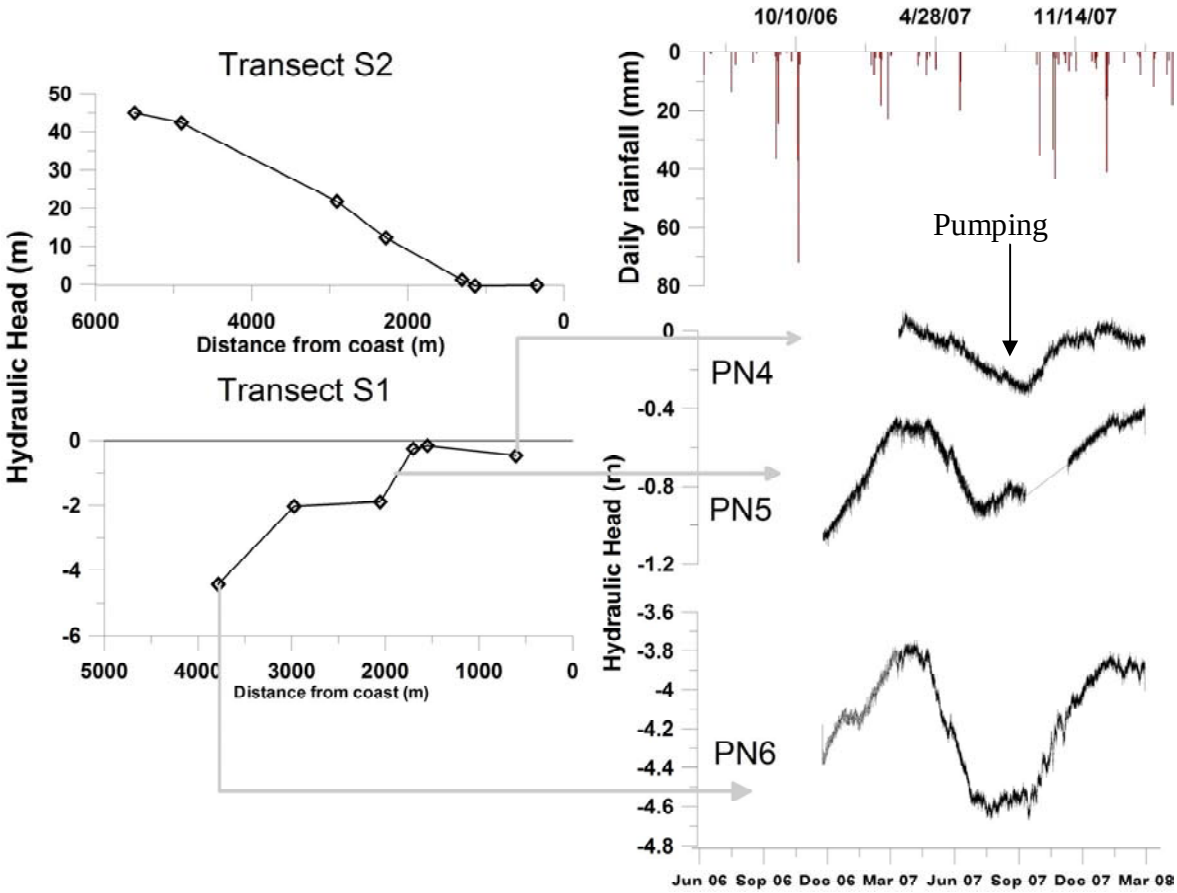

Fig. 3 Measured hydraulic heads along transect S1 and transect S2 in august 2006, continuous recorded heads in boreholes PN4, PN5 and PN6 and daily rainfall measured in Oued Souhil climatic station.

Leduc et al. (2009) studied the environmental modifications and rural development in the Merguellil catchment, Kairouan plain, central Tunisia and reported that it was not possible to find traces of irrigation water return to groundwater. They argued that this was due to the important depth of the unsaturated zone. However, the climatic context is different from that observed in Korba plain. The seasonal head variation reaches 30 cm, 60 cm and 90 cm for respectively PN4, PN5 and PN6.

Fig. 4 shows pseudo-sections of the inverted resistivity model for T1, with high resolution, and for T2. The RMS error is acceptable (about 5%) except for T1 with low resolution (18%). Both profiles are calibrated with a borehole: PN4 for T1 and 13207 for T2. The resistivity varies mainly with depth. The high resistivities measured in T2 (>1400 Ωm) corresponds to the consolidated sandstone layer. According to borehole 1307 lithology,

saturated sands present a resistivity ranging between 130 and 700 Ωm. Below this layer, the resistivity lowers to 30 Ωm indicating the presence of the clayey layer saturated with salty water. Indeed, low resistivities suggest that the pores of sediments have been filled by salty water (Yaouti et al., 2009). Besides, the depth profile of EC measured in Borehole 13207, shows that the EC reaches 25 mS/cm at 23 m below the groundwater level. The clayey layer also suggests that the bedrock, formed of Miocene marls, is not far below. The same phenomenon is observed for T1 profile, where the resistivity of saturated clays reaches 4 Ωm. The low resistivitiy values indicate that the clay is saturated with seawater and that the pseudo-section plotted the seawater-freshwater interface at only 6 m below the soil level.

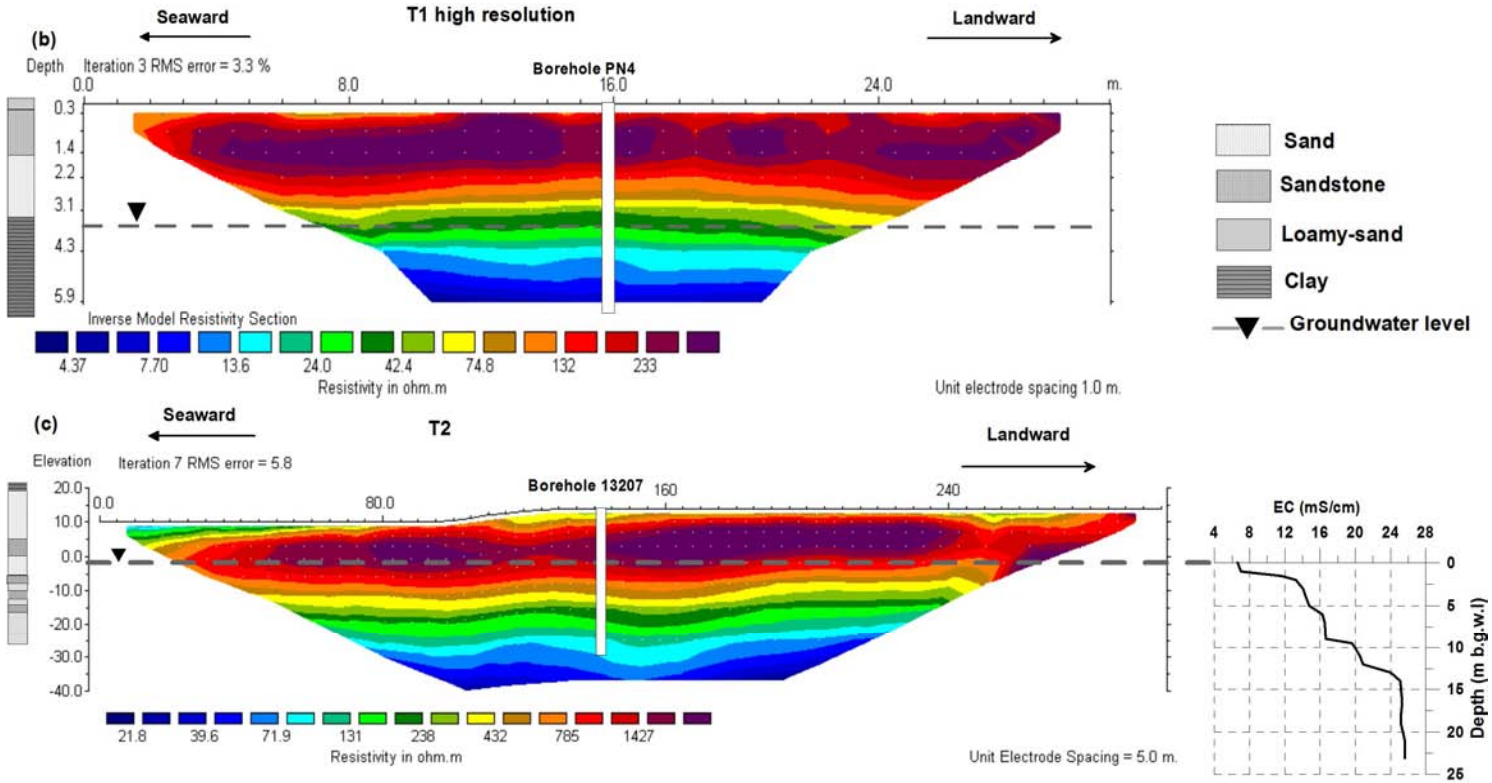

Fig. 4 Vertical pseudo-sections of the inverted resistivity measured in (b) T1 with high resolution and (c) T2. Depth profile of EC measured in well 13207 is also shown

4.2. Identification of groundwater salinity sources

4.2.1 Water types and classification using HCA

Basic statistics (Minimum, Maximun, Mean, Standard Deviation and number of samples) computed for major ions, nitrate, pH, EC and ionic ratios are reported in Tab 1 (Appendix B (raw data is available on the CD attached to the present report)). EC ranges between 3.37 and 17.19 mS/cm in transect S1 and between 1.65 and 7.93 mS/cm in transect S2, indicating a real state of salinization that makes groundwater unsuitable for both drinking (WHO, 2008) and irrigation purposes (Ayers and Westcot, 1994). Note that the highest value of EC (17.19 mS/cm) was measured in P1 in June 2006. This well is located at 836 m from the shoreline and the sample was taken after many hours of continuous pumping. Otherwise, electrical conductivities in this well fluctuates around 5 mS/cm. Barica (1972) reported that in desert oasis areas fresh water (TDS 500–3500 mg/L) could lie above saline groundwater (TDS 7.000–12.000 mg/L). Curiously PN5 which is located at more than 2000 m from the shoreline shows a constant high salinity reaching 9.98 mS/m. Moreover, plotted in a Piper diagram (Fig. 4), 80% of the samples in transect S1 are Na-Ca-Cl type (PN4, P19, PN5, P1, P11, P14, P15, P15B, P15D, P2 P3 P4 P5B, P8 and P9). This water type is mainly found in saline waters. The remaining samples present Na-Mg-Cl-HCO_3, Na-Ca-Mg-Cl and Na-Ca-Cl-HCO_3 water types. In transect S2, Na-Ca-Cl type characterizes 63% of the samples. The other water types are Na-Ca-Mg-Cl, Ca-Na-Cl, Na-Ca-Cl-SO_4, and Ca-Na-Cl-HCO_3.

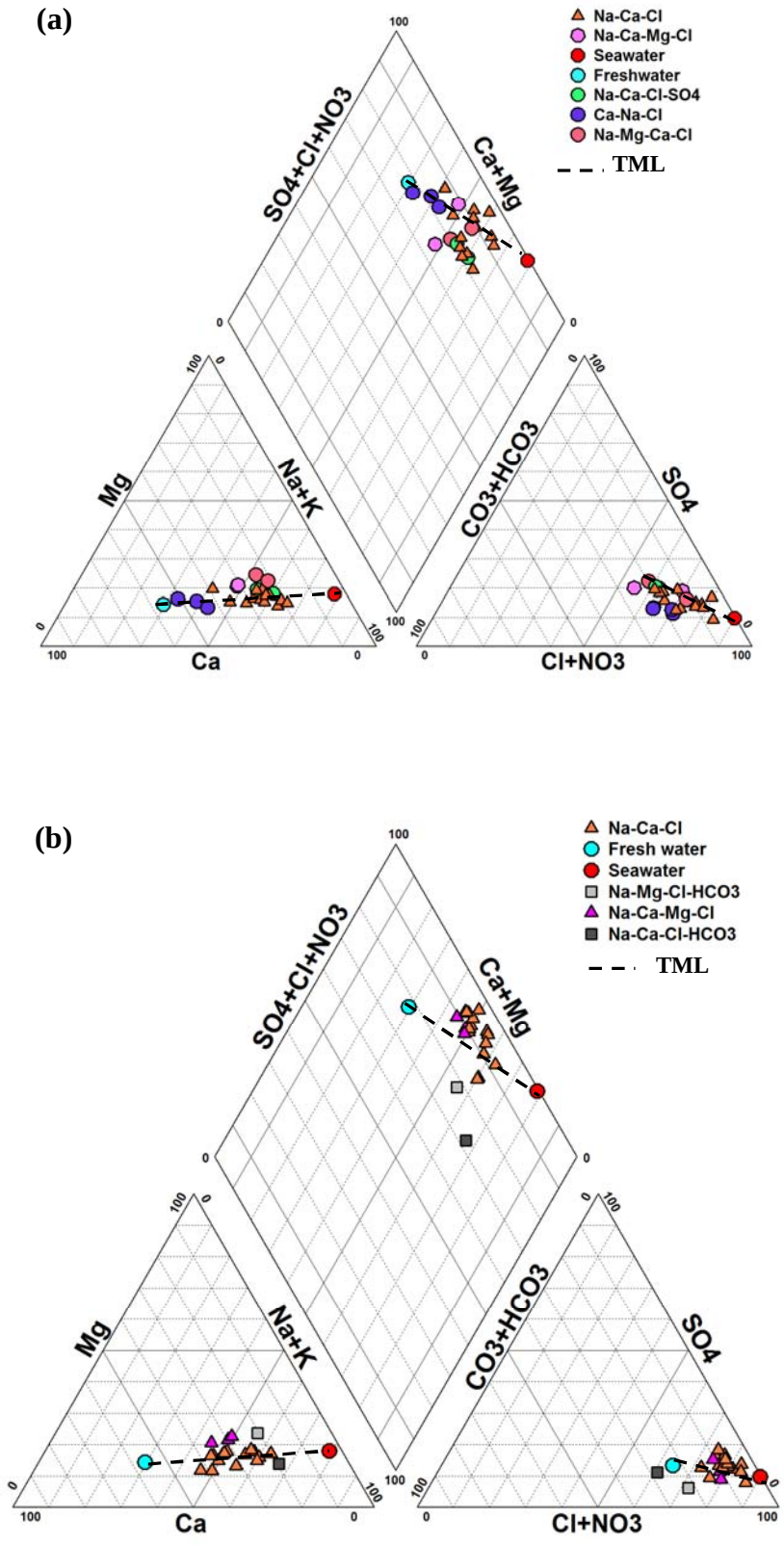

Fig. 5 Piper diagram for (a) Transect S1 (b) transect S2

This grouping is more or less compliant with the HCA if we consider the phenonline 10 (Fig. 6). Wells can be gathered in two clusters for both S1 and S2:

Transect S1

- Cluster 1.1: groups wells PN5, P19, P15B, P2, P5B, P6, P11, PN4, P15D, P1, P8 and P9. Those wells are characterised by high EC (4.68-6.29 mS/cm) and Na-Ca-Cl water type. Note that well P15B is located at about 8.5 km from the shoreline.
- Cluster 1.2: gathers wells P3, P7, P12, P14, P15, P15C and P8894, presenting lower EC (3.74-4.52 mS/cm) and Na-Mg-Cl-HCO_3, Na-Ca-Mg-Cl, Na-Ca-Cl-HCO_3 and Na-Ca-Cl water types. We have noticed that wells P12, P8894 P3 and P7 have been deepened by the farmers and are extracting water from depths higher than 50 m below soil level.

Transect S2

- Cluster 2.1: is composed of wells P17, P18, P20, P17B, MD1 and MD2, located at 1 km from the shoreline and presenting high EC (4.87-6.79). All samples are Na-Ca-Cl water type.
- Cluster 2.2: groups wells P16, P21, P21B, P30, P31, PN2, KS1, KS2, P5972, P25, P28, P33, P34 and PN3 with the lowest EC measured in this study (1.71-4.84 mS/cm). Water types are Na-Ca-Mg-Cl, Ca-Na-Cl, Na-Ca-Cl, Na-Ca-Cl-SO_4, and Ca-Na-Cl-HCO_3.

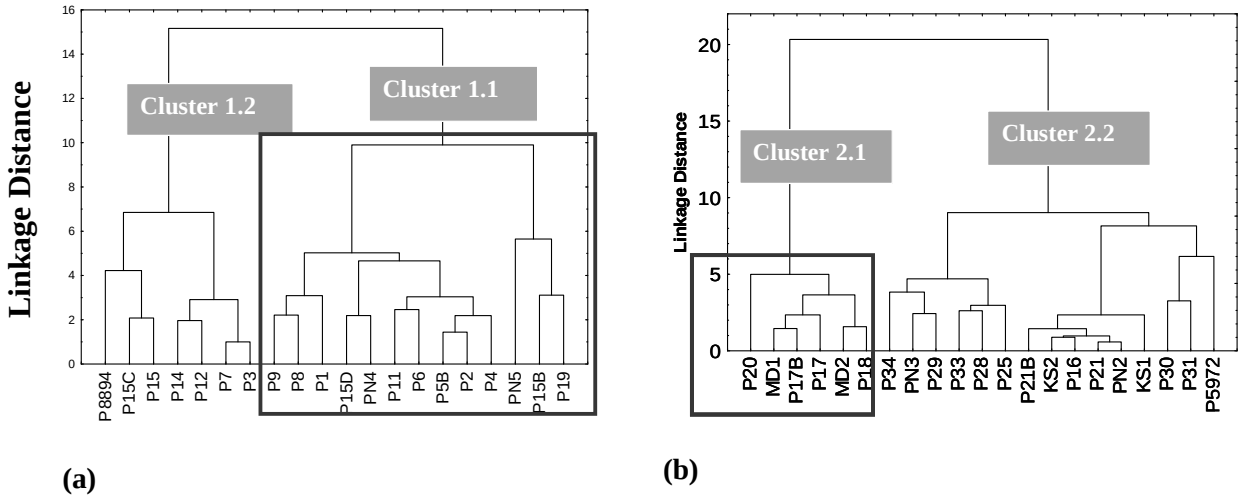

Fig. 6 Tree diagram from HCA in Q-Mode for (a) transect S1 (b) transect S2 for samples issued from the dry season (August 2006)

4.2.2 Spatial and temporal evolution

Fig. 7 presents spatio-temporal evolution of major ions in transect S1. It shows that the groundwater mineralization follows the flow path from the sea landwards. Indeed, concentrations decrease from the sea towards the internal areas. Wells located along 4 km from the sea present all high concentrations with regard to all major ions. Furthermore, the piezometric depression cone is located at about four kilometres from the shoreline, thus it is possible that seawater is influencing the groundwater's composition even at that important distance.

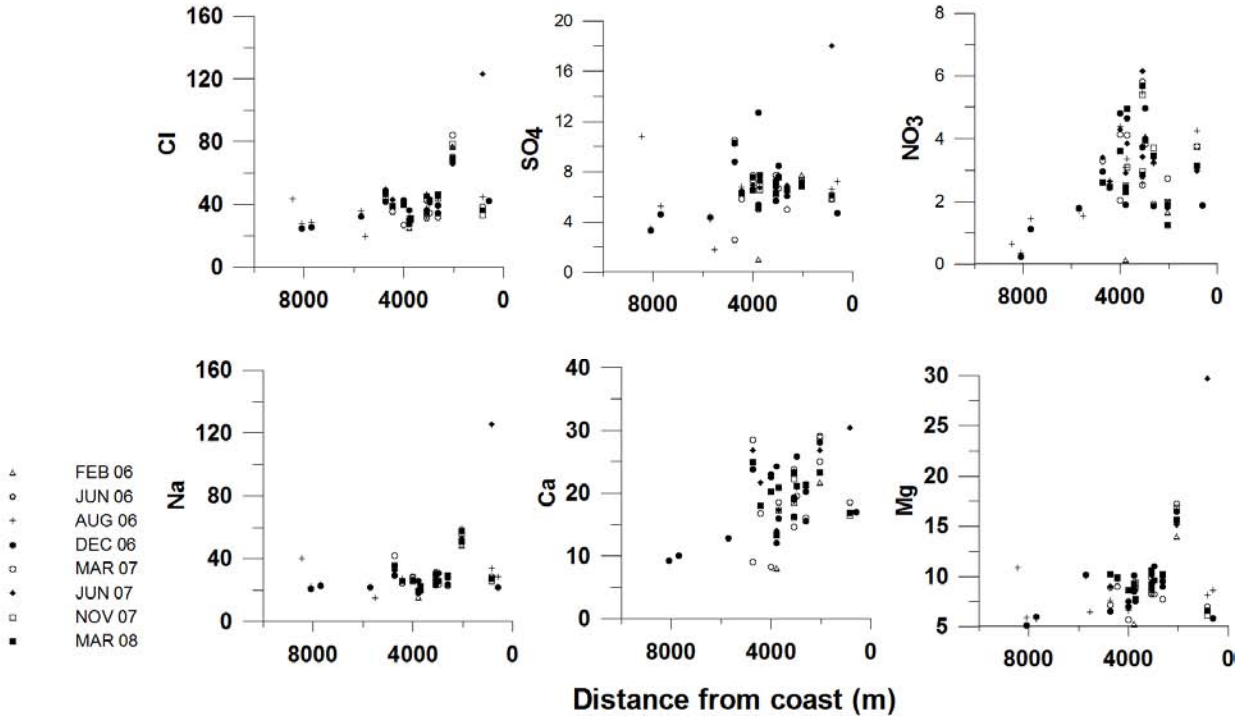

Fig. 7 Time and spatial evolution of Major elements (Na, Ca, Mg, Cl, SO4 and NO3) along transect S1. Concentrations are expressed in meq/L and distance in meters

To study the temporal trend, we have taken as an example PN5 well as it is equipped with an automatic data logger (Fig. 8). We notice that significant temporal variations are only visible for chloride, sodium and HCO_3. Inversely, Mg, SO_4, NO_3 and Ca show a constant trend. As chloride and sodium are mostly associated with seawater intrusion and HCO_3 to natural recharge, it is possible that these trends express the annual fluctuation of salinity controlled by the regional flow. Groundwater enrichment through irrigation return flow associated with nitrate and SO_4 is possibly a long term process. This analysis

should be confirmed, firstly, by applying statistical trend tools such as seasonal Mann-Kendall test (Gibbons et al., 2009) and, secondly, by using a longer time series.

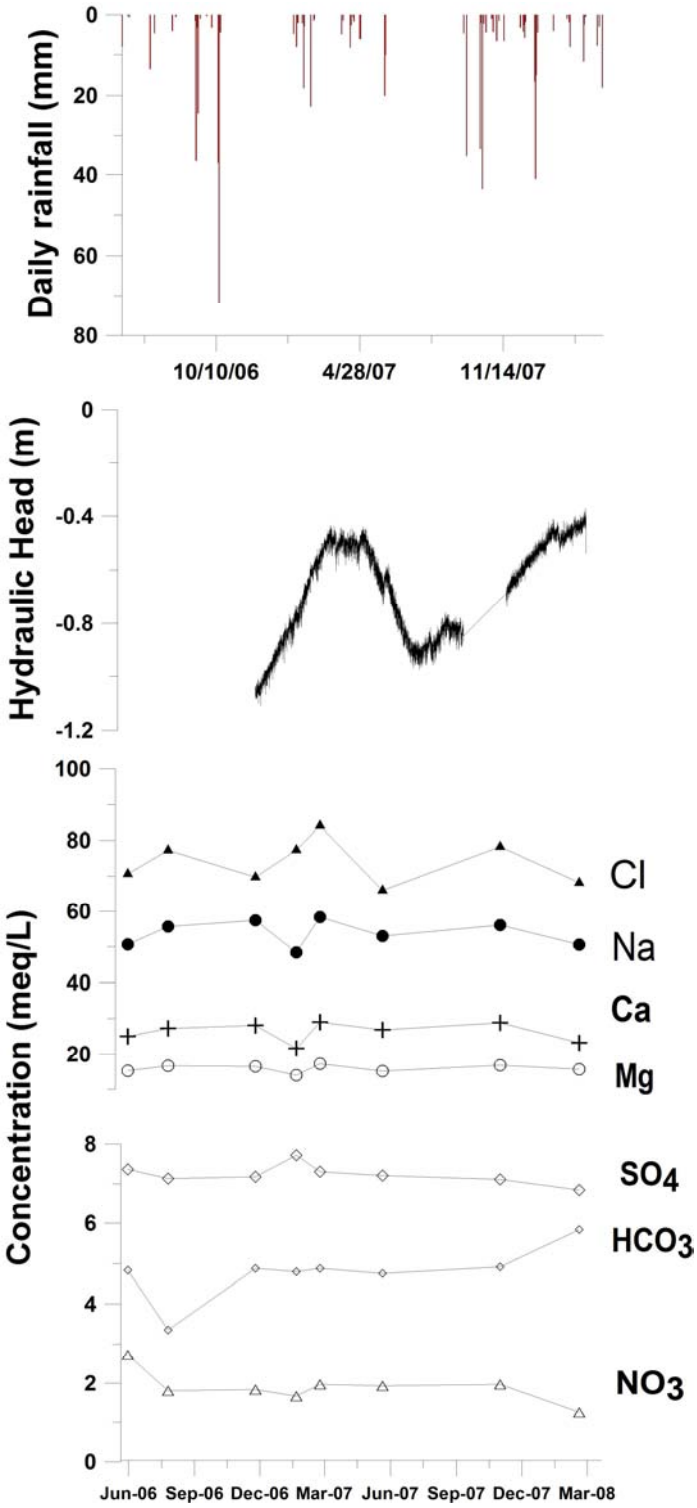

Fig. 8 Time evolution of major ions, nitrate and hydraulic heads measured in PN5. Rainfall is measured in Oued Souhil climatic station.

4.2.3 Ionic ratios and PCA analysis

Seawater is characterized by the following specific molar ionic ratios: Na/Cl=0.86, SO_4/Cl=0.05, Br/Cl=0.0015, Ca/(HCO_3+SO_4)=0.34 and Mg/Ca=5.2 (Vengosh and Rosenthal, 1994).

The mean average of the molar ratio Na/Cl was 0.72 and 0.9 for respectively S1 and S2. Both values are different from the seawater ratio. However ratio values (especially that in transect S1) are below the dissolution ratio of halite (=1), suggesting a marine influence (De Montety et al., 2008). The other calculated molar ratios are different from those characterizing seawater: mean Mg/Ca=(0.53 for S1 and 0.64 for S2), mean SO4/Cl=(0.17 for S1 and 0.26 for S2) and mean Ca/(HCO_3+SO_4)=(1.73 for S1 and 1.17 for S2). Besides the mean Br/Cl molar ratio, calculated for 11 wells in transect S1 for the dry season was about 3.5 10^{-3}. The outcome of this analysis is that ionic ratios method is not suitable for all case studies, mainly because the mixing of freshwater with seawater is not a conservative process. Ben Hamouda (2009) used the ionic ratios to assess seawater intrusion at a larger scale in the Korba coastal aquifer and came to the same conclusion. Hence, this method has to be compared to other identification techniques.

PCA analysis, applied to both transects, show that data is mainly explained by two principal component factor (Tab. 1) accounting for 74.3 % and 72.8 % of the cumulative variance for respectively S1 and S2. Factor loadings evaluation differs according to the author. Koh et al. (2007) (Koh et al., 2007) defines a high loading as greater than 0.75, and a moderate loading as ranging between 0.40 and 0.75. Thus, loadings of less than 0.4 are considered insignificant. Factors description is discussed in the following section:

- The first factor F1 accounts for 56.3 and 56.9 % of the total variance for respectively S1 and S2. It is contributed by the following variables: EC, Cl, Na, Mg, Ca and SO4, as their loadings are higher than 0.77 for both transects (Tab. 2). This group of variables is often associated, in the literature, to the seawater intrusion process (Koh et al., 2007; Trabelsi et al., 2007).

Tab. 1 Eigenvalues of correlation matrix and cumulative total variance

	Factor	Eigenvalue	Tot. Var. (%)	Cum-Eigenvalue	Cum. Tot.Var. (%)
S1	**1**	5.07	56.29	5.07	56.29
	2	1.62	18.04	6.69	74.33
	3	1.02	11.37	7.71	85.69
	4	0.60	6.64	8.31	92.33
	5	0.29	3.28	8.60	95.61
	6	0.25	2.75	8.85	98.36
	7	0.08	0.90	8.93	99.26
	8	0.05	0.61	8.99	99.86
	9	0.01	0.14	9.00	100.00
	Factor	**Eigenvalue**	**Tot. Var. (%)**	**Cum-Eigenvalue**	**Cum. Tot.Var. (%)**
S2	**1**	5.13	56.98	5.13	56.98
	2	1.42	15.78	6.55	72.76
	3	0.99	11.01	7.54	83.77
	4	0.73	8.16	8.27	91.93
	5	0.49	5.48	8.77	97.40
	6	0.18	1.97	8.94	99.37
	7	0.05	0.51	8.99	99.88
	8	0.01	0.07	9.00	99.95
	9	0.00	0.05	9.00	100.00

- The second factor F2 explains 18.04 % and 15.78 % of the total variance for respectively S1 and S2. Nitrate loading is respectively 0.59 for S1 and 0.57 for S2. Potassium loading is equal to 0.82 for S2 and -0.77 for S1. Grassi et al. (2007) state that potassium, nitrate and sulphate are associated to N-fertilizers. They also found a positive correlation between nitrate and potassium. Therefore, Factor F2 is related to agricultural contamination.

The fourth factor F4, issued from PCA applied to S1, and accounting for 6.64 % of the total variance, presents a moderate loading for HCO_3. Thus, it can be associated to natural recharge by rainwater (Trabelsi et al., 2007).

To analyse the factor scores for different wells, we have performed the biplot of variables and samples (Fig. 9). For transect S1, we can distinguish three groups of wells plotting respectively on F1, F2 and F4. In addition, we have plotted the spatial distribution of factors along each transect in the purpose of assessing the relationship between hydrodynamic flows and geochemical processes (Fig. 10). The spatial distribution of factor scores for F1, F2 and F3 shows that seawater intrusion, associated to F1, is contributing to the chemistry of most of the wells located along 4000 m from the shoreline. Beyond this limit, seawater does not seem to have an influence on the groundwater composition. An exception is made for the well P15B, located at about 8500 m from the shoreline, which presents a high score for F1. This well is probably a singular case that is affected by fossil seawater. In transect S2,

factor F1 presents high score along 1500 m from the shoreline. This distance marks the seawater influence limit in transect S2. Even though groundwater flows seaward a mixing process between seawater and freshwater is possible.

Tab. 2 Factor loadings for variables. Moderate to strong loadings are highlighted in grey

	Variable	Factor 1	Factor 2	Factor 3	Factor 4
S1	**Ec**	0.91	-0.25	-0.11	0.12
	Ca	0.88	0.30	-0.27	0.06
	Mg	0.83	-0.31	0.02	-0.11
	Na	0.91	-0.31	0.18	-0.05
	K	-0.12	-0.77	-0.52	-0.18
	HCO_3	-0.55	-0.52	-0.15	0.61
	Cl	0.96	-0.20	-0.01	-0.04
	SO_4	0.77	0.16	0.33	0.37
	NO_3	0.34	0.59	-0.70	0.13
	Variable	**Factor 1**	**Factor 2**	**Factor 3**	**Factor 4**
S2	**Ec**	0.98	-0.03	0.01	-0.13
	Ca	0.78	0.21	-0.03	0.11
	Mg	0.94	-0.06	-0.23	-0.07
	Na	0.95	-0.11	0.06	-0.19
	K	-0.02	0.82	0.16	-0.52
	HCO3	-0.31	-0.58	-0.52	-0.52
	Cl	0.98	0.01	0.10	-0.11
	SO4	0.84	-0.18	-0.08	0.26
	NO3	0.02	0.57	-0.79	0.20

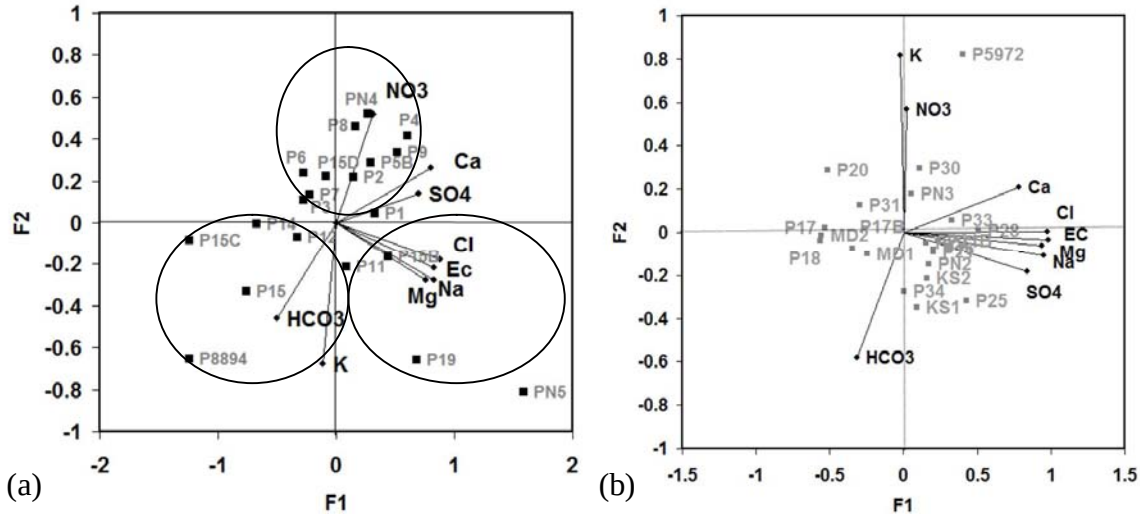

Fig. 9. Biplot of variable loadings and sample scores for F1vs F2, (a) S1 and (b) S2

The impact area of factor F2, related to the agricultural contamination, begins at 2000 m and 1500 m from the shoreline in respectively transect S1 and transect S2. This result can be explained by the fact that samples mixed with seawater have a low concentration of nitrate. Indeed, seawater usually does not contain nitrate. PN4

(located at about 600 m from the shoreline in transect S1) is the only well presenting a high score for F2. The water table is at only 3.5 m below soil level, which is favourable to nitrate enrichment. Besides, groundwater at this well is likely to be a fresh water lens lying on salt water. Note that most of the wells, in both transects, present a high score for factor F2, which demonstrates the important contribution of agricultural pollution in the groundwater's composition. Factor F4, explaining natural recharge, has a very limited area of impact mainly located in transect S1 in the internal areas at more than 4000 m.

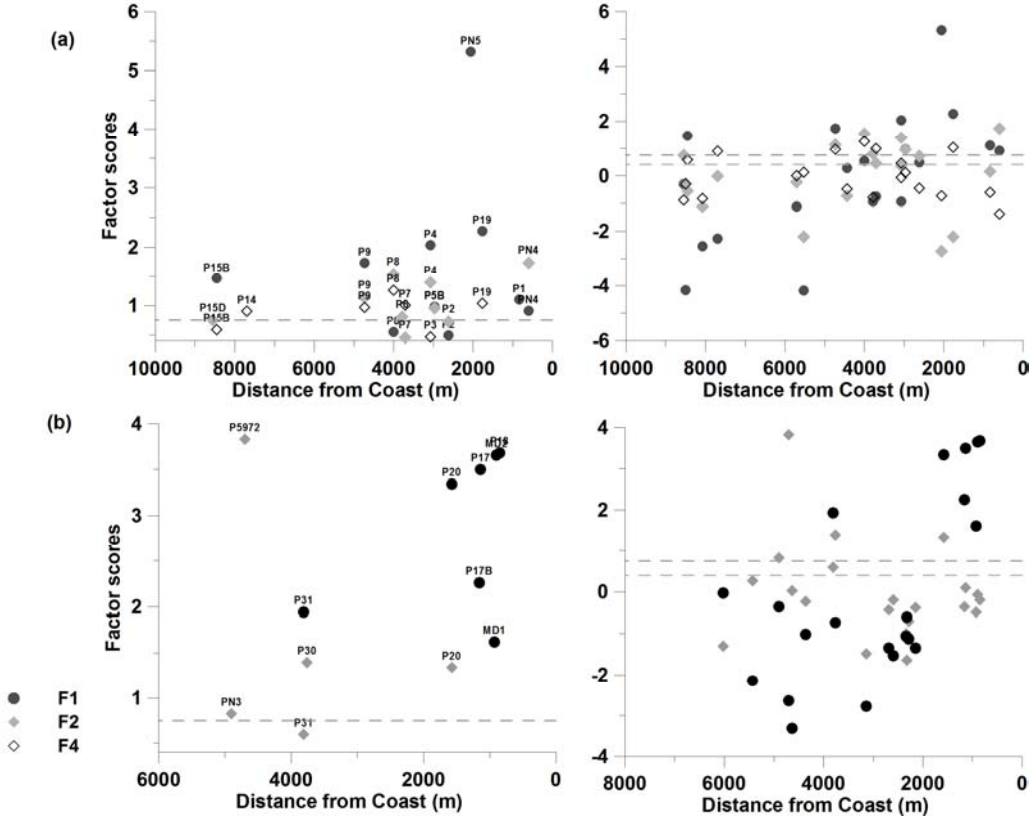

Fig. 10 Spatial distribution of F1, F2 and F4 factor scores for (a) transect S1 and (b) transect S2. Limits for appreciating the significant loadings (0.4-0.75) are dashed in grey.

4.2.4 Oil field Brine contamination

Oil field brine or deep-basin contamination occurs due to natural subsurface migration through faults (Richter and Kreitler, 1991) or during the production of oil and gas (Otton, 2006). In the Cap Bon peninsula, onshore and offshore petroleum wells have been in exploitation since 1949. Hounslow (1995) proposes a rectangular diagram with the molar

ratios Na/(Na+Cl) and Ca/(Ca+SO_4) as respectively the X axis and the Y axis. This diagram is used to differentiate the origin of groundwater contamination among oil field brine, evaporites seawater and alkali lakes. Samples collected in august 2006 for both transects as well as samples resulting from the campaign performed in 1964 were reported separately in this diagram. Fig. 11 shows that an important number of wells plot in the oil field brine triangle.

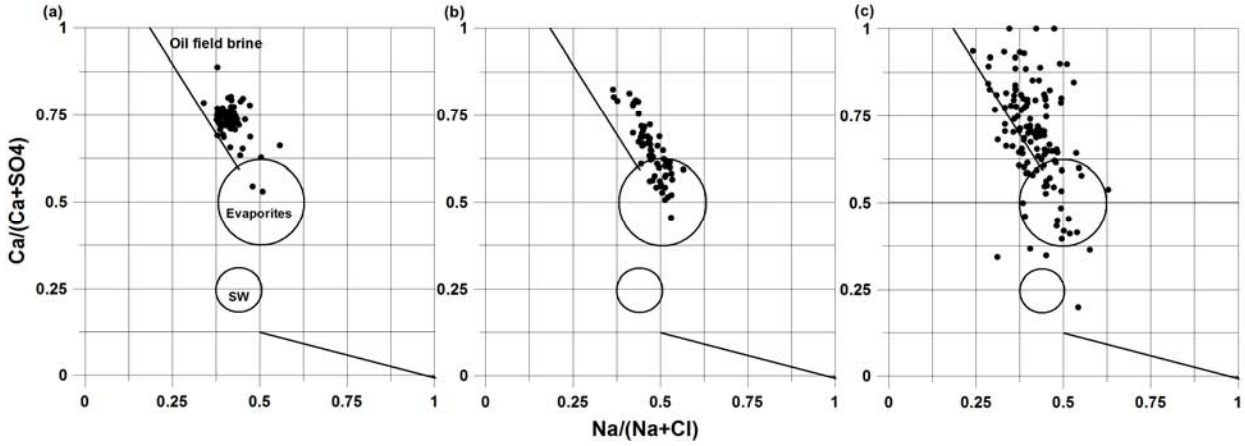

Fig. 11 Hounslow diagram for brine contaminated water differentiation for (a) S1 all samples (b) S2 all samples (c) All samples issued from 1964 database.

Moreover, the average molar ratio Br/Cl measured for 11 samples in transect S1 is about 3.5 10^{-3} (twice the marine ratio) which represents another indicator of oil field brine contamination (Richter and Kreitler, 1991). The high salinities reported, since the sixties, in the internal areas located at more than 6 km from the shoreline (Fig.2) could then partially originate from natural oil field brine migration.

4.3. Seawater intrusion processes

Studying hydrochemical processes accompanying the conservative mixing of seawater and freshwater is interesting for the assessment of the seawater intrusion. In the next chapter we are thoroughly analysing these questions. In each transect, we have isolated a group of wells likely to be affected by seawater intrusion. Seawater fractions and ionic deltas were calculated. Besides, modelling of the mixing between two end members, fresh-brackish water and seawater, was performed using PHREEQC (Parkhurst, 1995). The outcome of this study was that cation exchange processes (Fig. 12) are actively taking place along the two flow paths (transect S1 and transect S2). Besides we have

noticed an excess of Ca in both transects that can be explained by a combination of gypsum leaching and dedolomitization. The study also showed that redox processes are contributing to groundwater composition.

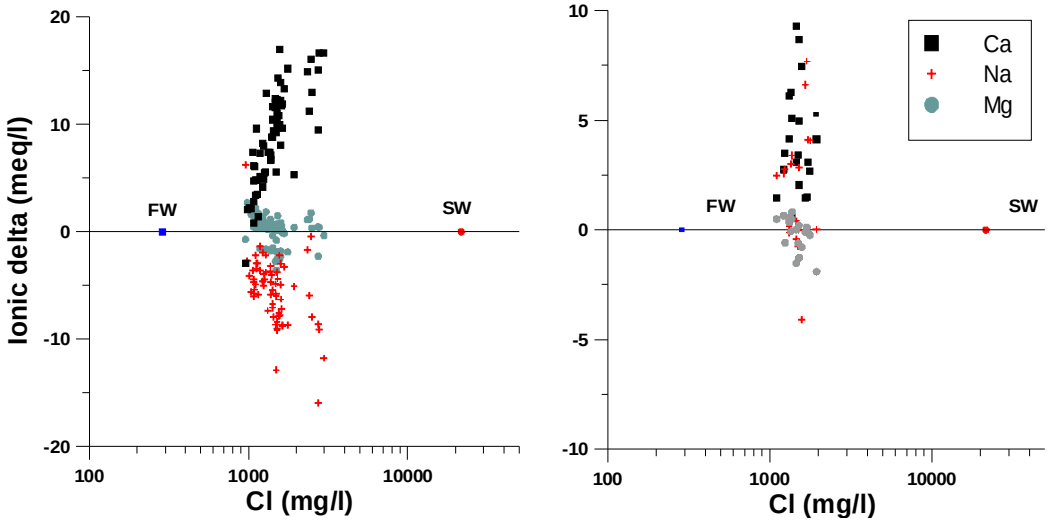

Fig. 12 Ionic deltas of Ca, Na and Mg versus Chloride for both Transects (Calculated for all campaigns)

4.4. Nitrate as a fingerprint of agricultural and irrigation-induced salinization

Most of the sampled wells, in both transects S1 and S2, present high concentrations of nitrate, ranging between 15 and 381 mg/L. The average concentration of all measured samples is about 185 mg/L and 93% and 100 % of the samples, respectively in transect S1 and transect S2, present a concentration exceeding the drinking water limit of 50 mg/L. This situation reflects the groundwater's contamination expansion due to agricultural residual products, mainly N-fertilizers. The high measured molar ratios of Br/Cl ($3.5\ 10^{-3}$) is also an indicator of agricultural substances contamination. Indeed, methyl bromide has been widely used, for a long time, as a pesticide in cultivated areas (Andreasen and Fleck, 1997; Ghabayen et al., 2006). Grassi et al. (2007) reported that nitrate concentrations are correlated to rainfall and the unsaturated zone thickness. Fig. 13 depicts nitrate concentrations of all measured samples vs. depth below soil level. It is evident that the upper horizons show the highest recorded concentrations (>370 mg/L at a depth of 6.5 m) and inversely samples measured at about 30 m deep presented lower concentrations (70 mg/L). However even samples taken at more than 20 m below soil

level presented high concentrations (308 mg/L at a depth of 22.5 m). Hence, it is probable that nitrates are transferred vertically towards groundwater.

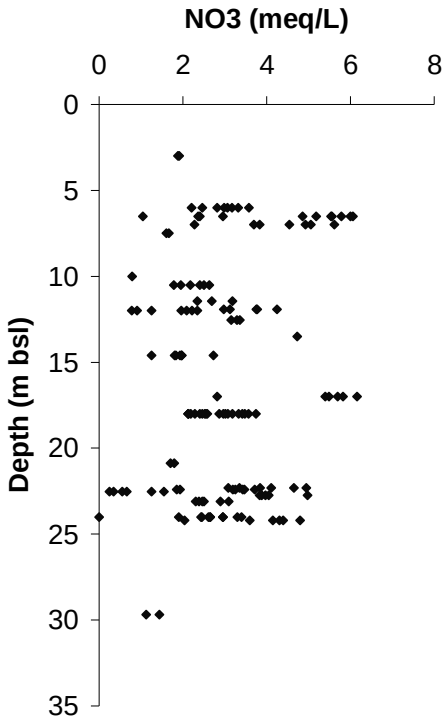

Fig. 13 Nitrate concentrations vs. the thickness of the vadose zone in S1 and S2

Fig. 14 shows the evolution of nitrate concentrations in wells PN5, P1, P11, P2 and P3 over the period from June 2006 to March 2008. We have plotted daily rainfall, to study possible correlations between precipitations and groundwater concentrations. The observation well P2 showed a decrease in concentration in the wet season, probably due to a dilution effect under natural recharge. Apart from this well, no trend at this scale of time was observed. Grassi et al. (2007) observed positive correlations between nitrate concentrations and rainfall at the beginning of the autumn. However, they used a larger time series (over 6 years) and filtered their data on the basis of the vadose zone thickness.

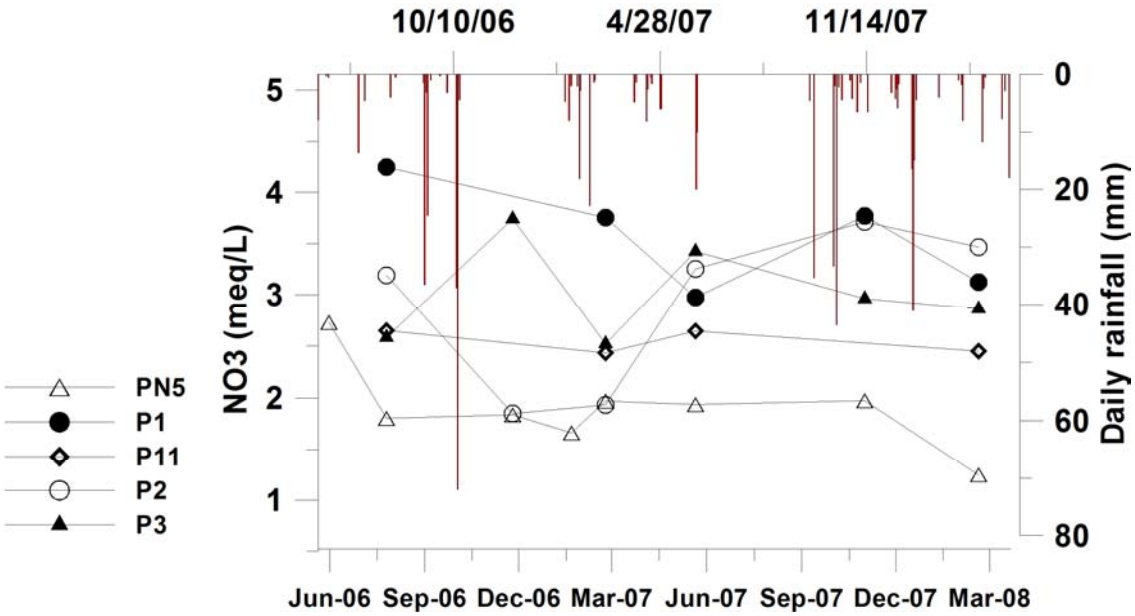

Fig. 14 Nitrate concentrations measured for wells P1, P2, P3, P11 and PN5 in transect S1 vs. rainfall measured in Oued Souhil climatic station

It is interesting to notice that nitrate plotted vs. seawater fraction (calculations are presented in the next chapter) revealed that, in general, samples mixed with seawater, at a ratio above 10%, are less concentrated with regards to nitrate (Fig. 15). Kim at al. (2004) observed the same trends in the coastal region of Kunsan (Korea), known to have complex contaminant sources. In the case of nitrate contaminated aquifers, the ratio NO_3/Cl can be used as an indicator to identify seawater intrusion.

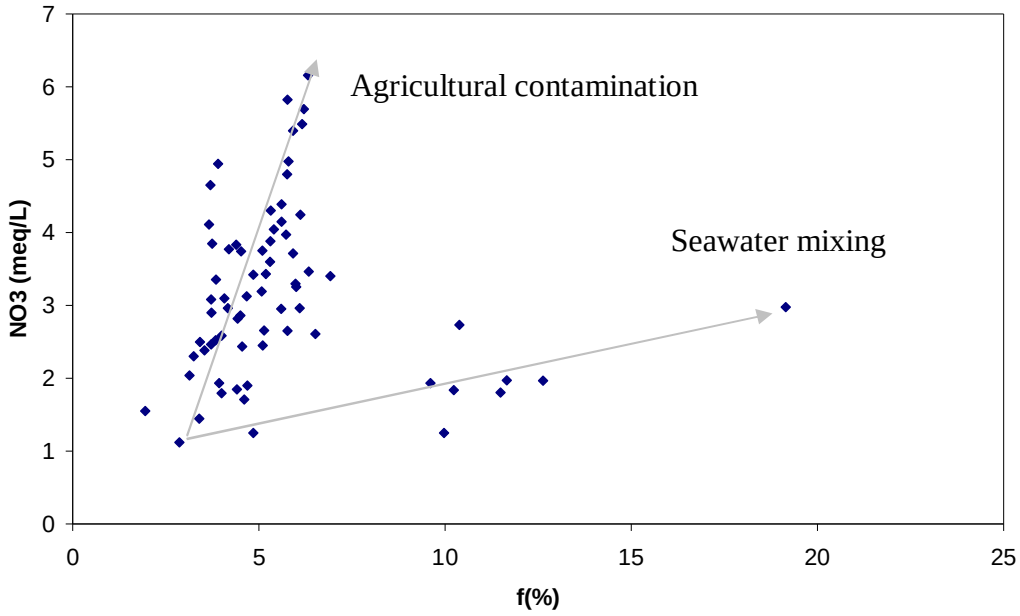

Fig. 15 Nitrate concentrations vs. seawater fraction for all measured samples in transects S1 and S2

5. Conclusion

A variety of techniques were combined to study the salinization origins and processes in Korba coastal irrigated plain. Those techniques comprised geochemical investigations and modelling using PHREEQC, hydrodynamic monitoring and plotting, electrical tomography imaging and multivariate statistics analysis applied to hydrochemical variables. Surveys that were applied confirm the complexity and superposition of various processes contributing to groundwater composition. The hydrodynamic survey confirmed the observation of a high piezometric depression cone located at about 4000 m in transect S1, where the hydraulic head is estimated to -5m. Inversely, groundwater flows seaward in transect S2. The continuous records of the hydraulic heads, in three observation wells located along transect S1, revealed that groundwater levels were linked to natural recharge in the wet season and to the pumping in the dry season. The immediate groundwater recharge through irrigation return flow is not observed even in PN4 where the groundwater is at only 3.5 m below the soil level. The ERT imaging survey showed that the seawater/freshwater interface is not far below the soil level in two observed profiles T1 and T2 located respectively at 600 and 1200 m from the shoreline. Resistivities considerably decreased at depths of 6 and 40 m below the soil level for respectively T1 and T2 indicating that the soil has been saturated by salty water.

The study of the most common ionic ratios, characterizing seawater intrusion, was not concluding, except the Na/Cl ratio which clearly suggested a marine influence.

HCA analysis was a useful tool for grouping wells and isolating those which are potentially affected by seawater mixing process. The Hounslow diagram applied to samples, issued from the study presented herein and those collected in 1963 before the seawater intrusion expansion, suggests that natural oil field brine contamination could be considered as a source of salinity.

PCA showed that the groundwater chemistry is mainly affected by two factors F1 and F2. The first factor F1 was related to seawater intrusion, whereas the second one F2 was linked to agricultural contamination through N-fertilizers.

The spatial distribution of factors was useful to delineate the area of impact of each factor. Geochemical processes zoning was estimated and was correlated to the flow paths. According to PCA results, seawater strongly contributes to groundwater chemistry along 4000 m from the shoreline in transect S1. The seawater intrusion penetration length

can be estimated to 4000 m in transect S1. PCA also revealed that agricultural contamination was controlling the groundwater composition in internal areas.

The loading of nitrate toward groundwater seems to be a long term process. The study suggests that nitrate and other agricultural residual substances are leached by the rainfall from the upper soil layers. The soil quality survey will be presented in chapter 4 and the study of the processes occurring at the seawater/freshwater will be discussed in the following chapter.

References

Andersen, M.S., Nyvang, V., Jakobsen, R. and Postma, D., 2005. Geochemical processes and solute transport at the seawater/freshwater interface of a sandy aquifer. Geochimica et Cosmochimica Acta 69(16): 3979-3994.

Andreasen, D.C. and Fleck, W.B., 1997. Use of Bromide:chloride ratios to differentiate potential sources of chloride in a shallow, unconfined aquifer affected by brackish-water intrusion. Hydrogeology journal, 5: 17-26.

Appelo, C.A.J. and Postma, D., 2005. Geochemistry, Groundwater and Pollution, second ed. Balkema, Rotterdam.

Ayers, R., S., and Westcot, D., W., 1994. Water quality for agriculture-FAO irrigation and drainage paper. FAO-Food and Agriculture Organization of the United Nations, Rome, Italy.

Barica, J., 1972. Salinization of groundwater in arid zones. Water Research, 6(8): 925-933.

Bear, J., Cheng, A.H.D., Sorek, S., Ouazar, D. and Herrera , I., 1999. Seawater Intrusion in Coastal Aquifers - Concepts, Methods and Practices. Kluwer Academic Publishers, Dordrecht.

Ben Hamouda, M.F., Leduc, C., Tarhouni, J. and Zouari, K., 2009. Origine de la minéralisation dans l'aquifère plio-quaternaire de la côte orientale du cap Bon (Tunisie). Sècheresse, 20 (1): 78-86.

Ben Moussa, A., Zouari, K. and Oueslati, N., 2008. Geochemical study of groundwater mineralization in the Grombalia shallow aquifer, north-eastern Tunisia: implication of irrigation and industrial waste water accounting. Environmental Geology.

Bouhlila, R. and Laabidi, E., 2008. Impacts of calcite dissolution on seawater intrusion processes in coastal aquifers: Density dependent flow and multi species reactive transport modeling. Calibration and Reliability in Groundwater Modelling Credibility of Modelling. IAHS Publications, 320: 220-225.

Cardona, A., Carrillo-Rivera, J., Huizar-Alvarez, R. and Garniel-Castro, E., 2004. Salinization in coastal aquifers of arid zones: an example from Santo Domingo, Baja California Sur, Mexico. Environmental Geology, 45: 350-366.

De Franco, R., G. Biella, L. Tosi, Teatini, P., Lozej, A., B. Chiozzotto, M. Giada, F. Rizzetto, C. Claude, A. Mayer , Bassan, V. and Gasparetto-Stori, G., 2009. Monitoring the saltwater intrusion by time lapse electrical resistivity tomography: The Chioggia test site (Venice Lagoon, Italy). Applied Geophysics, doi:10.1016/j.jappgeo.2009.08.004.

D.G.R.E, 1964. Etude hydrogeologique de la nappe de Korba, Direction Générale des Ressources en Eau, Tunis, Tunisia.

De Montety, V., Olivier, R., Christine, V.-C., Bernard, B., Daniel, H. and Vincent, V., 2008. Origin of groundwater salinity and hydrogeochemical processes in a confined coastal aquifer: Case of the Rhône delta (Southern France). Applied Geochemistry, 23: 2337–2349.

FAO, 1997. Seawater intrusion in coastal aquifers, guidelines for study, monitoring and control. Water Reports no. 11. FAO Land and Water Development Div., Rome, Italy, 161 pp.

Geotomo Software, 2010. RES2DINV ver. 3.59 for Windows XP/Vista/7, Rapid 2-D Resistivity & IP inversion using the least-squares method.http://www.geoelectrical.com/downloads.php.

Ghabayen, S.M.S., McKee, M. and Kemblowski, M., 2006. Ionic and isotopic ratios for identification of salinity sources and missing data in the Gaza aquifer. Journal of Hydrology, 318: 360-373.

Gibbons, R.D., Bhaumik, D. and Aryal, S., 2009. Statistical Methods for Groundwater Monitoring, Second Edition. John Wiley & Sons, 374 pp.

Gomis-Yagües, V., Boluda-Botella, N. and Ruiz-Bevia´, F., 2000. Gypsum precipitation/dissolution as an explanation of the decrease of sulphate concentration during seawater intrusion. Journal of Hydrology, 228: 48–55.

Grassi, S., Cortecci, G. and Squarci, P., 2007. Groundwater resource degradation in coastal plains: The example of the Cecina area (Tuscany - Central Italy). Applied geochemistry, 22: 2273-2289.

Hounslow, A., 1995. Water quality data: analysis and interpretation. Lewis Publishers, 397 pp.

Hsissou, J., Mudry, J., Mania, J., Bouchaou, L. and Chauve, P., 1999. Utilisation de rapport Br/Cl pour déterminer l'origine de la salinité des eaux souterraines : exemple de la plaine du Souss (Maroc). C.R. Acad. Sci. Paris, Sciences de la terre et des planètes, 328: 381-386.

Hussain, M., Ahmed, S.M. and Abderrahman, W., 2008. Cluster analysis and quality assessment of logged water at an irrigation project, eastern Saudi Arabia. Journal of Environmental Management, 86: 297-307.

Hussein, M.T., 2003. Hydrochemical evaluation of groundwater in the Blue Nile Basin, eastern Sudan, using conventional and multivariate techniques. hydrogeology journal, 12 144-158.

Kerrou, J., Renard, P. and Tarhouni, J., 2010. Status of the Korba groundwater resources (Tunisia): observations and three-dimensional modelling of seawater intrusion. Hydrogeology Journal, DOI 10.1007/s10040-010-0573-5.

Kim, K., Rajmohan, N., Kim, H.J., Hwang, G.-S. and Cho, M.J., 2004. Assessment of groundwater chemistry in a coastal region (Kunsan, Korea) having complex contaminant sources: a stoichiometric approach. Environmental Geology 46: 763-774.

Koh, D.-C., Ko, K.-S., Kim, Y., Lee, S.-G. and Chang, H.-W., 2007. Effect of agricultural land use on the chemistry of groundwater from basaltic aquifers, Jeju Island, South Korea. Hydrogeology journal, 15: 727–743.

Kumar, M., Kumari, K., Singh, U.K. and Ramanathan, A., 2009. Hydrogeochemical processes in the groundwater environment of Muktsar, Punjab: conventional graphical and multivariate statistical approach. Environmental Geology, 57: 873-884.

LECCA et al., 1999. A modular approach to the Korba aquifer sea-water intrusion study, 2, Simulation, data manipulation, and visualization for the 3D model. Natuur-en Geneeskundige Vennootschap, Gand, BELGIQUE, 309 pp.

Leduc, C. et al., 2007. Impacts of hydrological changes in the Mediterranean zone: environmental modifications and rural development in the Merguellil catchment, central Tunisia Hydrological Sciences Journal, 52(6): 1162 - 1178.

Martínez, J., Benavente, J., García-Aróstegui, J.L., Hidalgo, M.C. and Rey, J., 2009. Contribution of electrical resistivity tomography to the study of detrital aquifers affected by seawater intrusion-extrusion effects: The river Vélez delta (Vélez-Málaga, southern Spain). Engineering Geology, 108(3-4): 161-168.

Melloul, A. and Collin, M., 1992. The 'principal components' statistical method as a complementary approach to geochemical methods in water quality factor identification; application to the Coastal Plain aquifer of Israel. Journal of Hydrology, 140 49-73.

Milnes, E. and Renard, P., 2004. The problem of salt recycling and seawater intrusion in coastal irrigated plains: an example from the Kiti aquifer (Southern Cyprus). Journal of Hydrology, 288: 327-343.

Morell, I., Gimhez, E. and Esteller, M.V., 1996. Application of principal components analysis to the study of salinization on the Castellon Plain (Spain). The Science of the Total Environment 177: 161-171.

Otton, J.K., 2006. Environmental Aspects of Produced-water Salt Releases in Onshore and Coastal Petroleum-producing Areas of the Conterminous U.S. - A Bibliography U.S. Geological Survey

Paniconi, C., Khalifi, I., Lecca, G., Giacomelli, A. and Tarhouni, J., 2001. Modeling and analysis of seawater intrusion in the coastal aquifer of Eastern Cap-Bon, Tunisia. Transport in Porous Media, 43: 3-28.

Papatheodorou, G., Lambrakis, N. and Panagopoulos, G., 2007. Application of multivariate statistical procedures to the hydrochemical study of a coastal aquifer: an example from Crete, Greece. Hydrological Processes, 21(11): 1482-1495.

Parkhurst, D., 1995. User's guide to PHREEQC: a computer program for speciation, rreaction-path, advective-transport and inverse geochemical calculations, US Geol Surv Water-Res.

Post, E.A., 2004. Groundwater salinization processes in the coastal area of the Netherlands due to transgressions during the Holocene, VRIJE UNIVERSITEIT, Amsterdam, 137 pp.

Pulido-Leboeuf, P., Pulido-Bosch, A., Calvache, A.V., M.-L. and Andreu, J.-M., 2003. Strontium, SO42−/Cl- and Mg2+/Ca2+ ratios as tracers for the evolution of seawater into coastal aquifers: the example of Castell de Ferro Aquifer (SE Spain). C.R. Acad. Sci. Paris, Sciences de la Terre et des Planètes, 335 1039-1048.

Richter, B.C. and Kreitler, C.W., 1991. Identification of sources of ground-water salinization using geochemical techniques: , U.S. Environmental Protection Agency, Okalahoma.

Slama, F., Bahri, A., Bouarfa, S., Chaumont, C. and Bouhlila R., 2004. Pratiques d'irrigation et rôle du drainage pour le contrôle de la salinité -cas du périmètre irrigué Kalaât Landelous en Tunisie, Projet européen Inco-Wademed sur la "Modernisation de l'agriculture irriguée dans les pays du Maghreb", Rabat.

Smedema, L., K., and Shiati, K., 2002. Irrigation and salinity: a perspective review of the salinity hazards of irrigation development in the arid zone. Irrigation and Drainage Systems, 16: 161-174.

Trabelsi, R., Zairi, M. and Dhia, H.B., 2007. Groundwater salinization of the Sfax superficial

aquifer, Tunisia. Hydrogeology journal, 15: 1341-1355.

Vengosh, A. and Benzvi, A., 1994. Formation of a salt plume in the coastal-plain aquifer of Israel- The Beer-Toviyya Region. Journal of Hydrology, 160((1-4)): 21-52.

Vengosh, A. and Rosenthal, E., 1994. Saline groundwater in Israel: its bearing on the water crisis in the country. Journal of Hydrology. 156: 389-430.

WHO, 2008. Guidelines for drinking-water quality, third edition, incorporating first and second addenda. WHO-World Health Organization, 515 pp.

Yakirevich, A., Melloul, A., Sorek, S., Shaath, S. and Borisov, V., 1998. Simulation of seawater intrusion into the Khan Yunis area of the Gaza Strip coastal aquifer. Hydrogeology journal, 6: 549–559.

Yaouti, F.E., Mandour, A.E., Khattach, D., Benavente, J. and Kaufmann, O., 2009. Salinization processes in the unconfined aquifer of Bou-Areg (NE Morocco): A geostatistical, geochemical, and tomographic study. Applied geochemistry, 24 16-31.

Chapter 3. Hydrochemical processes accompanying seawater-freshwater mixing as indicators of seawater intrusion evolution: Case of Korba coastal aquifer Tunisia[1]

Abstract

Groundwater sampling and piezometric measurements were carried out along two flow paths (corresponding to two transects) in Korba coastal plain (North east of Tunisia). The study aims to identify hydrochemical processes occurring when seawater and freshwater mix. Those processes can be used as indicators of seawater intrusion progression. Seawater fractions in the groundwater were calculated using the chloride concentration. Hierarchical cluster analysis (HCA) was applied to isolate wells potentially affected by seawater. In addition, PHREEQC was used to simulate the theoretical mixing between two end members: seawater and a fresh-brackish groundwater sample. Geochemical conventional diagrams showed that the groundwater chemistry is explained by a mixing process between two end members. Results also revealed the presence of other geochemical processes, correlated to the hydrodynamic flow paths. Direct cation exchange was linked to seawater intrusion, and reverse cation exchange was associated to the freshwater flushing into seawater. The presence of these processes indicated that seawater intrusion was in progress. An excess of Ca, that could not be explained by only cation exchange processes, was observed in both transects. Dedolomitization combined to gypsum leaching is the possible explanation of the groundwater Ca enrichment. Finally, redox processes were also found to contribute to the groundwater composition along flow paths.

[1] Partially presented at the SWIM 21 - 21st Salt Water Intrusion Meeting Azores 2010.
Submitted to Environmental earth sciences

1. Introduction

Coastal aquifers are vulnerable to seawater intrusion leading to groundwater salinization. This phenomenon is worsened by heavy pumping which is a result of agricultural expansion. Indeed, seawater and fresh groundwater are naturally and hydraulically connected through an interface. Fresh water, which is less dense than seawater, floats on top. The boundary between salt water and fresh water can be an abrupt one called sharp interface (Meadows et al., 2004). In other situations, the transition zone is not distinct, and it is brackish with salt water and fresh water mixing. Heavy pumping makes large amounts of fresh water to be withdrawn leading seawater to intrude fresh groundwater. The interface is thus displaced landward. Moreover, in arid and semi arid regions the extracted water is not renewed through natural recharge. This is because of disturbance made in water budget and climate change (Ranjana et al., 2006).

The mixing of seawater within freshwater is well studied and is reported in several case and theoretical studies (e.g. Bear et al., 1999). However, most of these studies focus on the density driven flow and transport of miscible fluids (Andersen et al., 2005). The chemical reactions occurring in the seawater/freshwater interface and their relationship with the hydrodynamic processes are less reported in literature (e.g Andersen et al., 2005; Bouhlila and Laabidi, 2008; Jeen et al., 2001; Rezeia and Carrera, 2004).

The simple mixing of seawater and fresh groundwater is characterized by an increase of chloride concentration. Jones (1999) demonstrates that a ratio of 5% of seawater would induce a water with a chloride concentration exceeding 1000 mg/l.

The mixing process can easily be identified using trilinear plots (e.g Piper diagram) and bivariate plots of chloride versus major ions (Richter and Kreitler, 1991). In fact, the mixed solution will plot on the theoretical line joining the two end members. The simple mixing is, yet, usually accompanied by ion exchange (Appelo and Postma, 2005). Ion exchange reactions along a flow path are also identified as ion chromatographic processes (Beekman and Appelo, 1990; Lambrakis, 2006; Petalas and Lambrakis, 2005). The solid phase, mainly clay minerals, changes the sorbed calcium and part of the magnesium for sodium as follows (Andersen et al., 2005; Custodio and Bruggeman, 1987):

$$Na^{+} + \frac{1}{2}Ca \text{ - } X_2 \rightarrow Na\text{ - }X + \frac{1}{2}Ca^{2+}$$

$$\frac{1}{2}Mg^{2+} + Na\text{ - }X \rightarrow Na^{+} + \frac{1}{2}Mg\text{ - }X + Ca^{2+}$$

Where X is the soil exchanger. It is interesting to note that even in sandy aquifers, presenting low clay fractions, exchange processes still occur (Richter and Kreitler, 1991). An exchange between calcium and magnesium can also take place when seawater intrudes fresh water:

$$Mg^{2+} + Ca\text{-}X \rightarrow Mg\text{-}X + Ca^{2+}$$

In this situation the ratio Mg/Ca decreases. Calcite dissolution can also lead to a similar result (Rezeia and Carrera, 2004; Smart et al., 1988). Magaritz et al. (1980) state that the mixing zone between freshwater and seawater can form a favourable environment for recent formation of dolomites. Pulido (2004) found that dolomotization and dedolomitization act as major hydrochemical processes characterizing the groundwater salinization due to seawater intrusion. Besides carbonate equilibrium and ion exchange, redox reactions are considered as important processes governing the chemistry of the seawater/freshwater mix (Kim et al., 2003; Panteleit et al., 2010). Sulphate reduction is reported in several experimental and modelling studies (Andersen et al., 2005; De Montety et al., 2008; Gomis-Yagües et al., 2000). It results in general from bacterial activities. Gomis-Yagües et al. (2000) suggest that observed sulphate reduction during seawater intrusion can originate from gypsum precipitation. Custodio and Bruggeman (1987) explain that ionic exchange processes occur when seawater/freshwater interface is in movement or when salinization/desalinization state is in evolution. Hence, these processes can be used as indicators of the seawter intrusion progress (Jones, 1999; Sivan et al., 2003; Sivan et al., 2005).

The present study presents results of experimental investigations performed in the Korba coastal plain North-East Tunisia. This aquifer is encountering, since the seventies, seawater intrusion caused by over pumping for agricultural purposes. The objectives are to identify the relationship between hydrodynamic and geochemical processes along a flow path and to evaluate the evolution of seawater intrusion using geochemical methods.

2. Hydrogeological settings

Korba coastal aquifer is located in the north-eastern Cap-Bon peninsula of Tunisia (Fig. 16). The aquifer covers about 438 km² and it is constituted of two geological units (Ben Hamouda, 2009). The first unit was formed during the Pliocene and Quaternary ages by deposition of eroded products from the Djbel Sidi AbedErrahmen anticline and the Dakhla syncline. The Pliocene formation is sandstone with alternating marl units and having a mean thickness of 85m. The Quaternary alluvium is composed of detrital sediment (sand,

gravel, and silt) with thin clay lenses and has a thickness that varies between 20 m and 25 m. The second unit is constituted of a Miocene marl formation underlying the first unit (Paniconi et al., 2001) (Fig. 17). The hydraulic transmissivity ranges from 5.10^{-5} to 10^{-2} m^2/s.The climate in the studied area is semi-arid with Mediterranean influence. The annual mean precipitation is 450 mm while mean annual evapotranspiration is 1100 mm. the annual aerial recharge rate ranges between 8 and 10% Ennabli (1980). This aquifer is being intensively exploited, mainly for agricultural purposes, since the seventies. This situation caused groundwater level to decrease steadily leading to the creation of a wide depression between Diar El Hojjej and Tafelloun villages where the measured hydraulic head reached 12 m under the mean sea level in 2004 (Kerrou et al., 2006). Besides piezometric depression, groundwater salinity has been increasing since the seventies (Fig. 2). It reaches in some regions 15g/L.

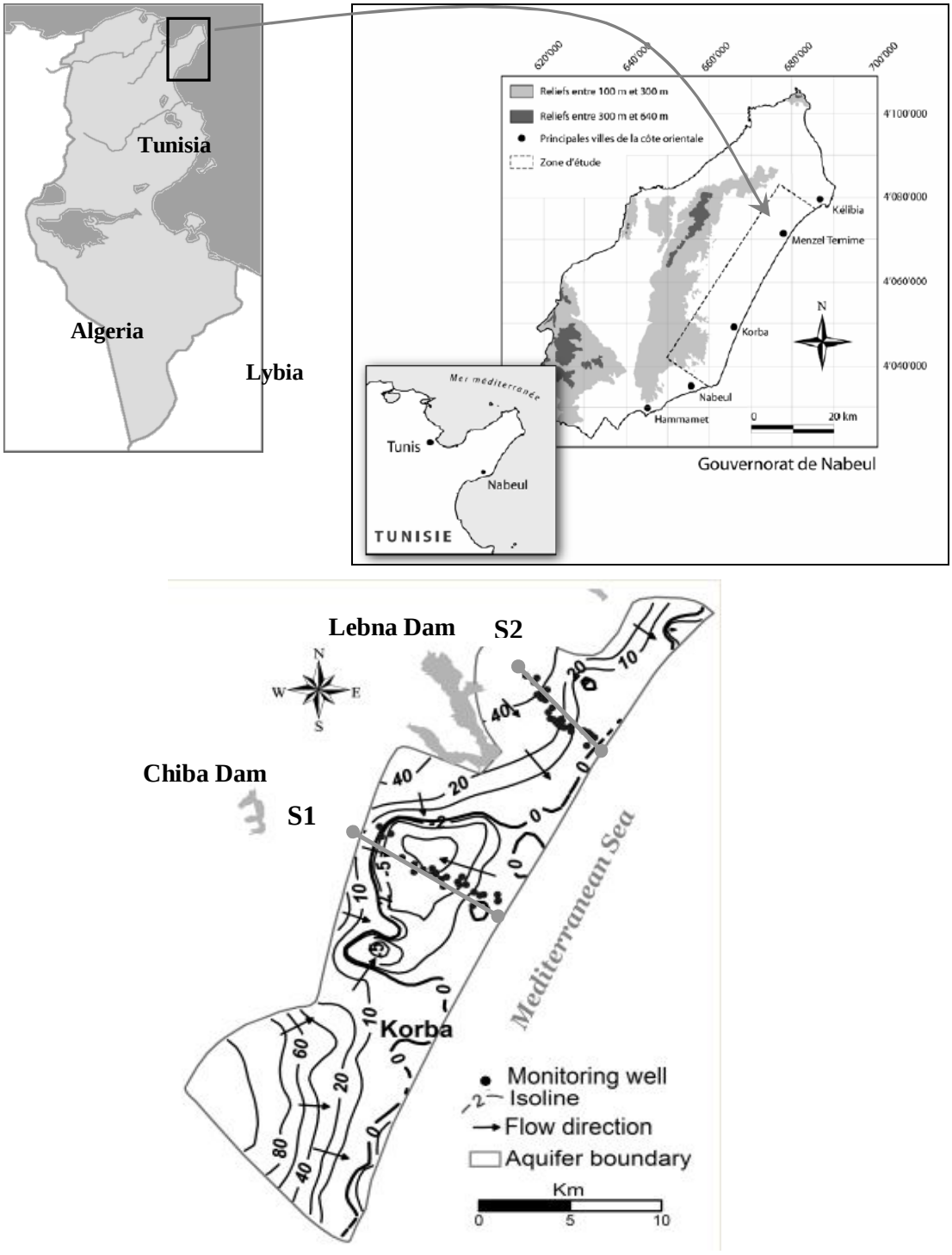

Fig. 16 Location of Korba plain, iso-contours of measured hydraulic heads in 2004 (Kerrou et al., 2010) and location of transects S1 and S2

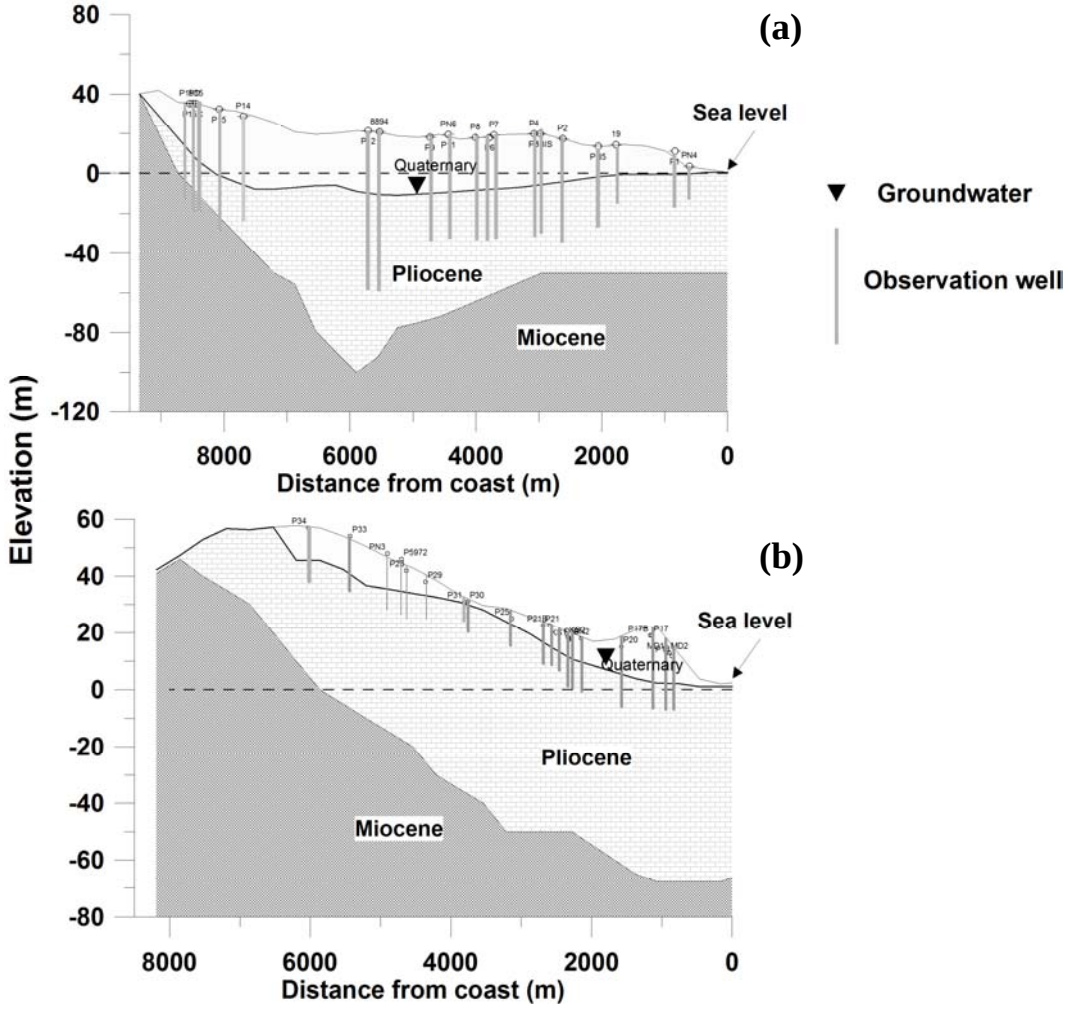

Fig. 17 Schematic cross sections of transects (a) S1 and (b) S2 and locations of observation wells.

3. Materials and methods

3.1. Groundwater investigations

Monitoring network systems were established since the sixties in the Korba coastal aquifer contributing thus to the set up of an important database describing the hydraulic and geochemical state of the groundwater. In this study, we have identified two transects perpendicular to the shoreline and following flow paths (S1 and S2) (Fig. 16). The first transect S1 is located in an area characterized by both the inversion of the groundwater flow landward and the high salinities. The second transect S2 is located at about ten kilometres north of the first one and is not affected by seawater intrusion (Fig. 17). A monitoring network composed of piezometers, and a selection of exploited and abandoned wells was set up, in each transect, in June 2006 (Fig. 17). Field campaigns were carried out in June, August, and December 2006, March, June, November 2007 and March 2008. Temperature, pH and electrical conductivity were measured in situ. Samples were taken

from wells in exploitation before being refrigerated at 4°C. Major elements (Na, K, Ca, Mg, Cl and SO_4) and nitrate were analysed in the CHYN Laboratory with ionic chromatography after the samples were filtered (0.45 µm). Bicarbonates ions (HCO3 and CO3) were analysed using titration.

3.2. Geochemical methods

Water types were identified for each transect, using the conventional Piper diagram (Appelo and Postma, 2005). Piper diagram and the diagram proposed and modified after Chadha (1999) were also used to identify geochemical processes occurring in the groundwater. The latter is a rectangular diagram with, in milliequivalent percentage, the sum between "calcium plus magnesium" and the sum "sodium plus potassium" in the X axis and the difference between the sum of bicarbonates and the sum of "chloride plus sulphates plus nitrate" in the Y axis (Chadha, 1999). Note that nitrates were introduced to both Piper and Chadha diagrams as the groundwater is known to be concentrated with regard to nitrate (Ben Hamouda, 2009).

Besides, observation wells were gathered into groups issued from Hierarchical Classification Analysis (HCA) following the Q-Mode (Hussein, 2003). Ward's method based on Euclidian distance as a measure of similarity was applied on 20 samples from transect S1 and 19 samples from transect S2, all collected in august 2006. The following group of variables was retained for HCA: Electrical Conductivity (EC), Na, K, Ca, Mg, Cl, SO_4, and HCO_3. In addition, variables were standardized before HCA application (Melloul and Collin, 1992).

3.2.1 Seawater fraction and ionic deltas

Seawater fraction in the groundwater is often estimated using chloride concentration since this ion is considered as a conservative tracer, not affected by ion exchange (Custodio and Bruggeman, 1987). Other techniques of calculations, mainly based on regional statistical trends, are also proposed in literature (Park et al., 2003). The seawater fraction for conservative mixing is calculated as follows (Appelo and Postma, 2005):

$$f_{sea} = \frac{m_{Cl^-,sample} - m_{Cl^-,fresh}}{m_{Cl^-,sea} - m_{Cl^-,fresh}}$$

Where $m_{Cl^-,sample}$ is the Cl^- concentration of the sample, $m_{Cl^-,sea}$ is the Cl^- concentration of the Mediterranean sea (value taken from the literature (De Montety Veronique et al., 2008)) and $m_{Cl^-,fresh}$ represents the Cl^- concentration of the fresh water. The sample

considered as fresh water is usually taken from the beginning of the recharge area of the aquifer and is characterised by a Ca-HCO_3 type (Pulido-Leboeuf, 2004) or a Ca-Mg-Na-HCO_3 (Custodio and Bruggeman, 1987). In this study, the fresh water sample will be selected considering the least measured value of the electrical conductivity. As the groundwater presents, since 1964 high chloride concentrations (>130 mg/l) the mixing problem is thus a mixing between a fresh-brackish water (according to Stuyfzand classification (Stuyfzand, 1986)) and seawater. Once calculated, the seawater fraction is used for determining the concentration of each ion *i* resulting from the conservative mixing of seawater and the fresh-brackish water:

$$m_{i,mix} = f_{sea} m_{i,sea} + (1 - f_{sea}).m_{i,fresh}$$

Where $m_{i,sea}$ and $m_{i,fresh}$ are the concentration of the ion *i* of respectively seawater, and fresh-brakish water. For each ion *i*, the difference between the concentration of the conservative mixing $m_{i,mix}$ and the measured one $m_{i,sample}$ simply represents the concentration resulting from any chemical reaction occurring within mixing:

$$m_{i,react} = m_{i,sample} - m_{i,mix}$$

Those potential deviations from the simply mixed composition result from various chemical processes and are also known as the ionic deltas. Thus the calculation of these deviations is important for identifying and quantifying potential chemical reactions (Grassi et al., 2007; Pulido-Leboeuf, 2004). When $m_{i,react}$ is positive, groundwater is getting enriched for ion *i* whereas a negative value of $m_{i,react}$ indicates a depletion of the ion *i* compared to the theoretical mixing (Andersen et al., 2005).

3.2.2 Conservative mixing and geochemical modelling

Besides the calculation of seawater fraction and ionic deltas, we used PHREEQC (Parkhurst, 1995) to generate 20 solutions issued from the conservative seawater fresh-brackish water mixing with fractions ranging from 100% to 0.1 %. Ionic ratios and bivariate lines corresponding to the generated solutions will form respectively the theoretical mixing ratios and the theoretical mixing lines (TML). Another way of studying the processes accompanying the conservative seawater fresh-brackish water mixing is comparing the saturation indexes of usual minerals met in coastal aquifers (Calcite,

dolomite, gypsum and halite) of measured samples to those of the mix solutions computed using PHREEQC (Post, 2002; Pulido-Leboeuf, 2004).

4. Results and discussions

4.1. Groundwater fluctuations

Measurements of the hydraulic head along the first transect S1 revealed an important piezometric depression reaching 5 meters at 4 km from the shoreline. Inversely, in transect S2 the groundwater flow is still seaward (Fig. 3).

4.2. Water types and classification

Water types (Fig. 5) and classification were discussed in the second chapter. The calculated seawater fractions varied from 1.4 % to 19.2 % in transect S1 and from 0.06 % to 9 % in Transect S2.

To study seawater intrusion, only samples potentially affected by the mixture with seawater are retained. For transect S1, as we ignore the introduction length of seawater landward, we excluded from the study the group of wells located at more than 6 km (wells P8894, P15C, P15, P14, P12 and P15D) from the shoreline. In addition, this selection was compliant with HCA analysis results (Fig. 6). Selected wells in transect S2 are those of cluster 2.1 (wells P20, P17, MD1, MD2, P18, P17B). This group of wells is located along 1500 m from the shoreline:

4.3. Ion exchange

The modified Chadha diagram (Fig. 18) as well as Piper diagram (Fig. 5) illustrate that a certain number of wells lie on the theoretical mixing line between fresh-brackish water and

seawater.

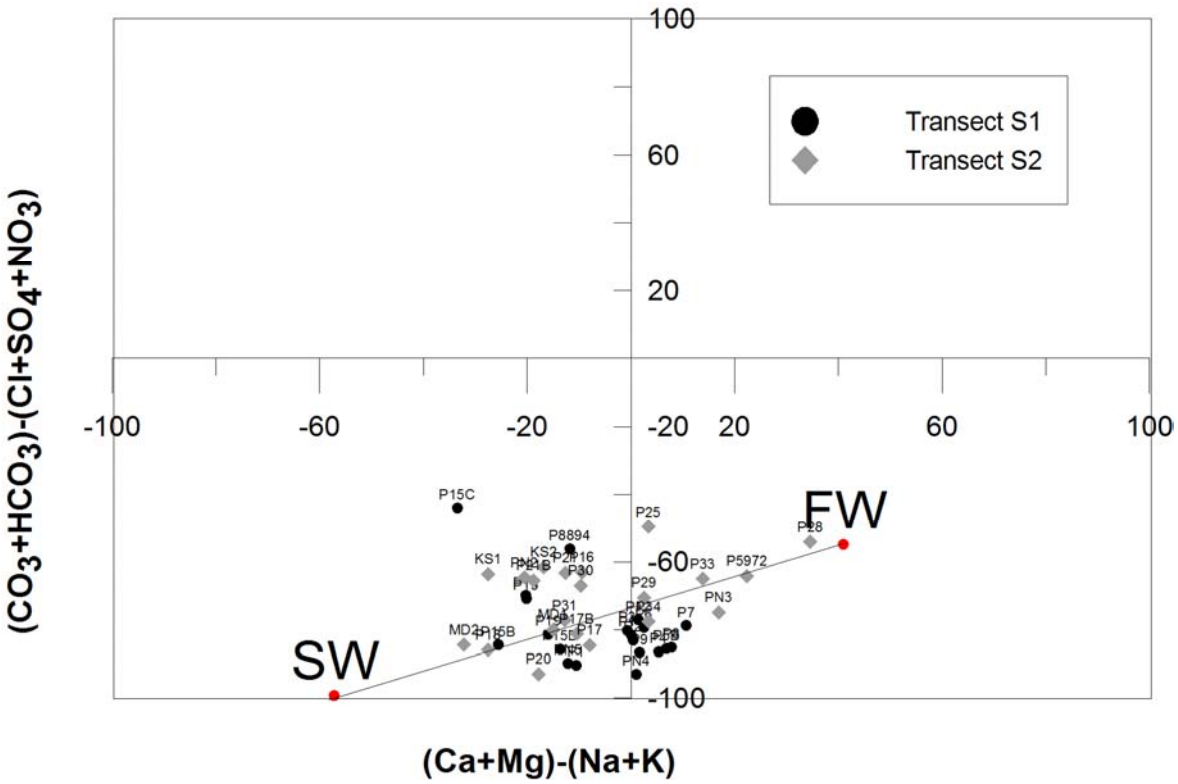

Fig. 18. Modified Chada diagram for (a) transect S1 and (b) transect S2 august 2006 survey

However, other wells plot under or above the TML indicating the presence of other geochemical processes taking place within the mixing. Fig. 20 illustrates the calculated ionic deltas versus chloride for both transects at different seasons. The majority of samples in transect S1 are depleted in Na and enriched in Ca and Mg. The loss of Na and gain of Ca and Mg suggests a direct cation exchange usually observed in similar situations when the seawater is replacing fresh water (Appelo and Postma, 2005; Cardona et al., 2004; De Montety et al., 2008; Yaouti et al., 2009). Yet, some samples are always or seasonally depleted in Mg and enriched in Ca indicating a possible exchange between these two cations (Fig. 20).

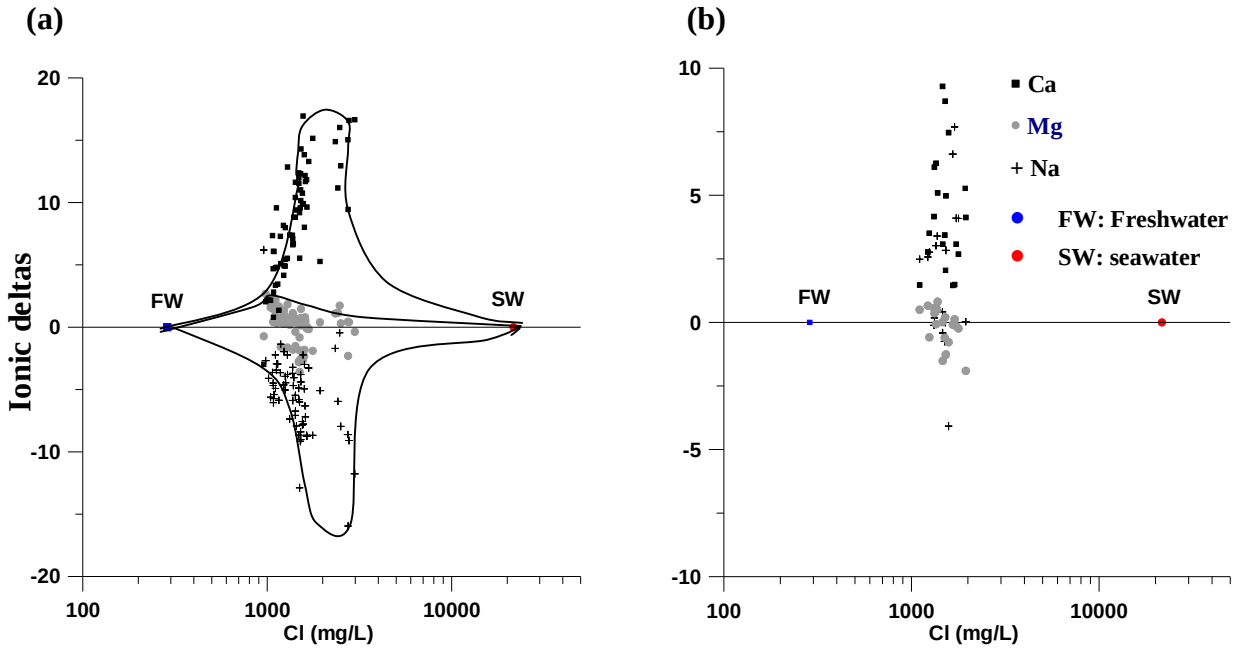

Fig. 19 Ionic deltas of Na, Ca and Mg versus Chloride for (a) transect S1 (b) transect S2

Custodio and Bruggeman (1987) explain that cation exchange processes take place in the freshwater/seawater interface until the exchange capacity of the exchanger is satisfied except in the sandy aquifers and in the case of a dynamic interface announcing a progressing seawater contamination. This explanation suits this transect of the Korba aquifer as it is mainly constituted of Quaternary sands. Besides, the inversion of the flow landward was reported since the seventies (Ennabli, 1980) which announces that seawater is still intruding fresh water.

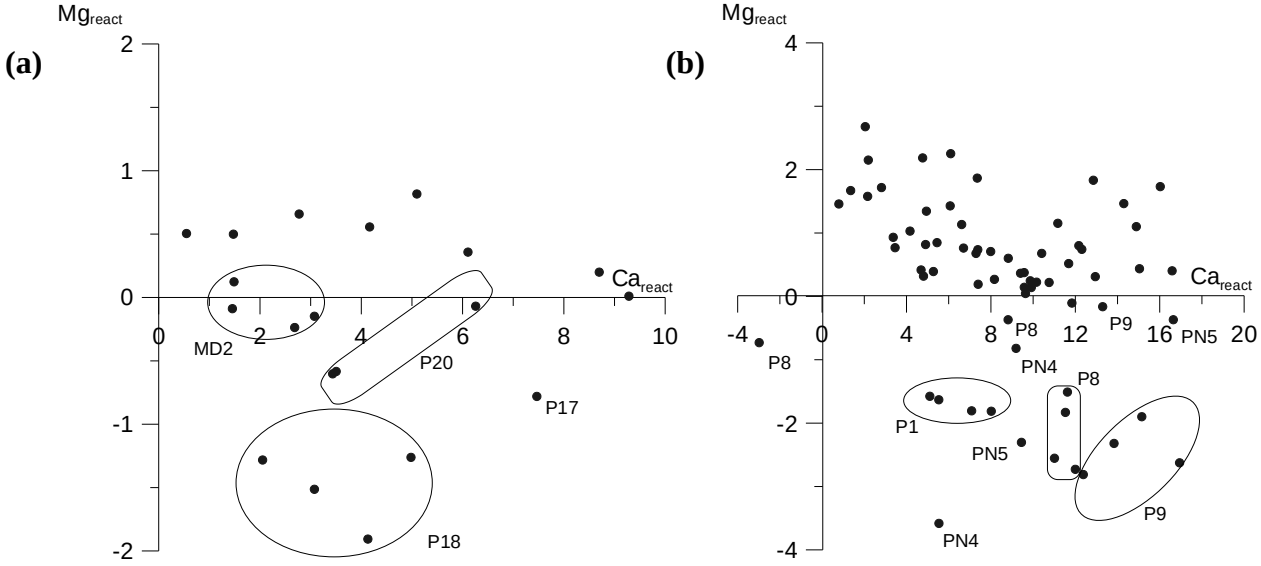

Fig. 20 Mgreact versus Careact calculated for all observation campaigns in (a) transect S2 and (b) transect S1

Note that, ion exchange is observed during all seasons and in wells located at about 4400 m (Fig. 21).

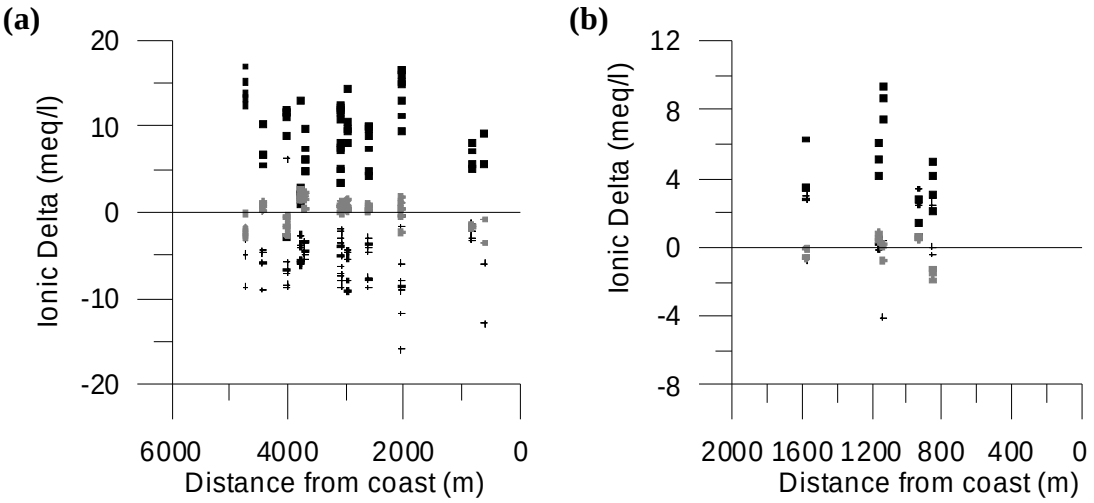

Fig. 21 Spatial and distribution of ionic deltas for samples issued from all campaigns (a) Transect S1 and (b) Transect S2

Inversely, samples of transects S2 are enriched in Na and in Ca. As the flow is seaward in this transect (Fig. 19), one can suggest that inverse cation exchange is taking place indicating the flushing of freshwater into seawater. In this case, samples should be depleted in Ca which is not the case. Another explanation could be that other sources are enriching the groundwater with Ca. This suggestion is supported by the fact that even in transect S1, Ca_{react} +Mg_{react} is sometimes more important than Na_{react} (Fig. 22).

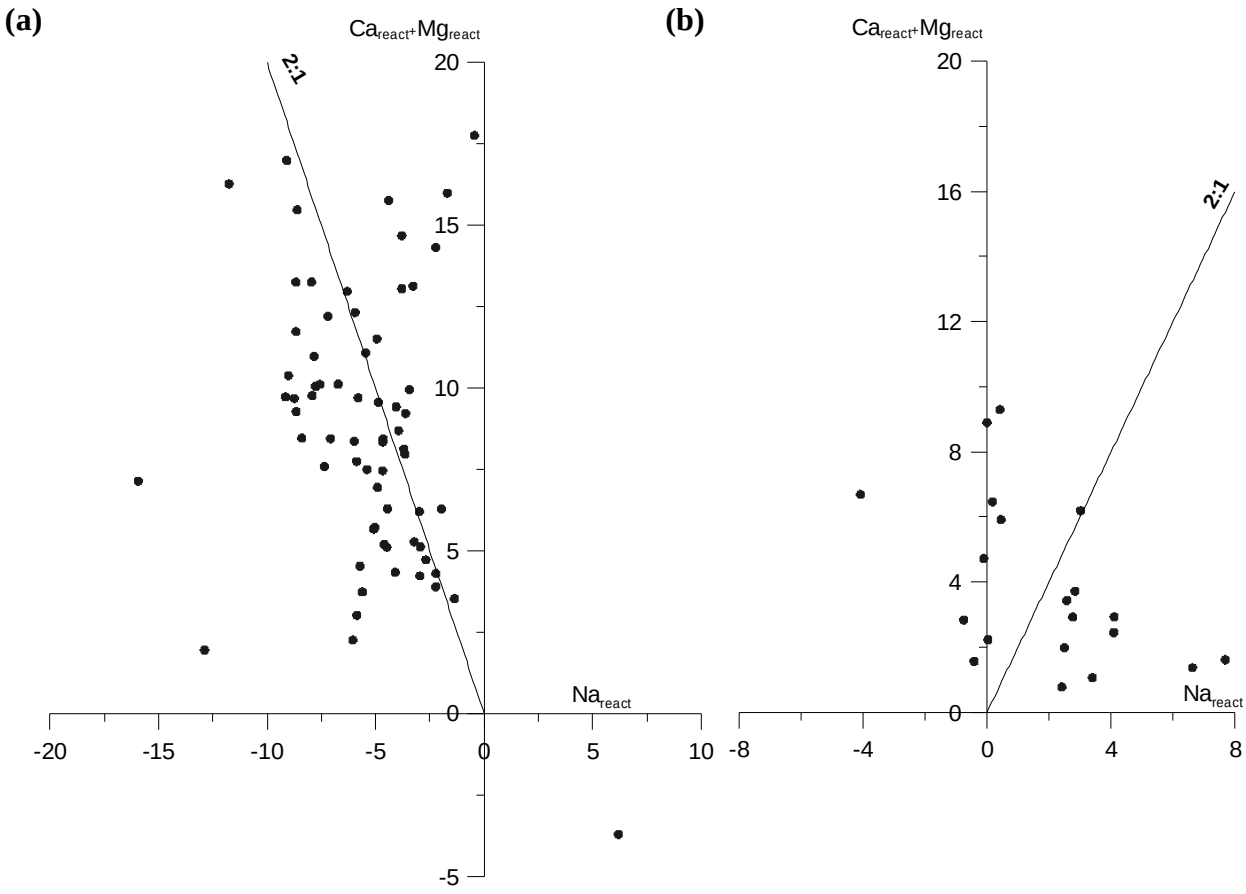

Fig. 22 $Ca_{react}+Mg_{react}$ versus Na_{react} calculated for all observation campaigns in (a) Transect S1 (b) Transect S2

4.4. Carbonate equilibrium and gypsum dissolution

The possible sources of Ca reported in the literature are gypsum dissolution or leaching and dedolomitization (Lambrakis, 2006). The latter is known as the transformation of dolomite into calcite via the dissolution of the first one and the precipitation of the second one (Appelo and Postma, 2005). Dedolomitization is usually possible when groundwater is in equilibrium with calcite and dolomite and simultaneously gypsum dissolution takes place (Farber et al., 2007; Lorite-Herrera et al., 2008). The dissolution of gypsum is written as follows:

$$CaSO_4 \rightarrow Ca^{2+} + SO_4^{2-}$$

In this case groundwater will show excess in Ca, Mg and SO_4. In the present study all samples issued from both transects and diverse campaigns are either in equilibrium or slightly oversaturated with respect to calcite and dolomite and undersaturated with respect to gypsum (Fig. 23).

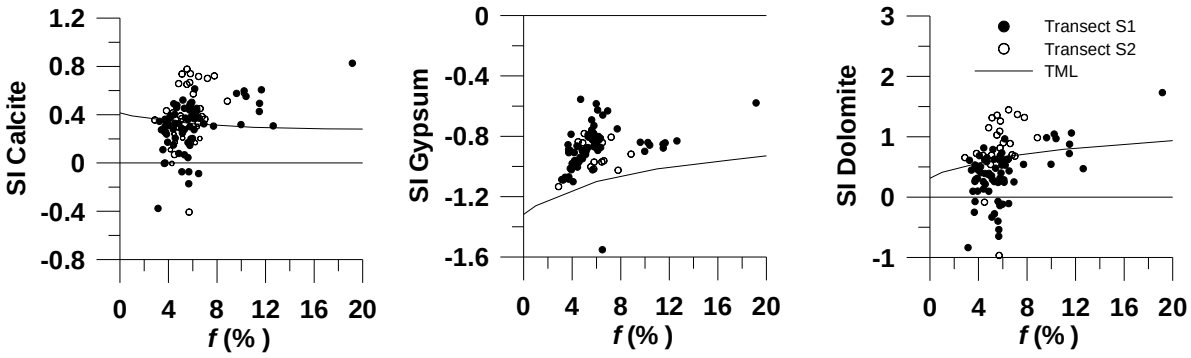

Fig. 23 Calcite, dolomite and gypsum saturation indexes along simulated for samples collected in august 2006 in tansects S1 and S2 and theoretical mixed solutions versus seawater fraction

In addition, Fig. 25 shows that samples in both transects are enriched in SO_4, except well PN5 in transect S1 and well P18 in transect S2. Two sources of sulphate are to be considered, gypsum dissolution and fertilizers. As the presence of gypsum (Fig. 25) is not reported in the geological surveys in the region, one can suppose that the major source of gypsum are fertilizers. Slama et al. (2007) reported, on the basis of a geochemical modelling study using brackish water, that gypsum can appear in the topsoil as a result of evapotranspiration and salt accumulation. This salt is then leached, under rainfall, towards the groundwater constituting thereby another possible source of gypsum. Moreover, the saturation indexes, with regards to gypsum, of all samples, are higher than those of the TML (Fig. 23), suggesting, therefore another source of SO_4 other than seawater (Pulido-Leboeuf, 2004).

Pulido-Leboeuf (2004) and Lombrakis et al (2006) reported that only samples containing more than 40% of seawater are concerned by dolomitization processes. Besides, Magaritz (1980) states that Mg/Ca ratio exceeding 1 is necessary for dolomite formation. Samples collected in this study present a seawater fraction that does not exceed 20% and their Mg/Ca never reached the value of 1 (Fig. 24).

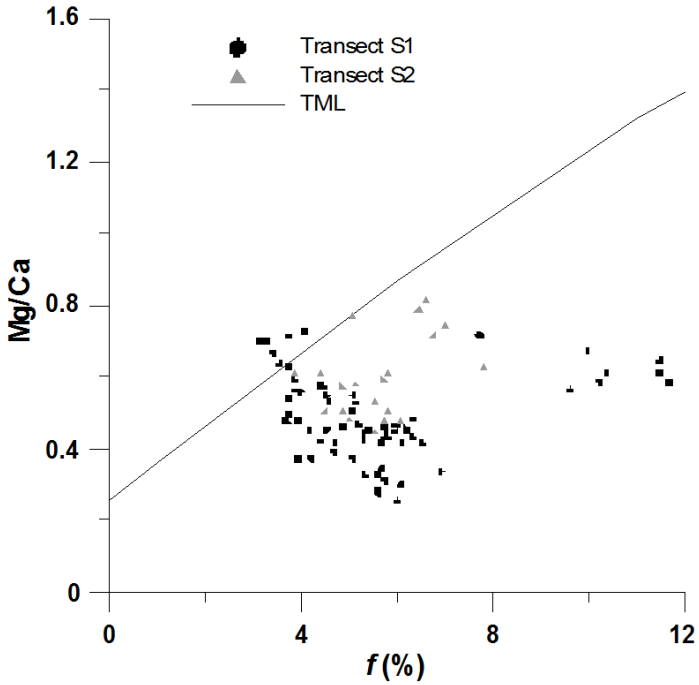

Fig. 24 Mg/Ca ratio calculated for S1 and S2 (all measured samples) versus seawater fraction

These results lead us to conclude that, in our case, dedolomitization is a possible process to consider, whereas a dolomitization phenomenon is rather to be excluded. Moreover, in their study, Smart et al. (1988) found that dolomite does not precipitate even though samples are supersaturated with regard to this mineral as opposed to results proposed by Magaritz et al (1988) stating that dolomite formation in the mixing zone is more frequent than it is thought to be. De Montetey (2008) explains that cation exchange inducing Ca^{2+} and Mg^{2+} enrichment affects carbonate equilibrium and causing thus the water to be supersaturated with regard to calcite and/or dolomite. This is to note that different hydrochemical processes are interconnected. Pulido (2004) compared the theoretical saturation indexes to those calculated for measured samples in order to test the possible sulphate reduction and dolomitization. Fig. 23 reproduces calcite, dolomite and gypsum saturation indexes calculated in both transects and for all campaigns as a function of seawater fraction. We notice a seasonal deviation between the theoretical saturation states and the ones calculated for the samples. Pulido (2004) explains that these deviations are principally due the non-conservative nature of dissolution and precipitation of the calcite and to the CO_2 flux.

4.5. Redox processes

Post (2002) states that redox processes often occur in coastal aquifers when seawater and freshwater mix. Indeed, seawater is an important source of SO_4 (usually involved in redox processes). Besides, sediments in coastal areas are rich in organic matter (Post, 2002). Thus, SO_4 reduction is a well known phenomenon in coastal aquifers (De Montety et al., 2008). Fig. 25 shows that, only PN5 (all samples) and P18 (only one sample) are depleted in SO_4 and enriched in HCO_3.

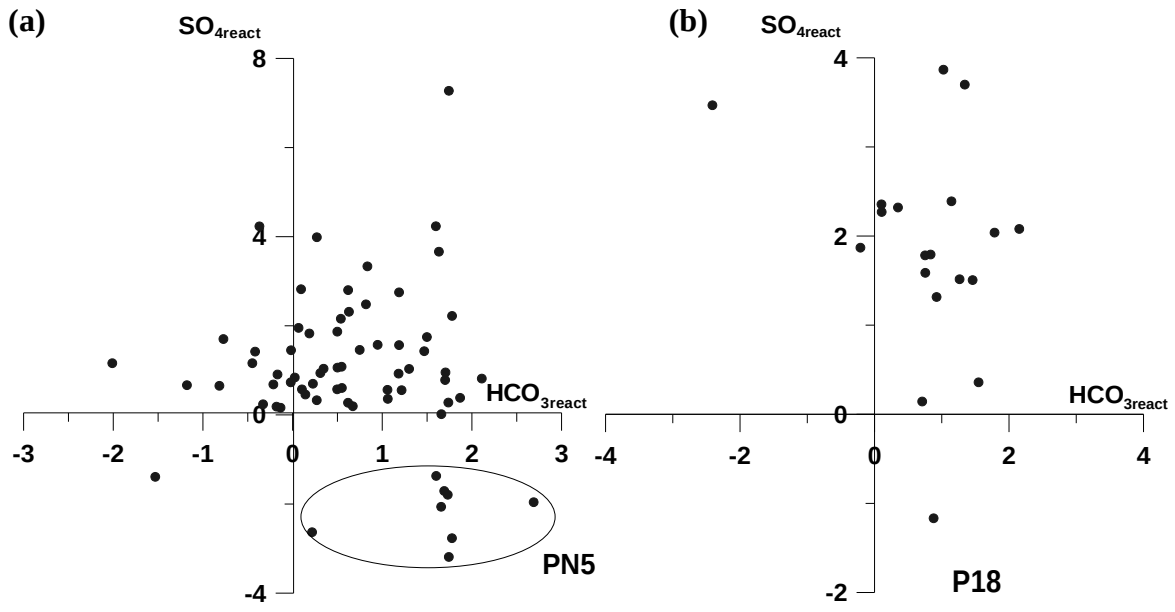

Fig. 25 $HCO3_{react}$ vs. $SO4_{react}$ calculated for all observation campaigns in (a) transect S1 (b) transect S2

Gomiz et al. (2004) demonstrated that SO_4 depletion can result from gypsum dissolution/precipitation. Yet, both wells are undersaturated with regard to gypsum. Therefore, SO_4 depletion originates from reduction. Note that PN5 and P18 present both high seawater fractions (max=12.6% for PN5 and Max= 7.8 for P18). If we consider SO_4 reduction, redox processes seem to be limited in space unlike, cation exchange. However, the excess of SO_4 can hide those processes.

Kim et al. (2003) observed that HCO_3 could be enriched along flow paths as a result of increasing microbial productivity. Fig. 26 depicts the spatial evolution of HCO_3 along the flow path in S1 and S2. It demonstrates that HCO_3 concentration increases along the two flow paths suggesting the presence of redox processes.

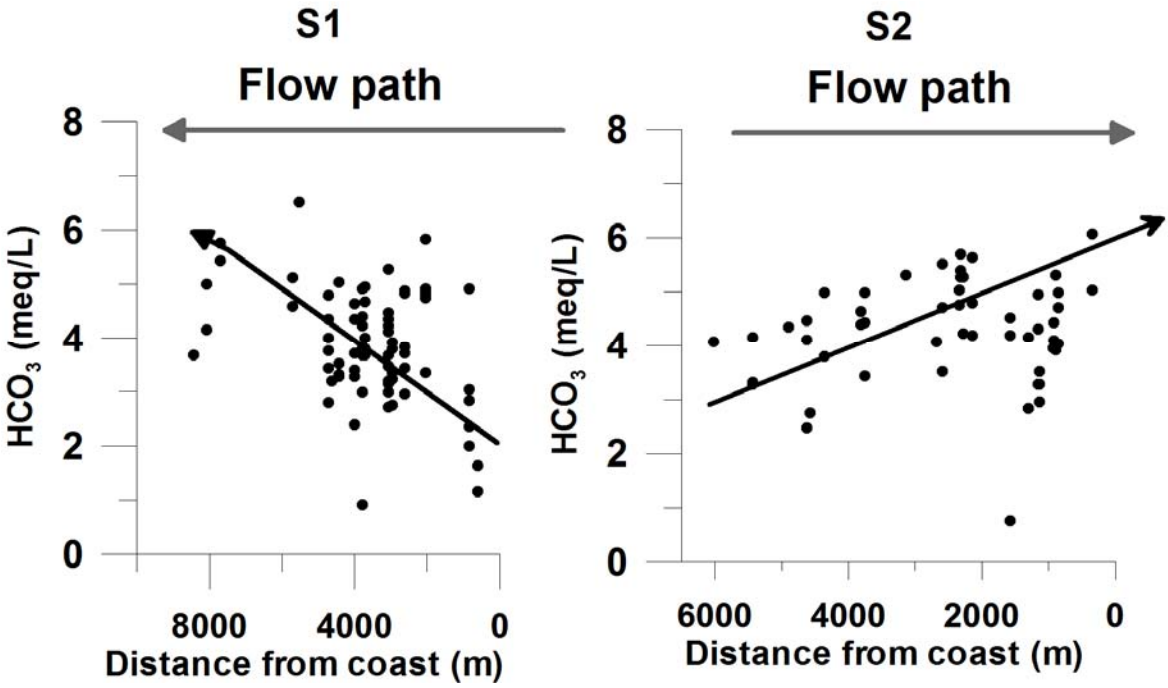

Fig. 26 Spatial evolution of HCO3 concentrations (for all measured samples) in transects S1 and S2

To conclude this study, we present a schematic section of different processes occurring in respectively transect S1 and transect (Fig. 27)

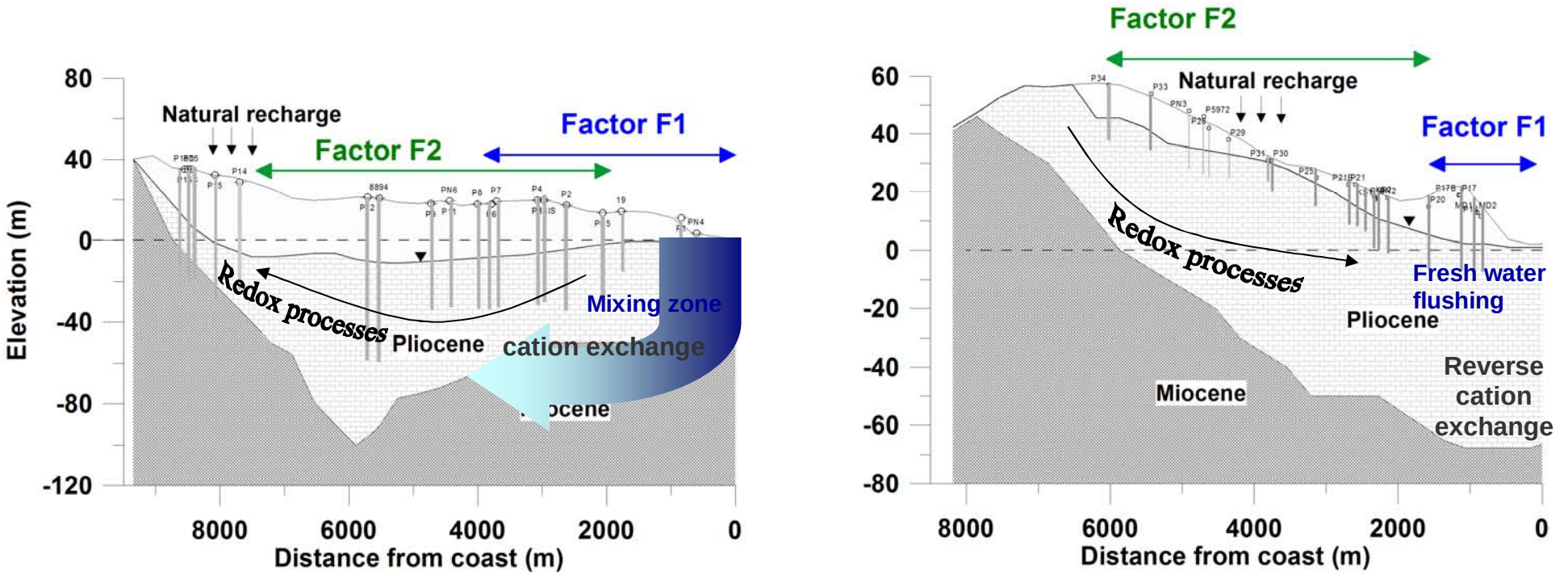

Fig. 27 Major Processes and spatial distribution of Factors (PCA) occurring in (a) transect S1 and (b) transect S2

5. Conclusion

Hydrochemical processes were explored at the interface of seawater/freshwater along two flow paths. Results reveal that in each transect a group of wells is concerned by the seawater/freshwater mixing phenomenon. Seawater fractions varied from 1.4 % to 19.2 % and from 0.06 % to 9 % in respectively transect S1 and transect S2. Seawater seems to contribute to the composition of groundwater along 4000 m and 1500 m from the shoreline in respectively S1 and S2. The mixing of seawater with the fresh-brackish water was confirmed, using Piper and the modified Chahda diagrams. A certain number of wells plotted at the TML. However, it was evident that the mixing was not conservative and thus was accompanied by other geochemical processes as samples fluctuated around the TML. The study of the Ionic Deltas revealed that cation exchange was highly acting as a major process in transect S1 where the flow was landwards. Indeed all samples were depleted in Na and enriched in Ca. Cation exchange was observed during all seasons and in wells located at about 4400 m. Inversely, in transect S1, nearly all samples were enriched in Na which could suggest reverse cation exchange. However, Ca depletion was not observed. Yet, reverse cation exchange can be hidden by an excess of Ca confirmed by the observation that even in transect S1 the enriched Ca is higher than the depleted Na. Besides, the excess of Ca, we have detected SO_4 enrichment of almost all samples. These observations suggest that dissolution of gypsum would be a potential source of both Ca and SO_4. Gypsum sources are mainly fertilizers or precipitation by evaporation at the topsoil. Besides, the study of the carbonate equilibrium suggests that dedolomitization can take place contributing therefore to the excess of Ca. Redox processes were observed along flow paths and were contributing to the groundwater composition.

To confirm the conclusions of the analysis presented herein, it would be interesting to model geochemical reactions along a flow path using PREEQC or NRTPATH (Plummer, 1994).

Finally the presented study focused on samples with seawater fractions less than 20%. It would be interesting to extend the analysis for samples presenting more than 20 % of the seawater fraction. This would be possible by performing vertical and continuous sampling in well P1 located at 600 m from the shoreline in transects S1.

References

Andersen, M.S., Nyvang, V., Jakobsen, R. and Postma, D., 2005. Geochemical processes and solute transport at the seawater/freshwater interface of a sandy aquifer. Geochimica et Cosmochimica Acta 69(16): 3979-3994.

Appelo, C.A.J. and Postma, D., 2005. Geochemistry, Groundwater and Pollution, second ed. Balkema, Rotterdam.

Bear, J., Cheng, A.H.D., Sorek, S., Ouazar, D. and Herrera , I., 1999. Seawater Intrusion in Coastal Aquifers - Concepts, Methods and Practices. Kluwer Academic Publishers, Dordrecht.

Beekman, H., E., and Appelo, C., A., J., 1990. Ion chromatography of fresh- and salt-water displacement: Laboratory experiments and multicomponent transport modelling. Journal of Contaminant Hydrology, 7: 21-37.

Ben Hamouda, M.F., Leduc, C., Tarhouni, J. and Zouari, K., 2009. Origine de la minéralisation dans l'aquifère plio-quaternaire de la côte orientale du cap Bon (Tunisie). Sècheresse, 20 (1): 78-86.

Bouhlila, R. and Laabidi, E., 2008. Impacts of calcite dissolution on seawater intrusion processes in coastal aquifers: Density dependent flow and multi species reactive transport modeling. Calibration and Reliability in Groundwater Modelling Credibility of Modelling. IAHS Publications, 320: 220-225.

Cardona, A., Carrillo-Rivera, J., Huizar-Alvarez, R. and Garniel-Castro, E., 2004. Salinization in coastal aquifers of arid zones: an example from Santo Domingo, Baja California Sur, Mexico. Environmental Geology, 45: 350-366.

Chadha, D., K.,, 1999. A proposed new diagram for geochemical classification of natural waters and interpretation of chemical data. Hydrogeology Journal 7: 431-439.

Custodio, E. and Bruggeman, K.A., 1987. Groundwater Problems in Coastal Areas UNESCO, Paris.

De Montety, V., Olivier, R., Christine, V.-C., Bernard, B., Daniel, H. and Vincent, V., 2008. Origin of groundwater salinity and hydrogeochemical processes in a confined coastal aquifer: Case of the Rhône delta (Southern France). Applied Geochemistry, 23: 2337–2349.

Ennabli, M., 1980. Etude hydrogéologique des aquifères du nord-est de la Tunisie pour une gestion intégrée des ressources en eau. Doctorat d'Etat Thesis, Ministère de l'agriculture. République Tunisienne.

Farber, E., Vengosh, A., Gavrieli, I., Marie, A., D. Bullen, T., Mayer, B., Polak, A. and Shavit, U., 2007. The geochemistry of groundwater resources in the Jordan Valley: The impact of the Rift Valley brines. Applied geochemistry, 22: 494-514.

Gomis-Yagües, V., Boluda-Botella, N. and Ruiz-Bevia´, F., 2000. Gypsum precipitation/dissolution as an explanation of the decrease of sulphate concentration during seawater intrusion. Journal of Hydrology, 228: 48–55.

Grassi, S., Cortecci, G. and Squarci, P., 2007. Groundwater resource degradation in coastal plains: The example of the Cecina area (Tuscany - Central Italy). Applied geochemistry, 22: 2273-2289.

Hussein, M.T., 2003. Hydrochemical evaluation of groundwater in the Blue Nile Basin, eastern Sudan, using conventional and multivariate techniques. hydrogeology journal, 12 144-158.

Jeen, S.-W., Kim, J.-M., Ko, K.-S., Yum, B. and Chang, H.-W., 2001. Hydrogeochemical characteristics of groundwater in a mid-western coastal aquifer system, Korea. Geosciences Journal, 5(4): 339-348.

Jones, B.F., Vengosh, A., Rosenthal, E., and Yechieli, Y. , 1999. Chapter 3: Geochemical Investigations. In: C.A.H.D. Bear J., Sorek S., Ouazar, D., and Herrera, I. (Editor), Seawater Intrusion in Coastal Aquifers - Concepts, Methods and Practises. Kluwer Academic Publishers, Dordrecht, The Netherlands, pp. 51-72.

Kerrou, J., Renard, P. and Tarhouni, J., 2010. Status of the Korba groundwater resources (Tunisia): observations and three-dimensional modelling of seawater intrusion. Hydrogeology Journal, DOI 10.1007/s10040-010-0573-5.

Kim, J., H., , Kim, R., H., , Lee, J. and Chang, H., W., , 2003. Hydrogeochemical characterization of major factors affecting the quality of shallow groundwater in the coastal area at Kimje in South Korea. Environmental Geology, 44: 478-489.

Lambrakis, N., 2006. Multicomponent heterovalent chromatography in aquifers. Modelling salinization and freshening phenomena in field conditions. Journal of Hydrology, 323(1-4): 230-243.

Lorite-Herrera, M., Jiménez-Espinosa, R., Jiménez-Millán, J. and Hiscock, K.M., 2008. Integrated hydrochemical assessment of the Quaternary alluvial aquifer of the Guadalquivir River, southern Spain. Applied geochemistry, 23: 2040-2054.

Magaritz, M., Goldenberg, L., Kafri, U. and Arad, A., 1980. Dolomite formation in the seawater–freshwater interface. Nature 287.

Meadows, D.G., Caballero, J.P., Kruse, S.E. and Vacher, H.L., 2004. Variation of Salinity in Brackish-Water Lenses of Two Florida Keys. Journal of Coastal Research, 20(2): 386-400

Melloul, A. and Collin, M., 1992. The 'principal components' statistical method as a complementary approach to geochemical methods in water quality factor identification; application to the Coastal Plain aquifer of Israel. Journal of Hydrology, 140 49-73.

Paniconi, C., Khalifi, I., Lecca, G., Giacomelli, A. and Tarhouni, J., 2001. Modeling and analysis of seawater intrusion in the coastal aquifer of Eastern Cap-Bon, Tunisia. Transport in Porous Media, 43: 3-28.

Panteleit, B., Hamer, K., Kringel, R., Kessels, W. and Schulz, H., D., 2010. Geochemical processes in the saltwater-freshwater transition zone: comparing results of a sand tank experiment with field data. Environmental earth sciences.

Park, S.C., Yun, S.T., Chae, G.T., Yoo, I.-S., Shin, K.S., Heo, C.-H. and Lee, S.-K., 2003. Regional hydrochemical study on salinization of coastal aquifers, western coastal area of South Korea. Journal of Hydrology, 2005(313): 182–194.

Parkhurst, D., 1995. User's guide to PHREEQC: a computer program for speciation, rreaction-path, advective-transport and inverse geochemical calculations, US Geol Surv Water-Res.

Petalas, C. and Lambrakis, N., 2005. Simulation of intense salinization phenomena in coastal aquifers: the case of the coastal aquifers of Thrace. Journal of Hydrology, 324(1-4): 51-64.

Plummer, L.N., Prestemon, E.C. and Parkhurst, D.L., 1994. An Interactive Code (NETPATH) For Modeling NET Geochemical Reactions Along a Flow PATH Version 2.0. U.S. Geological Survey Water-Resources Investigations Report 94-4169

Post, V.E.A., 2002. Chemistry for modellers aqueous geochemistry in coastal areas, 17th Salt Water Intrusion Meeting, Delft, The Netherlands.

Pulido-Leboeuf, P., 2004. Seawater intrusion and associated processes in a small coastal complex aquifer (Castell de Ferro, Spain). Applied geochemistry, 19: 1517–1527.

Ranjana, P., Kazamaa, S. and Sawamotob, M., 2006. Effects of climate change on coastal fresh groundwater resources. Global Environmental Change, 16(4): 388-399.

Rezeia, M. and Carrera, J., 2004. Reactive transport modeling of calcite dissolution in the fresh-salt water mixing zone. Journal of Hydrology, 311: 478-487.

Richter, B.C. and Kreitler, C.W., 1991. Identification of sources of ground-water salinization using geochemical techniques: , U.S. Environmental Protection Agency, Okalahoma.

Sivan, O., Yechieli, Y., Herut, B. and Lazar, B., 2003. Dynamics and Geochemical Evolution of Seawater Intruding into a Coastal Aquifer, The Second International Conference on Saltwater Intrusion and Coastal Aquifers-Monitoring, Modeling, and Management, Mérida, Yucatán, México.

Sivan, O., Yechieli, Y., Herut, B. and Lazar, B., 2005. Geochemical evolution and timescale of seawater intrusion into the coastal aquifer of Israel. Geochimica et Cosmochimica Acta, 69(3): 579-592.

Slama, F., Labidi, E., Bouhlila, R., Perrochet, P., Renard, P. and Milnes, P.E., 2007. Geochimical modelling of soil and groundwater salinisation under irrigation with saline water. In: IAHS (Editor), MODELCARE, Calibration and Reliability in Groundwater Modelling, Copenhagen, Danemark.

Smart, P.L., Dawans, J.M. and Whitaker, F., 1988. Carbonate dissolution in a modern mixing zone. Nature, 335: 811-813

Stuyfzand, P.J., 1986. A new hydrochemical classification of water types: principles and application to the coastal dunes aquifer system of the Netherlands SWIM 9th, Delft.

Yaouti, F.E., Mandour, A.E., Khattach, D., Benavente, J. and Kaufmann, O., 2009. Salinization processes in the unconfined aquifer of Bou-Areg (NE Morocco): A geostatistical, geochemical, and tomographic study. Applied geochemistry, 24 16-31.

Chapter 4. Impact of Irrigation with brackish water on the soil and groundwater quality

Abstract

Soil and groundwater samples were taken from six irrigated plots in Korba coastal aquifer in Tunisia. Two sampling campaigns were carried out corresponding respectively to the dry (August 2006) and the wet season (April 2007). Irrigation water comes from groundwater and presents high electrical conductivities reaching 9 mS/cm. the objective was to identify the impact of irrigating with saline water on both soil and groundwater composition. Depth profiles of Electrical Conductivities of the soil saturated paste extracts (ECe) reveal that, during the dry season, the soil solution gets concentrated in the upper horizons. The salinity of the topsoil reaches 17.5 mS/cm. ECe decreases considerably after the wet season suggesting a leaching process under rainfall. Multivariate statistical analysis (HCA and PCA) shows that the soil solution chemistry is mainly controlled by three processes: salinization processes involving concentration under evaporation and mineral precipitation, N-fertilizers contamination and redox processes. The generalized Residual Alkalinity (RA) was applied to soil samples collected in three plots. It demonstrated that when the soil solution gets concentrated under evaporation, calcite than gypsum precipitates in agreement with Saturation Index calculations. The generalized RA concept also shows that the soil solution trends to a neutral saline pathway.

1. Introduction

Water scarcity, demographic pressure and climate change have increased the occurrence of irrigation with brackish water worldwide. Qadir et al. (2007) state that developing countries suffering from water scarcity will have to rely more on the use of non-conventional water resources. They report that marginal waters used for irrigation purposes generally originate from wastewater, agricultural drainage water, and groundwater containing different types of salts.

Kijne (2003) remind that saline waters have always been used for irrigation and focuses on the importance of considering the leaching fraction to cope with soil salinity problems. Bouarfa et al. (2009) demonstrated that farmers in the South of Tunisia, succeeded to manage the salinity problems by adapting their practices. Katerji et al. published an important series of researches for studying the relationship between water salinity and yields of several common crops (Katerji et al., 1996; Katerji et al., 1998; Katerji et al., 2000). They explained that salts limit the water absorption by roots causing a water stress to the plant through the mechanism of decreasing the water osmotic potential. Besides lowering the crop yields, irrigating with saline waters presents a serious threat for both soil and groundwater resources. The most important hazards associated to the use of brackish water in irrigation are salinization and alkalinisation, as they may permanently alter the soil structure (Sparks, 2003). It is worthwhile noting that the terms “saline soil” and “alkali soil” refer to soils that contain respectively sufficient soluble salts and exchangeable sodium to impair the plant production (Richards, 1954). When both of phenomena are superimposed, the soil is referred to as a saline-alkali soil. Hence, salinity and sodicity affecting soils are defined from an agricultural point of view and with regards to the plant tolerance (Hillel, 2000). Salama et al. (1999) define salinization as the process by which the concentration of dissolved salts in water and soil increases due to natural or human-induced processes. Hillel (2000) states that salts causing salinity may originate from the chemical decomposition of the rock minerals, referred to as “weathering”. A shallow groundwater can also cause soil salinization through upward flow mechanisms (Baba et al., 2006; Salama et al., 1999). In coastal areas, rainfall often mixes with sea spray forming another source of salts. Finally, irrigation with brackish water or insufficient drainage, mainly in arid environments, leads to an important accumulation of salts in the topsoil caused by evapotranspiration processes (Rhoades et al., 1992).

Depending on the origin of salts we can distinguish primary and secondary salinization processes. Primary salinization involves salt accumulation through natural processes

whereas secondary salinization is caused by anthropogenic activities mainly inappropriate irrigation practices. Hence, salinization depends on the irrigation system and management.
The chemistry of saline soils is mainly controlled by three major processes: the precipitation/dissolution of minerals, cation exchange and redox processes (Al-Droubi et al., 1977; Condom et al., 2002).
In Tunisia, the soil salinization hazard has been studied since the sixties. In fact, the Tunisian Government created a Research Centre for the Utilization of Saline Waters for Irrigation (*CRUESI*) in 1962 with the collaboration of the Special Fund of the United Nations and UNESCO (Rhoades et al., 1992). The objective was to test, at the field scale, various conditions and ways to irrigate with saline waters. Field studies were carried out in experiment stations representing various combinations of soils, climates and irrigation water compositions. The study concluded to several important observations and recommendations (CRUESI-Tunisie, 1970). Among these conclusions, was that winter rainfall, especially in coastal areas, could be exploited for leaching purposes by keeping the soil high in water content just prior to rain events (Rhoades et al., 1992). Slama et al. (2004) performed a salt balance at the plot scale in the irrigated area of Kalaat Landelous (North East of Tunisia), and found that rainfall contributes by 30% of the annual leached salt amount.

From an environmental point of view, accumulated salts in the topsoil form a potential stock of contaminants, threatening at the long term, groundwater quality. This phenomenon is known as the transport of solutes through irrigation return flow. Causapé et al. (2006) state that the return flows from irrigated agriculture are considered as the major diffuse or "non-point" contaminants. They contribute to the pollution of the receiving bodies, mainly, surface and groundwater. Besides, Causapé et al. (2004a and 2004b) performed a salt and water balance to study salt and nitrate loads in irrigation return flows in Ebro River Basin in Spain.

The study, presented herein, describes an experimental survey of the soil and groundwater quality in the Korba coastal plain (North East Tunisia). It aims to evaluate the impact of the irrigation with saline water on the soil and groundwater composition. An attempt for identifying hydrochemical processes occurring in the vadose zone is also presented. To fulfil these objectives, we have used conventional geochemical methods and multivariate statistical analysis techniques. Besides, the concept of Residual Alkalinity (Al-Droubi et

al., 1977) was applied to assess the salinization and alkalinisation trends and to predict the potential precipitated minerals under evaporation.

2. Materials and methods

2.1. Study area and irrigation practices

The experimental study was conducted in six irrigated plots in Korba coastal plain, located in the Cap-Bon peninsula North-East of Tunisia (Fig. 28). The Korba plain is an important agricultural region involving several irrigated areas. A variety of crops are cultivated in the studied area: truck farming, tomato, cereal, forage and arboriculture. Agricultural areas have been planned to receive irrigation water from Lebna Dam (located in the Cap-Bon) and from other dams located in the North East of Tunisia. Yet, groundwater remains the principal source for irrigation water. Indeed, about 9000 equipped wells were recorded (Ben Hamouda, 2009).

The plots are aligned on two transects perpendicular to the shoreline. A description of the irrigated plots is given in Tab. 3. The fields are intensively exploited reaching in some cases three crops per year, as for the other irrigated areas in Tunisia. Tomato is the dominant crop in Korba plain and it is generally alternated with wheat, barley or truck farming or forage. Indeed, farmers are encouraged by food industries (through donation of free tomato seedlings) to cultivate tomato in spite of the recorded poor yields (lowering to 10 t/ha) and the grants proposed, by the local authorities, to abandon the tomato cropping.

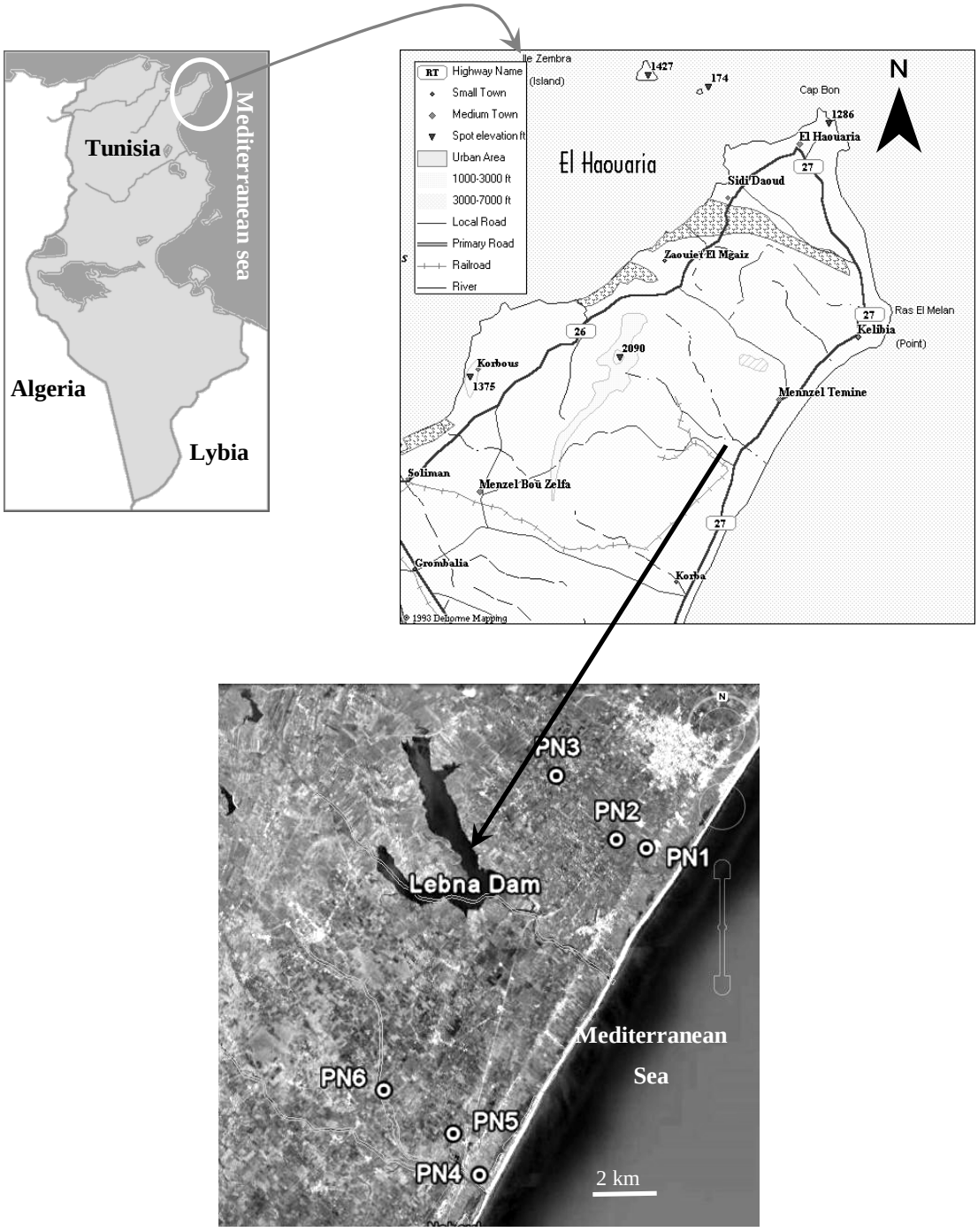

Fig. 28. Location of the six plots (map sources: google earth software)

The irrigation systems have been modernized and traditional ones were converted to water-conserving technologies, mainly drip irrigation. This was enhanced by a national program for agricultural water management and conservation, aiming to rationalize the use of water for irrigation (Al Atiri, 2004). However, several field studies reported that farmers, lacking training and information are misusing drip irrigation and are, in some cases, over irrigating crops (Slama et al., 2004; Slatni et al., 2004). The main cropping season for tomato starts usually in March and ends in June. The Cap Bon peninsula is also famous for being among the first regions in Tunisia to have introduced fertigation techniques. Farmers in Korba plain are widely using those techniques, especially with drip irrigation.

Tab. 3. Description of the studied plots

Transect	Plot	Coast distance (m)	Surface (ha)	Irrigation water source	Irrigation system	Cropping system	Tomato yield [1]
S2	PN1	1304	1.6	PN1B [3]	Drip irrigation	Wheat/ Tomato	NA
	PN2	2338	2.5	Wells KS1 and KS2 [2]	Surface irrigation	Tomato/olive/ truck farming	NA
	PN3	4901	1.3	Well PN3	Drip and sprinkler irrigation	Tomato/ wheat	NA
S1	PN4	605	0.8	Well P1	Drip irrigation	Tobacco/ truck farming	NA
	PN5	2056	6	Well PN5	Drip irrigation	Tomato/truck farming/ forage	10 T/ha
	PN6	4436	14.5	Well P11	Drip irrigation	Tomato/olive/ truck farming	60 T/ha

[1] Estimation indicated by the farmer. NA: non available

[2] Surface water from Lebna Dam is available but the farmer found it expensive to use

[3] Located at about 800 m from the irrigated plot: the farmer is sharing the water resource in return of a percentage of the harvest

2.2. Soil and groundwater sampling and analysis

The first soil sampling campaign was performed by the end of the dry season, after the irrigation has ended, in August-September 2006 and the second one by the end of the wet season (April 2007). Note that, because of access reasons the wet season campaign was

solely conducted for plots located in transect S1. Indeed, two farmers denied the access to their fields, as they were already cultivated. Thus, data analysis will focus on samples collected in transect S1. Soil samples were taken each 30 cm for the first meter and each 50 cm for the layers below. The total sampled depth reached 4 m, 15 m and 19.5 m for respectively PN4, PN5 and PN6. Various techniques, depending on the lithology, were used for extracting soil samples. Core drilling was suitable for clayey layers, whereas a rotary drilling using a tri-cone roller bit was performed in sandy layers. A down-the-hole hammer bit was used in sandstone, mainly met in the layer located at the depth of 40 to 100 cm. Note that the drilling tasks were all carried out using air pressure without added fluids in order to prevent sample contaminations. The pH was measured on soil extracts with distilled water ratios of 1:2.5. Saturated soil pastes were prepared by adding deionised water to 200 g of soil according to the standard method described in Rhoades et al. 1999 (Rhoades et al., 1999). The Saturation Percentage (SP) varied from 19 to 83%. Electrical conductivities, major ions (Na^+, K^+, Ca^{2+}, Mg^{2+}, Cl^-, $SO4^{2-}$), nitrate and bicarbonates were measured on the soil saturated paste extracts. Major ions were analysed using Ion Chromatography at the soil department of the ministry of agriculture. Bicarbonates were measured using the titration method. The charge balance error was calculated and was found acceptable (ranging between 5-10%). The soil texture was determined, for all samples of transect S1 collected in august 2006, using particle size analysis, performed at the soil department. Six granular fractions were measured using the Robinson method. Soils were then classified according to the USDA[3] classification and using the free software TRIANGLE (Gerakis and Baer, 1999; Gerakis and Baer, 2010).

2.3. X-Ray Diffraction (XRD) analysis

The XRD analysis is known to be a useful technique for the semi-quantitative determination of clay, primary and secondary minerals (Sparks, 2003). The use of this technique for the identification of precipitated salts in irrigated soils is reported in several case studies (Abdelfattah et al., 2009; Job, 1992; Metternicht and Zinck, 2009). For instance, Metternicht and Zinck (2009) found that salt crusts were mainly formed of halite, quartz, and finally gypsum.

Small salt crusts have been visibly noticed at the soil surface at most of the investigated plots. However, no special attention was made while taking samples at the topsoil. Indeed, Ulery and Drees (2008) (Ulery and Drees, 2008) emphasizes that the conservation of

[3] United States Department of Agriculture

samples is crucial for the detection of minerals. The XRD was performed on 15 soil samples issued from the dry campaign and sampled in PN4, PN5 and PN6 plots, located in transect S1.

2.4. Geochemical indicators of salinization and sodicity hazards and trends

Salinity is quantified, in the literature, in terms of electrical conductivities at 25°C (EC), expressed in mS/cm (1 dS/m = 1 mmho/cm): The FAO[4] defines six classes for water with regard to salinity, ranging from non-saline to brine (Tab. 4) (Ayers and Westcot, 1994). Richards (1954) recommends using Electrical Conductivity measured on soil saturated paste extracts (ECe) as the most reliable parameter in describing the soil salinity. Saturation indexes of calcite, dolomite and gypsum were computed using PHREEQC (Parkhurst, 1995).

Tab. 4 Classification of saline waters (Rhoades et al., 1992)

Water class	Electrical conductivity dS/m	Salt concentration mg/l	Type of water
Non-saline	<0.7	<500	Drinking and irrigation water
Slightly saline	0.7 - 2	500-1500	Irrigation water
Moderately saline	2 - 10	1500-7000	Primary drainage water and groundwater
Highly saline	10-25	7000-15 000	Secondary drainage water and groundwater
Very highly saline	25 - 45	15 000-35 000	Very saline groundwater
Brine	>45	>45 000	Seawater

The sodium hazard is typically expressed as the *sodium adsorption ratio* (*SAR*) calculated as follows (Sparks, 2003):

$$SAR = \frac{\left[Na^{+}\right]}{\sqrt{\left[\frac{Mg^{2+} + Ca^{2+}}{2}\right]}}.$$

Where brackets indicate the total concentration of ions in meq/L. However, SAR has to be plotted vs. EC (e.g. Wilcox diagram) in order to identify the sodium hazard on the basis of known salinization and sodicity hazard classes (Rhoades et al., 1992).

[4] Food and Agriculture Organization of the United Nations

Later on, the concept of Residual Alkalinity (RA) will be developed to better analyse the salinization and alkalinization processes occurring when a solution is getting concentrated (Barbiéro et al., 2001; Bouarfa et al., 2009). RA is calculated as follows:

$$RA=Alkalinity-[cations]+[anions] \quad \text{in meq/l}$$

Where [cations] and [anions] are the concentrations in meq/L of respectively cations and anions involved in precipitation (Bouarfa et al., 2009). Alkalinity (Alk) is defined as "*the sum of weak base concentrations multiplied by the number of protons each base can neutralize, minus the number of protons in the solution*" (Barbiéro et al., 2001). Alkalinity is due, in most soils, to carbonate and it is calculated as follows:

$$Alkalinity = [HCO3^-]-[H^+] \quad \text{in meq/L}$$

Furthermore, Droubi et al. (1976) (Droubi et al., 1976) introduced the concept of generalized residual alkalinity to the successive precipitation of several minerals. As an example calcite residual alkalinity (RAcalcite) refers to the alkalinity of the solution after complete precipitation of the calcite and it is calculated as follows (Barbiéro et al., 2001) :

$$RAcalcite= Alk-[Ca^{2+}] \quad \text{in (meq/L)}$$

Similarly, if gypsum is the next mineral to precipitate after calcite, RAcalcite+gypsum is calculated as follows:

$$RAcalcite+gypsum= Alk-[Ca2^+]-[Mg^{2+}]+[SO4^{2-}] \quad \text{in (meq/L)}$$

Al-Droubi et al (1976) explained that when calcite precipitates, two possibilities are to be considered:

1. RAcalcite <0: Ca^{2+} concentration increases, pH and alkalinity decrease and the solution follows the neutral saline pathway
2. RAcalcite >0: Ca^{2+} concentration decreases, pH and alkalinity rise and the solution follows the alkaline pathway (Bouarfa et al., 2009).

If RAcalcite+gypsum is positive, after calcite precipitation, if we suppose that gypsum precipitates, Ca^{2+} concentration increases, SO_4 concentration decreases and pH and alkalinity decrease. If RAcalcite+gypsum is negative, the opposite evolution is observed.

To evaluate the trends followed by the concentration of each cation or anion when the solution is getting concentrated, chloride is used as a reference. Chloride is considered as a

tracer as it is not involved in neither precipitation nor dissolution processes. Concentration diagrams of chloride vs. the other elements allow predicting precipitation occurrence. When the concentration of an element is increasing at a lower rate than that of chloride, this element is involved in precipitation (Mohamedou et al., 1999). To calculate concentration factors, we have divided the concentration of chloride of each sample by the least measured chloride concentration (Nezli et al., 2007). The solution of the sample presenting the minimum chloride concentration will be considered as the initial solution.

2.5. Multivariate statistical analysis

Principal Component Analysis and Hierarchical Clustering Analysis in R-Mode, as described in chapter 2, were applied separately, on standardized data issued from respectively, the dry and the wet season campaigns and collected in PN4, PN5 and PN6 plots located in transect S1. Considered variables are: Clay+Silt ratio, major elements (Na, K, Ca, Mg, Cl, HCO_3 and SO_4) and nitrate.

PCA was used in several studies for the assessment of soil salinization and alkalinization (Mohamedou et al., 1999; Visconti et al., 2009).

3. Results and discussion

3.1. Soil textural classification

Soils range in texture from sand to clay for PN4 and from sand to clay loam for PN6. Soil samples collected in PN5 present a high rate of sand and their texture range from sand to sandy loam (Fig. 29). Light textured soils, are, in general, characterized by high permeabilities and small Cation Exchange Capacities. Thus, it is expected that the vadose zone acts as transfer matrix for diverse minerals and nutrients. Chhabra (1996) states that light textured soils are less affected by salinity offering a higher tolerable level of irrigation water salinity.

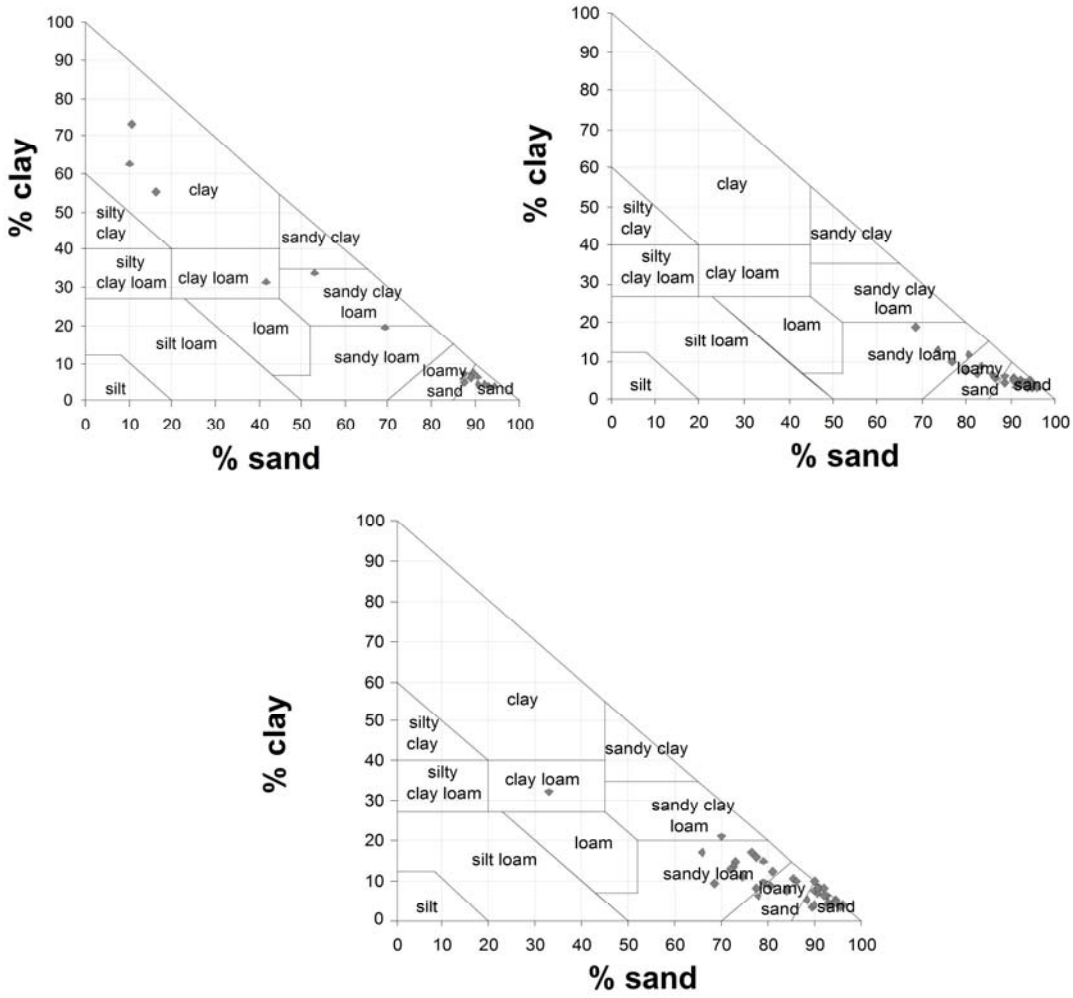

Fig. 29 Soil textural classification triangle for (a) PN4 (b) PN5 (c) PN6

3.2. Soil chemistry profiles

Table 3 summarizes the basic statistics of geochemical data for the dry and wet seasons for soil and groundwater samples.

Cations in soil water are classified as follows: $Na^{+}>Ca^{2+}>Mg^{2+}>K^{+}$ and anions as follows: $Cl^{-}>SO_4^{2-}>HCO_3^{-}>NO_3^{-}$. Piper diagram was plotted separately for the three soil profiles PN4, PN5 and PN6, using chemical data issued from the dry and the wet sampling campaigns (Fig. 30). In addition we added, to the diagram, the irrigation water chemistry measured in august 2006. The dominant water type is Na-Ca-Cl. We notice that the leaching process is controlling the soil solution chemistry in the first meter for PN4 (Fig. 30 encircled samples). The water type for theses samples is Na-Ca-HCO3. Besides, the groundwater sample plots among those of soil for the three plots PN4, PN5 and PN6 indicating the same origin.

Tab. 3 basic statistics of geochemical data for the dry and wet seasons for soil and groundwater samples

Transect	Plot		Nb		Depth (m)	SAR	pH 1:2.5	EC	Ca	Mg	Na	K	HCO3	Cl	SO4	NO3
S1	PN4	Soil	28	Min		2.30	8.26	0.48	1.80	0.26	2.33	0.09	0.07	1.49	0.00	0.00
				Max	4.00	6.14	10.06	4.09	11.25	3.71	16.79	0.71	3.10	27.43	4.19	3.50
				Mean		4.21	9.11	1.29	4.66	1.30	7.26	0.23	1.83	9.72	2.11	0.37
				SD		3.02	0.48	0.82	2.46	0.91	3.93	0.15	0.85	6.57	1.02	0.66
		groundwa	5	Min		7.65		4.45	16.43	6.12	25.69	0.29	2.00	33.35	5.80	2.97
				Max		22.86		17.19	30.38	29.72	125.31	2.01	4.92	123.36	18.02	3.77
				Mean		11.61		7.47	20.56	12.35	51.67	0.73	3.08	57.93	8.95	3.41
				SD		7.50		5.46	6.61	11.58	49.10	0.86	1.30	43.68	6.05	0.41
	PN5	Soil	66	Min		3.68	8.18	0.73	2.70	0.97	4.99	0.08	0.48	5.43	1.23	0.00
				Max	15.65	18.38	9.73	17.53	84.27	40.66	145.23	2.25	2.80	244.53	24.93	13.44
				Mean		6.15	8.85	2.20	7.51	3.06	14.14	0.26	1.32	20.84	2.54	1.25
				SD		6.74	0.38	2.19	10.20	5.03	18.61	0.33	0.47	30.95	3.04	1.89
		groundwater	7	Min		11.29		8.50	23.22	15.15	50.58	0.40	3.36	65.94	6.85	1.25
				Max		12.16		9.98	29.03	17.22	58.33	0.50	5.84	84.11	7.36	2.73
				Mean		11.74		9.18	26.92	16.18	54.52	0.44	4.78	73.42	7.16	1.93
				SD		0.33		0.59	2.12	0.83	3.13	0.03	0.73	6.56	0.17	0.44
	PN6	Soil	78	Min		2.20	7.81	0.69	1.81	0.55	3.31	0.05	0.00	2.22	1.04	0.00
				Max	19.50	7.85	9.95	4.64	21.58	8.71	30.57	3.28	2.84	46.53	9.98	11.09
				Mean		4.09	9.05	1.58	6.33	1.90	8.46	0.23	1.37	11.95	2.76	1.34
				SD		1.24	0.42	0.74	3.46	1.58	5.01	0.36	0.59	7.79	1.63	1.75
		groundwater	4	Min		6.58		4.82	16.81	8.97	24.42	0.43	3.28	35.50	5.82	2.43
				Max		7.31		5.65	21.68	9.90	27.21	0.46	5.04	42.84	6.78	2.65
				Mean		6.90		5.30	18.67	9.55	25.88	0.44	3.79	39.05	6.35	2.55
				SD		0.31		0.35	2.10	0.41	1.15	0.02	0.84	3.00	0.41	0.12
S2	PN1	Soil	32	Min		2.17	8.26	0.30	1.15	0.36	2.27	0.00	0.72	0.00	0.00	0.00
				Max	13.50	7.87	9.59	3.11	13.16	4.18	21.84	0.56	3.28	30.63	9.37	3.07
				Mean		3.81	9.03	0.95	3.91	1.22	6.46	0.13	1.61	7.91	2.41	0.65
				SD		1.46	0.34	0.81	3.39	1.06	5.46	0.13	0.80	9.02	2.23	0.76
		groundwa	1			4.32		4.94	12.60	6.30	13.29	0.09	2.84	15.31	6.20	4.73
	PN2	Soil	26	Min		2.59	8.26	0.33	1.04	0.27	3.42	0.04	0.48	2.01	0.79	0.04
				Max	10.50	7.08	9.59	4.02	15.27	7.31	21.90	0.34	2.70	43.73	8.53	4.13
				Mean		4.82	9.04	0.97	3.27	1.24	6.91	0.11	1.83	8.29	2.52	0.44
				SD		1.16	0.34	0.69	2.79	1.40	3.70	0.06	0.72	8.15	1.57	0.77
		groundwa	1			4.32		3.04	12.60	6.30	13.29	0.09	2.84	15.31	6.20	4.73
	PN3	Soil	14	Min		1.69	6.3	0.62	3.48	0.95	2.63	0.05	0.00	3.05	1.04	0.82
				Max	6.50	3.08	10.06	1.65	9.19	2.13	7.11	0.15	2.36	10.72	5.18	4.62
				Mean		2.42	8.633703704	1.02	5.71	1.48	4.62	0.09	1.05	7.09	2.42	2.07
				SD		0.46	0.71085078	0.29	1.57	0.34	1.37	0.03	0.85	2.26	1.14	1.17
		groundwat	1			4.52		3.05	13.61	6.91	14.49	0.09	4.36	17.76	6.73	5.78

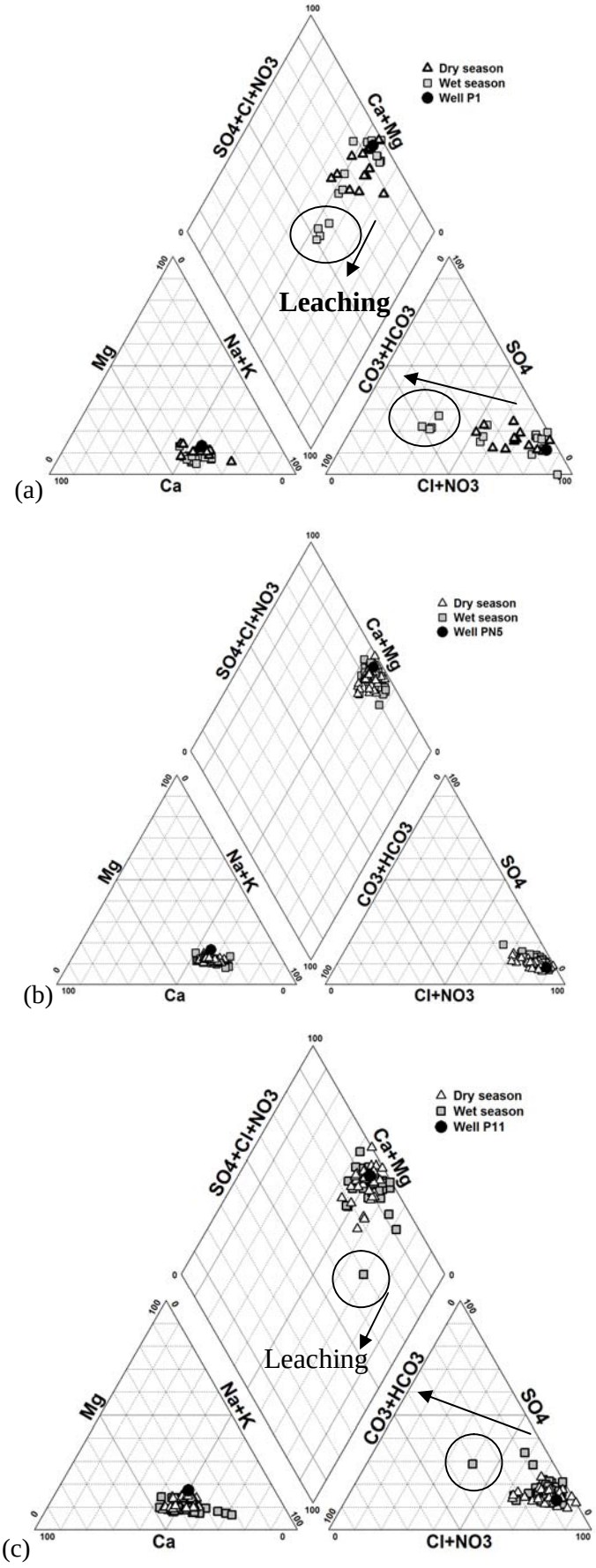

Fig. 30 Piper diagram for the dry and the wet season for (a) PN4, (b) PN5, (c) PN6 and the groundwater samples in august 2006 (a) P1, (b) PN5 and (c) P11

Depth profiles of ECe, major ions and nitrates measured in the dry and the wet season are plotted in Fig. 31. Besides, the ratio of clay and silt is depicted.

Fig. 31 and Fig. 32 show that, for the dry season, the soil samples located in the first layer (from the topsoil to the depth of 1m) presents high concentrations with regards to all the solutes. This concentration is also expressed in the high electrical conductivities ranging from 4.09 mS/cm (measured in the topsoil in PN4) to 17.53 mS/cm. We notice that this phenomenon is more important in transect S1 than it is in transect S2 where the irrigation water is more saline. Depth profiles of the wet season demonstrate an important decrease of the concentration of all major elements leading to the decrease of ECe. Indeed, ECe lowers from 17.53 to 2.73 mS/cm, from 4.64 to 1.88 mS/cm and from 2.25 to 0.67 mS/cm for respectively PN5, PN6 and PN4. Hence, accumulated salts are leached under rainfall. It is worthwhile noting that each of the three profiles in transect S1, presents peaks of high concentrations located mainly at layers containing a relative high ratio of clay and silt (Fig. 31). This observation indicates that the flow in the unsaturated zone is a piston flow (Appelo and Postma, 2005). The use of tritium in such profiles can be helpful in quantifying the infiltration rate (Baran et al., 2007).

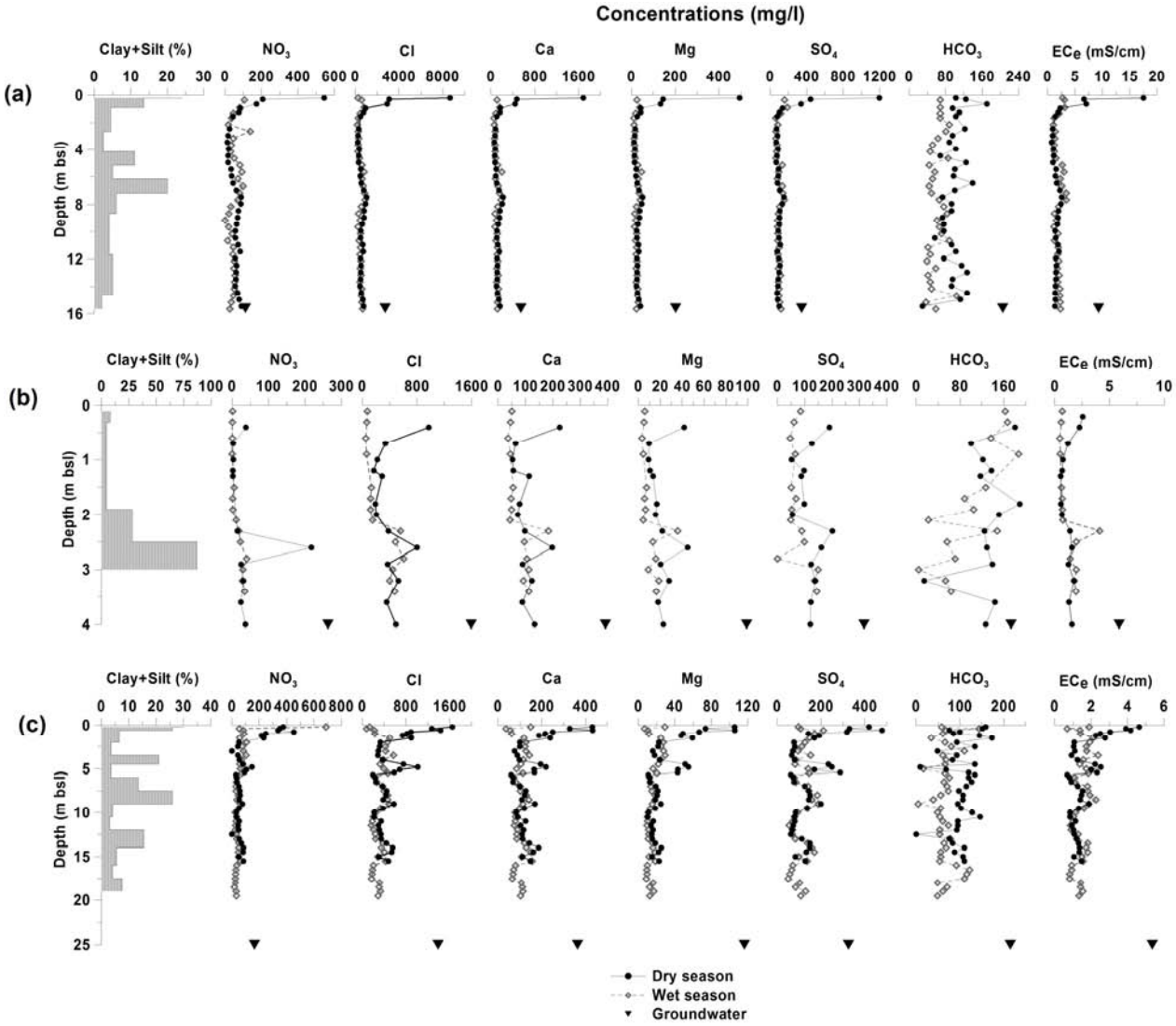

Transect S1

Fig. 31 Major ions and ECe profiles measured during the wet and the dry seasons in transect S1 for (a) PN5, (b) PN4 and (c) PN6. Groundwater concentrations are depicted with a black triangle. Concentrations are in mg/L

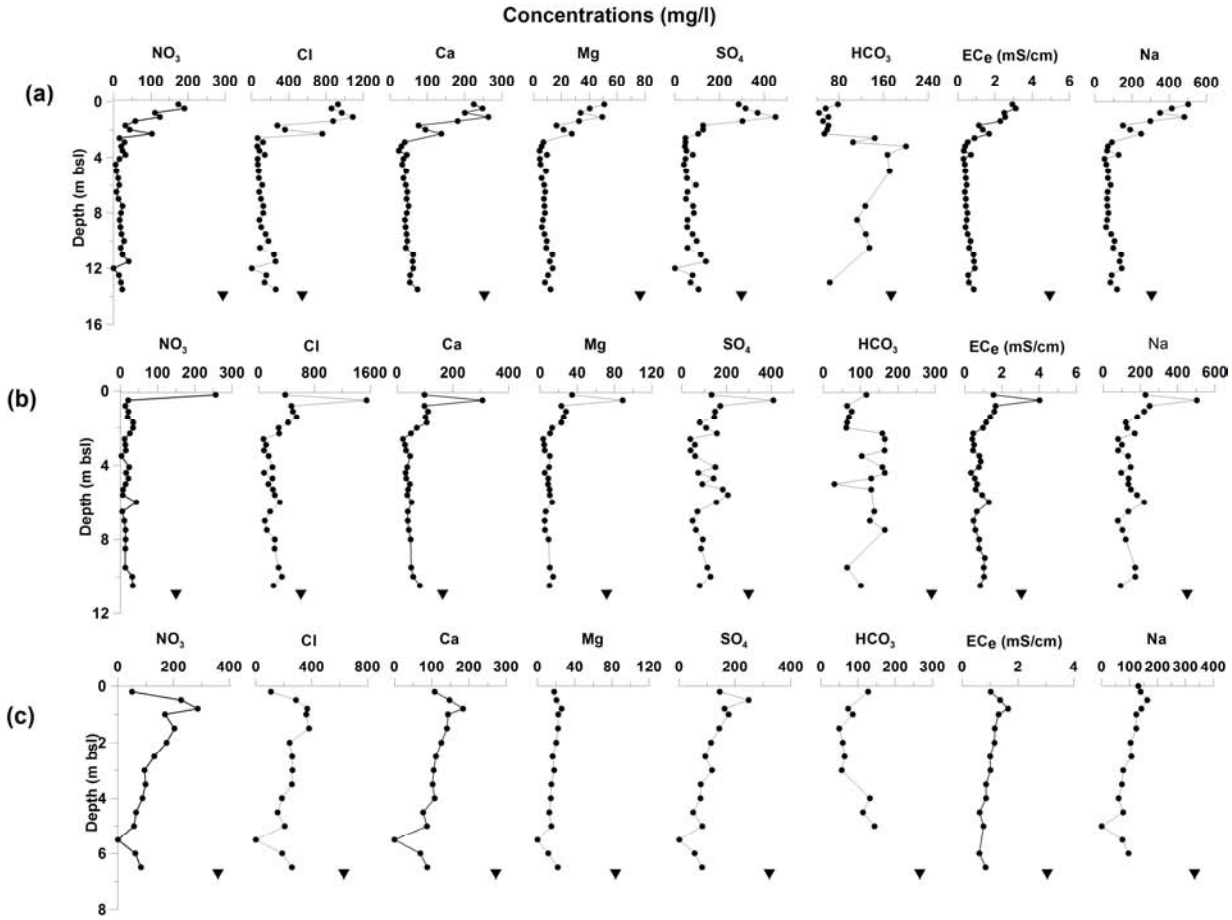

Fig. 32 Major ions and ECe profiles measured during the dry season in transect S2 for (a) PN1, (b) PN2 and (c) PN3. Groundwater concentrations are depicted with a black triangle. Concentrations are in mg/L

We performed a PCA and a HCA analysis for collected samples in PN4, PN5 and PN6 separately for each sampling season.

HCA analysis highlights that, for each season, variables cluster into two different groups (Fig. 33). For the wet season, the first cluster C1 gathers the ratio of clay+silt, HCO_3, SO_4, NO_3 and K. Grassi et al. (2007) state that NO_3, SO_4 and K are linked to pollution with N-fertilizers. Hence C1 counts for soil enrichment with agricultural substances in relationship with the presence of clay and silt. The second cluster, C2, groups, Mg, Ca, Na, Cl and ECe, considered in literature as the elements contributing to the global concentration of the solution and thus C2 is possibly related to salinity. For the dry season (Fig. 33) we observe the same clustering except for SO_4 which moves to the group of Mg, Ca, Na, Cl and ECe suggesting the involvement in the gypsum precipitation reaction.

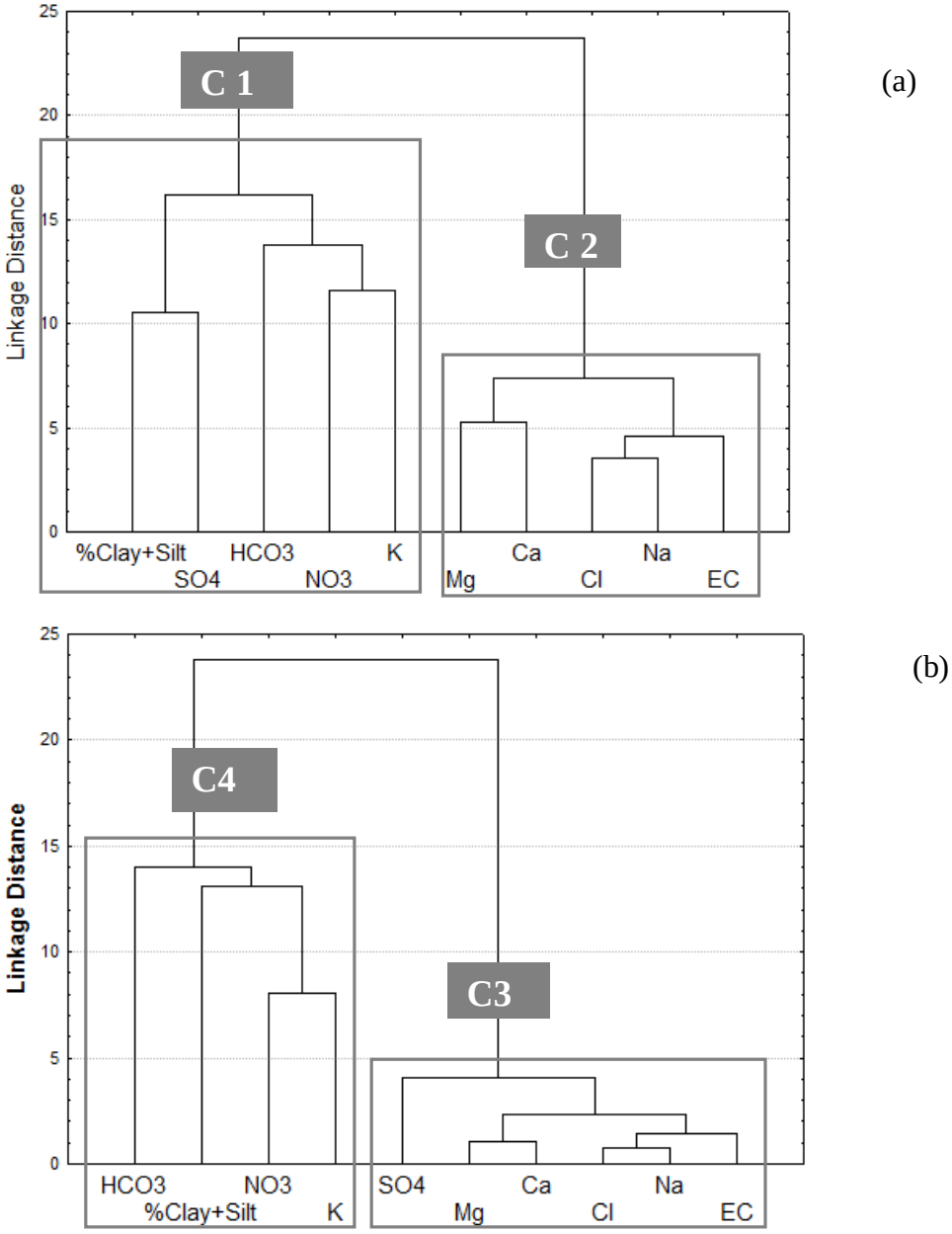

Fig. 33. Dendrogram from HCA in R-mode from (a) the wet season (b) the dry season

The analysis applied for the wet season showed that the data is explained by three principal component factors (Tab. 5) accounting for 76.16 % of the total cumulative variance. Significant loadings are taken higher than 0.75, moderate loading ranges between 0.40 and 0.75 and a loading of less than 0.4 is considered insignificant.

- The first factor F1 accounts for 51.03 % of the total variance and it is contributed by the following variables: ECe, Cl, Na, Ca, Mg, and SO_4 associated to salinity (Tab. 6) (Visconti et al., 2009).

- The second factor F2 explains 14.16 % of the total variance and is contributed by the Clay+Silt ratio (factor loading 0.54). Note that SO_4 shows a moderate loading for this factor (=0.45) and that NO_3 and HCO_3 show both moderate negative loadings (-0.44 for NO_3 and -0.50 for HCO_3). In general, SO_4, HCO_3 and NO_3 are involved in redox processes (De Montety et al., 2008; Kim et al., 2004; Koh et al., 2007). This factor is likely to be related to redox processes occurring within the presence of clay and silt.
- The third factor F3, accounts for 10.98 % of the total variance and it is mainly contributed by nitrate, presenting a high loading of 0.7. The ratio of Clay+Silt presents a mo+
- derate loading (0.6) for F3. Fine textured layers are likely to accumulate nitrate more than sandy ones (Baran et al., 2007). Therefore F3 would explain the nitrate pollution.

Tab. 5. Eigenvalues of correlation matrix and cumulative total variance.

	Factor	Eigenvalue	Tot. Var. (%)	Cum-Eigenvalue	Cum. Tot.Var.(%)
Wet season	**1**	5.10	51.03	5.10	51.03
	2	1.42	14.16	6.52	65.18
	3	1.10	10.98	7.62	76.16
	4	0.82	8.19	8.44	84.35
	5	0.67	6.67	9.10	91.02
	6	0.52	5.17	9.62	96.19
	7	0.24	2.42	9.86	98.60
	8	0.07	0.73	9.93	99.33
	9	0.05	0.53	9.99	99.86
	10	0.01	0.14	10.00	100.00
	Factor	**Eigenvalue**	**Tot. Var. (%)**	**Cum-Eigenvalue**	**Cum. Tot.Var. (%)**
Dry season	**1**	6.71	67.10	6.71	67.10
	2	1.11	11.12	7.82	78.22
	3	0.96	9.62	8.78	87.83
	4	0.87	8.72	9.66	96.55
	5	0.25	2.48	9.90	99.03
	6	0.06	0.60	9.96	99.63
	7	0.02	0.24	9.99	99.88
	8	0.01	0.07	9.99	99.95
	9	0.00	0.04	10.00	99.99
	10	0.00	0.01	10.00	100.00

Tab. 6 Factor loadings for variables. Moderate to strong loadings are highlighted in grey

		Factor 1	Factor 2	Factor 3
Wet season	Ece	0.96	-0.07	-0.07
	Ca	0.89	-0.11	0.01
	Mg	0.89	-0.32	-0.06
	Na	0.94	0.03	-0.12
	K	0.29	-0.59	0.13
	HCO3	-0.49	-0.50	0.06
	Cl	0.91	0.09	-0.33
	SO4	0.62	0.45	0.19
	NO3	0.34	-0.44	0.71
	%Clay+Silt	0.26	0.54	0.63
		Factor 1	Factor 2	Factor 3
Dry season	Ece	-0.99	0.05	0.11
	Ca	-0.98	0.05	0.11
	Mg	-0.99	0.05	0.12
	Na	-0.98	0.07	0.14
	K	-0.46	-0.28	-0.81
	HCO3	-0.08	0.76	-0.24
	Cl	-0.97	0.07	0.15
	SO4	-0.97	0.00	0.04
	NO3	-0.83	-0.09	-0.37
	%Clay+Silt	-0.22	-0.66	0.17

For the dry season data is explained by two factors accounting for 78.22 % of the total variance (Tab. 5)

- Factor F1 explains 67.10% of the data and contributed by: ECe, Cl, Na, Ca, Mg, SO_4 and NO_3. F1 is related to salinity and the process of concentration under evaporation (Tab. 6).
- F2 accounting for 11.2 % presents a high loading for HCO_3, and a negative moderate loading for the ratio of clay and silt. It can represent the alkalinity.

To study the different processes revealed through PCA along the vadose zone profiles, we have plotted the vertical distribution of each factor for the wet season (vertical distribution of factors for the dry season was highly distorted because of high factor score at the topsoil). Fig. 34 shows that the layers containing clay and silt, mainly in PN4 and PN6, are getting enriched with salts and nitrates. In PN5, irrigated with a high saline water (EC~9 mS/cm), the dominant process is probably salinization. Indeed, F1 presents high scores in this profile especially at the topsoil

and at the depth of 6 m b.s.l presenting a high clay+silt ratio. Note that no high scores for F1 were registered in the first two meters in PN4, indicating the leaching process under rainfall.

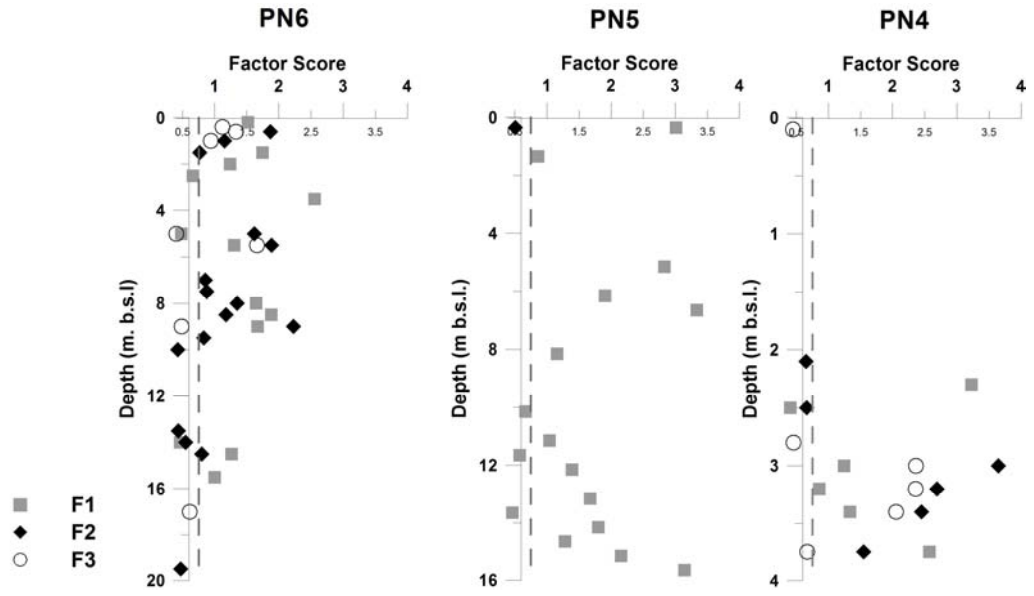

Fig. 34 Factor score profiles for PN4, PN5 and PN6 for (a) the wet season, (b) the dry season. The limit for appreciating the high loading (=0.75) is presented with a grey dashed line

3.3. XRD analysis and Saturation indexe calculations

Dominant minerals, detected using XRD analysis, are quartz followed by calcite (Fig. 35). No presence of gypsum neither anhydrite was observed in soil samples using this technique. This is possibly due to the sampling method as no precaution was taken while conserving the samples because the objective of the experiment was principally the study of soluble salts. Hence, gypsum can be altered by organic matter, mainly present in the topsoil samples.

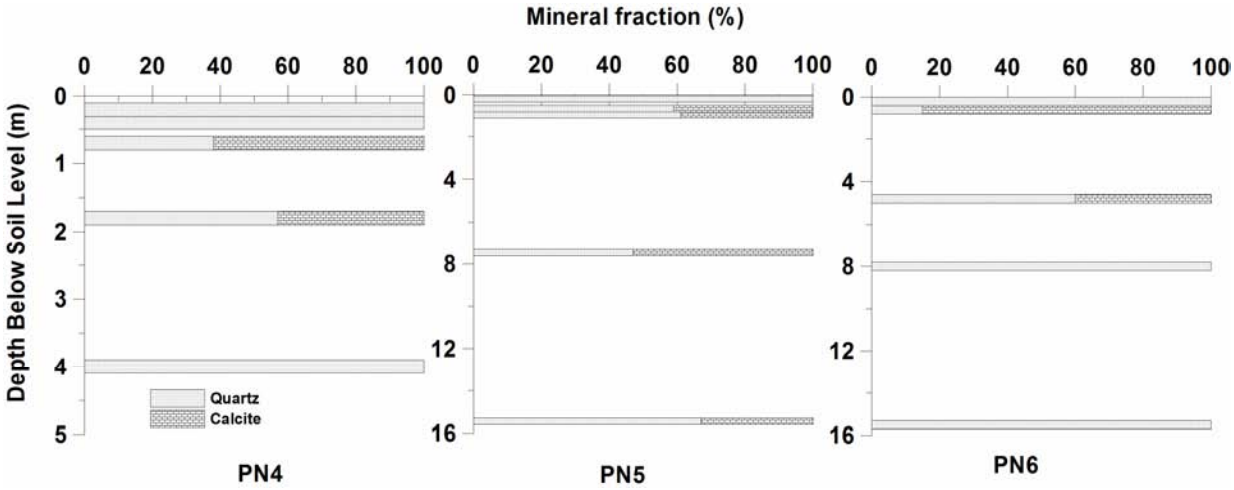

Fig. 35 Semi-quantitative estimation of quartz and calcite fraction measured in (a) PN4 (b) PN5 (c) PN6

Depth profiles of Saturation Indexes (SI) of calcite dolomite and gypsum calculated for PN4, PN5 and PN6 for the wet and the dry seasons are shown in Fig. 36. We observe that most of the samples are oversaturated or in equilibrium with regards to calcite and dolomite and undersaturated with regards to gypsum. Visconti et al. (2010) state that calcite and gypsum are abundant in areas under semi-arid and dry sub-humid climates. Besides, quaternary deposits in coastal areas are often rich in shell fragments (abundant in Korba plain) and calcite is known to be the primary constituent of marine organisms shells. However, gypsum (considered as a semi-soluble salt) is more soluble than calcite which is therefore less prone to dissolution in soils (Shahid and Abdelfattah, 2009; Visconti et al., 2010). Thus, calcite is more abundant in soils than gypsum. The XRD analysis is in agreement with this statement. Moreover, gypsum usually occurs together with calcite (Visconti et al., 2010).

Fig. 36 shows that, for the three plots, SI gypsum is higher in the dry season. However, this result is only visible in the topsoil. Moreover, the soil solution reaches equilibrium in the topsoil announcing possible gypsum precipitation.

Mohammadou et al (1999) reported that saturation with respect to gypsum was correlated with the concentration of the solution. Inversely the SI of calcite decreases during the wet season in the topsoil as a result of dissolution. However, the soil solution remains oversaturated with respect to calcite.

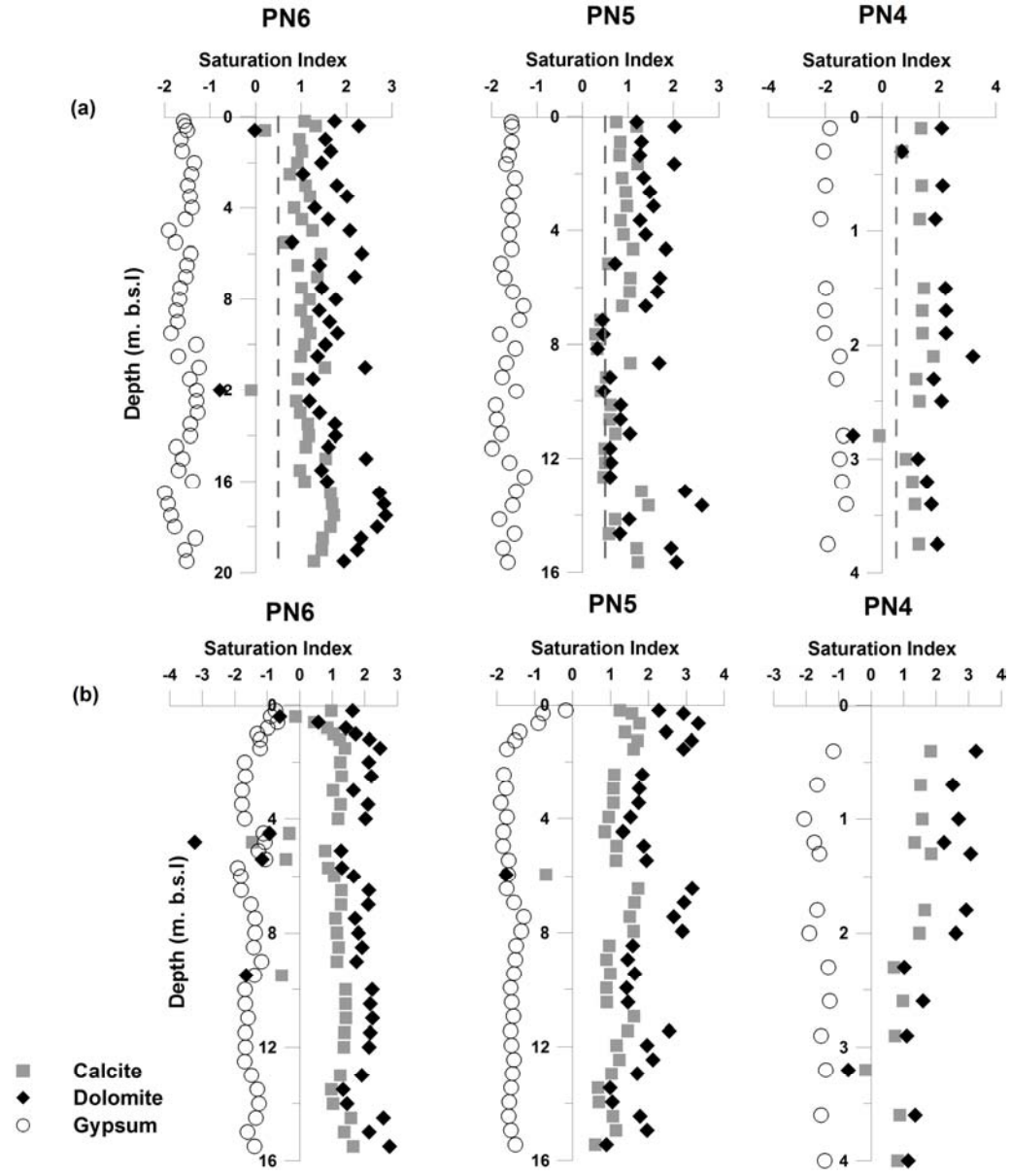

Fig. 36 Saturation indexes profiles for PN4, PN5 and PN6 during (a) the wet season and (b) the dry season

3.4. Soil and groundwater interactions

It is interesting to notice that soil water in the vicinity of groundwater is considerably less concentrated than groundwater. This result is observed in the six soil profiles and for all investigated solutes. An exception is made for the nitrate concentration in PN6 (Fig. 32 and Fig. 31).

Jemai (1998) in Mhiri et al. (1998) reported that the measured groundwater salinity in Tefelloun (Korba plain) increased from 5 to 7 mS/m after an exceptional rainy season in 1995. She argued that this sudden rise of groundwater salinity was a result of the leaching process acting on salts accumulated in the topsoil, during the last years.

Fig. 37 shows the concentrations of major ions and nitrates measured in the groundwater in august 2006 vs. those measured in the topsoil for PN6 and PN5 in the dry season. We have found strong correlations (R^2=0.98 for PN5, and R^2= 0.97 for PN6). Besides, as the groundwater is used for irrigation, it is evaporated in the topsoil and getting concentrated with a factor of 3 and 1.2 for respectively PN5 and PN6.

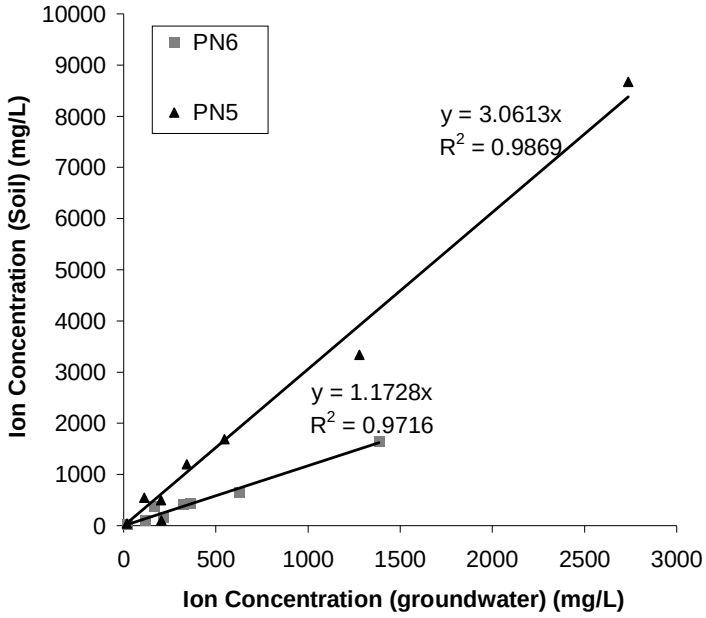

Fig. 37 Ion concentrations of groundwater vs. ion concentration measured in the soil saturated past extracts

3.5. Soil salinization trends and alkalinisation hazard assessment.

To assess the irrigation water's (coming from the groundwater) risk to induce soil salinization and/or alkalinization we have plotted the groundwater SAR versus EC (Fig. 38). The Wilcox diagram indicates that groundwater presents a high risk of salinization (Classes C3, C4). Moreover, many samples with EC exceeding 5 mS/cm plotted outside Wilcox diagram. However no risk of sodicity was detected. Soil samples are classified from medium to very high regarding salinity hazard. Note that, in the literature the threshold of soil salinity (expressed in ECe) for most of the crops is about 4 mS/cm (Rhoades et al., 1992). The risk of sodicity increased with the risk of salinity. The sodicity hazard ranged from low to high.

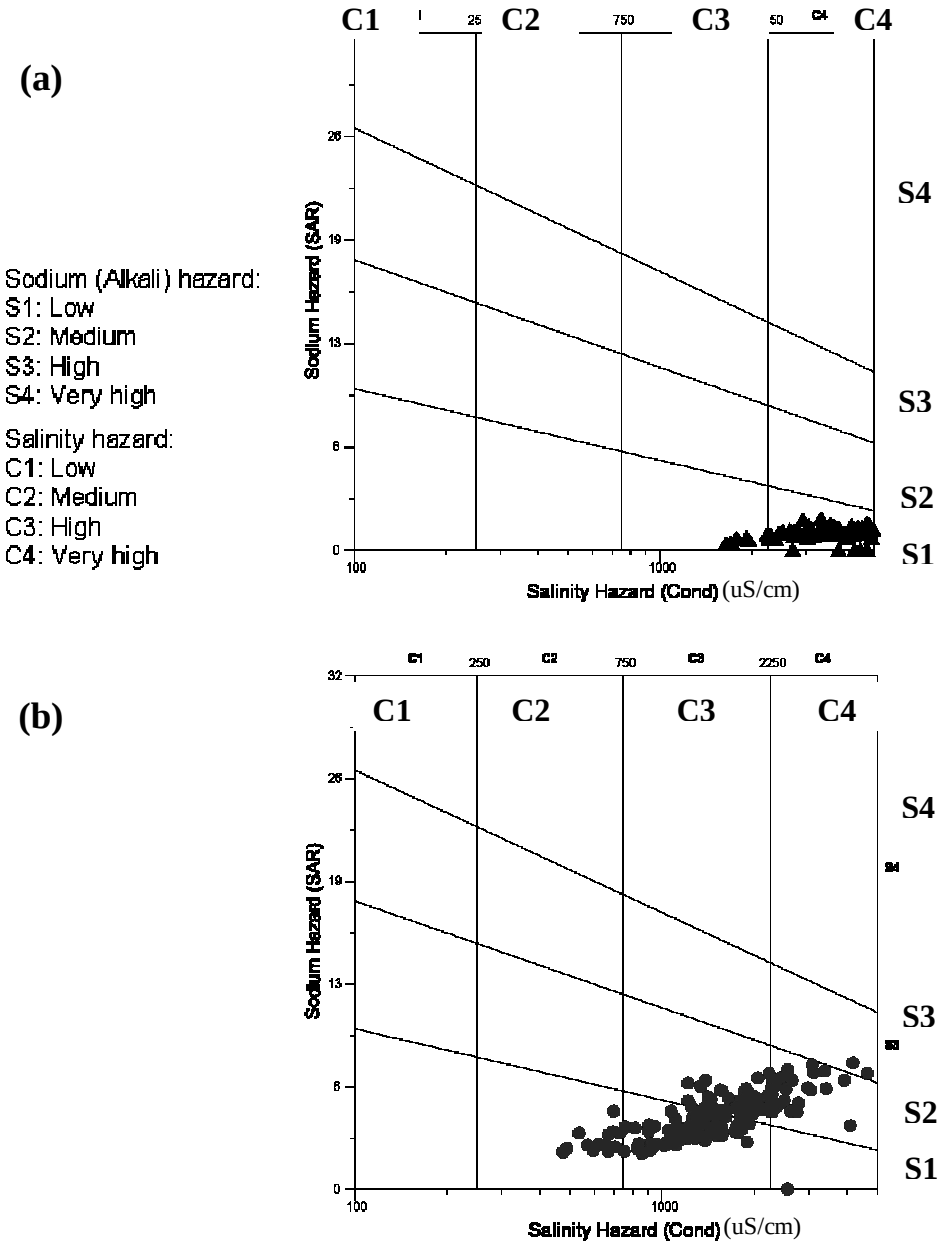

Fig. 38 Wilcox diagram for salinity (Electrical conductivity (uS/cm)) and sodium hazard for (a) groundwater (b) soil water

3.5.1 Salinization trends under evaporation

The concentration diagram (Fig.12) shows that Na and Mg concentrations increase at the same rate as chloride. Therefore these two elements are not involved in any precipitation. Inversely, Ca and SO_4 concentrations increase at a lower rate than chloride indicating respectively calcite and gypsum precipitation. RAcalcite is negative (Fig. 40), Ca increases and alkalinity decreases (Fig. 39) with agreement to RA concept. RAcacite+gypsum is also negative and the rate of decrease SO_4 becomes lower than the increase rate of Ca (Fig. 39) in compliance with the generalized RA concept. Hence, the soil solution is following a neutral saline trend and does not present a risk of alkalinization. Bouarfa et al. (2009) applied the RA concept to irrigation water in Fatnassa Oasis in Tunisia and found that the main trend was toward neutral salinity. Besides, Mohammedou et al. (1999) found the same sequence of precipitation, i.e. calcite>gypsum when applying the RA concept to clay dunes in the Senegal Delta in Mauritania.

Furthermore, Nezli et al (2007) and Barbiéro et al. (2001) investigated the role of fluorite in the control of salinization processes under evaporation.

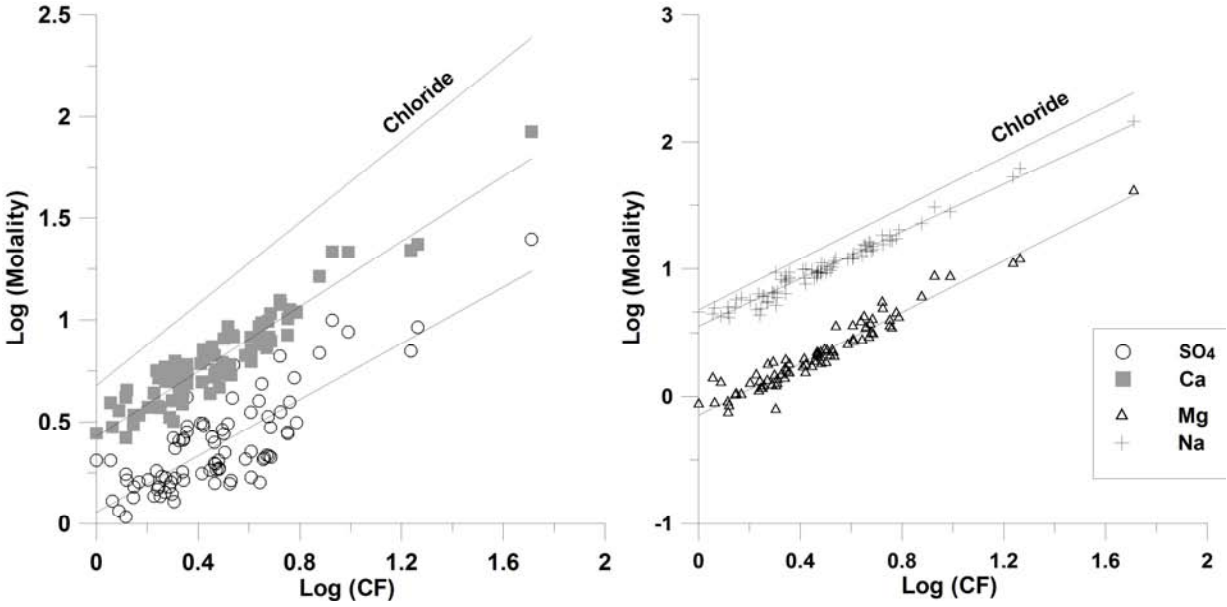

Fig. 39 Concentration diagrams for Ca, Mg, SO_4 and Na

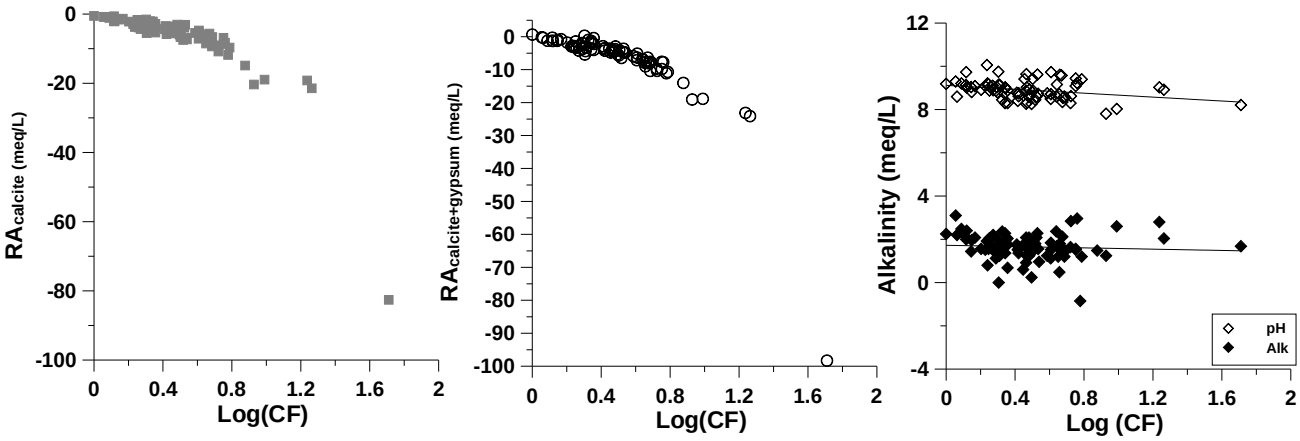

Fig. 40 Concentration diagrams for RAcalcite, RAcalcite+gypsum, alkalinity and pH

To confirm the generalized RA analysis, we have depicted the Log(CF) vs. Saturation Indexes of calcite, dolomite and gypsum (Fig. 41). We notice that the initial solution is already saturated with regards to calcite and undersaturated with regards to gypsum. This result would probably explain the detection of calcite using XRD analysis. When the solution begins to concentrate, the Saturation Index of gypsum increases and the solution equilibrates allowing gypsum to precipitate. Inversely, the Saturation Index of calcite decreases indicating precipitation, and then increases again after the Saturation Index of gypsum reaches equilibrium.

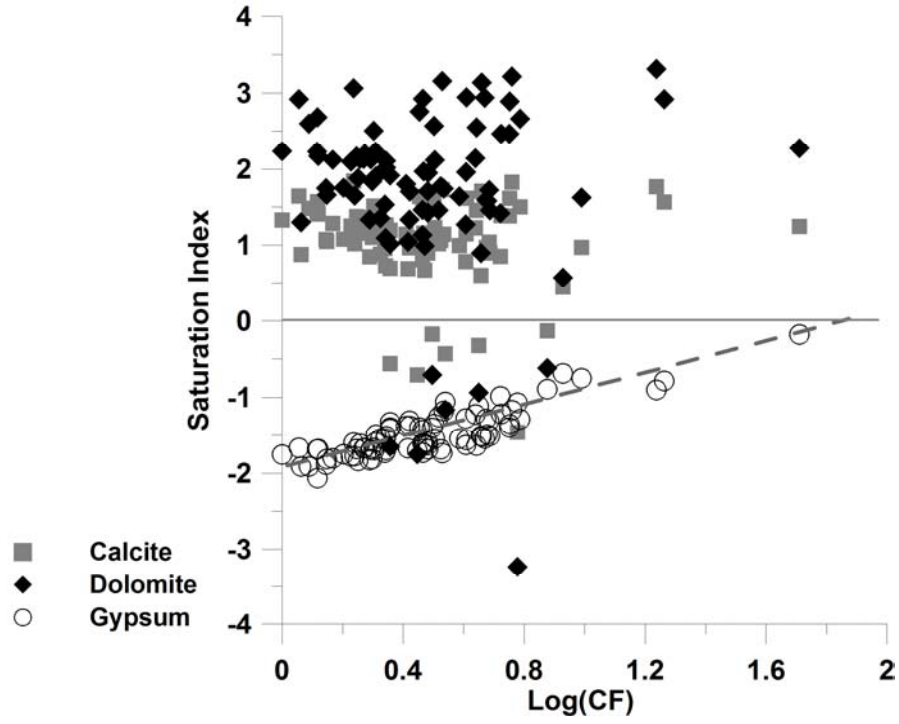

Fig. 41 Concentration Factor vs. Saturation Indexes of calcite, dolomite and gypsum. Equilibrium area is dashed in grey

4. Conclusion

The experimental data analysis showed that the soil solution is concentrated during the dry season because of the saline aspect of irrigation water and high rates of evapotranspiration. Indeed, ECe reached 17.5 mS/cm. Plotted in a Wilcox diagram for the assessment of salinity and sodicity hazard, groundwater showed high to very high risk of salinization and low risk of sodicity. Soil solution presents moderate to very high risk of salinization and medium to high risk of sodicity. Crop salt tolerance indicators worsen during the irrigation season resulting in poor yields. However, the light textured characteristic of the studied soils allows important leaching of the accumulated salts under rainfall. After the wet season, we observe a high rate of dilution in the topsoil (e. g. ECe decreases from 17.53 to 2.73 mS/cm in PNS5). Regarding groundwater quality, such soils present an important capacity for transfer of chemical substances.

Depth profiles of different ions showed that the groundwater was much more mineralized than the neighbouring soil water. However, Piper diagram suggests that water and soil present the same origins.

PCA is in agreement with HCA analysis revealed that three major processes are taking place in the soil solution: salinization processes related to concentration and precipitation, N-fertilisers contamination expressed in the high correlation between NO_3, K and SO_4 and finally redox processes.

The generalized RA was applied to all soil samples issued from transect S1 and collected in the dry season. It revealed that, when the soil solution gets concentrated, two minerals precipitate according to the sequence calcite>gypsum. The calculation of Saturation Indexes of respectively calcite and gypsum confirmed this result. The RA analysis also predicted that the soil solution would follow a neutral saline pathway.

.

References

Abdelfattah, M., A., Shahid, S., A. and Othman, Y., R., 2009. Soil Salinity Mapping Model Developed Using RS and GIS - A Case Study from Abu Dhabi, United Arab Emirates. European Journal of Scientific Research, 26(3): 342-351.

Al-Droubi, A., Fritz, B., Gac, J.-Y. and Tardy, Y., 1977. Prediction of the chemical evolution of natural waters during evaporation. In: T.Y.e.W.-r.i.S. Paquet H. (ed.) (Editor), Water-Rock Interaction : International Symposium, Strasbourg pp. 13-22.

Al Atiri, R., 2004. Les efforts de modernisation de l'agriculture irriguée en Tunisie, Projet européen Inco-Wademed sur la "Modernisation de l'agriculture irriguée dans les pays du Maghreb", Rabat.

Appelo, C.A.J. and Postma, D., 2005. Geochemistry, Groundwater and Pollution, second ed. Balkema, Rotterdam.

Ayers, R., S., and Westcot, D., W., 1994. Water quality for agriculture-FAO irrigation and drainage paper. FAO-Food and Agriculture Organization of the United Nations, Rome, Italy.

Baba, A., Howard, K., Gunduz, O. and Chambel, A., 2006. Groundwater in semi-arid mediterranean areas: desertification, soil salinization and ecosystems, Groundwater and Ecosystems. Springer Netherlands, pp. 47-58.

Baran, N., Richert, J. and Mouvet, C., 2007. Field data and modelling of water and nitrate movement through deep unsaturated loess. Journal of Hydrology, 345(1-2): 27-37.

Barbiéro, L., Valles, V., Régeard, A. and Cheverry, C., 2001. Residual alkalinity as tracer to estimate the changes induced by forage cultivation in a non-saline irrigated sodic soil. Agricultural Water Management, 50(3): 229-241.

Ben Hamouda, M.F., 2009. Origine de la minéralisation dans l'aquifère plio-quaternairede la côte orientale du cap Bon (Tunisie). Sècheresse, 20 (1): 78-86.

Bouarfa, S., S. Marlet , A. Douaoui, T. Hartani , I. Mekki, W. Ghazouani , I. Ben Aissa , B. Vincent , F. Hassani and Kuper, M., 2009. Salinity patterns in irrigation systems, a threat to be demystified, a constraint to be managed: Field evidence from Algeria and Tunisia. Irrigation and Drainage, 58 (S3): S273 - S284.

Causapé, J., Quìlez, D. and Aragüès, R., 2006. Irrigation efficiency and quality of irrigation return flows in the Ebro river basin: an overview. Environmental Monitoring and assessment, 117: 451-461.

Chhabra, R., 1996. Soil Salinity and Water Quality. Balkema, Brook-. field, VT, USA, 284 pp.

Condom, N., Marlet, S. and LAFOLIE, F., 2002. Hydrogeochemical modelling of soil salinisation, alkalinisation and sodification: presentation and calibration of the PASTIS model Actes de l'atelier du PCSI,, Montpellier, France.

CRUESI-Tunisie, 1970. Rapport technique. Recherche et formation en matière d'irrigation avec des eaux salées, 1963-1969 +multigr. tableaux, PNUD-UNESCO, Paris.

De Montety, V., Olivier, R., Christine, V.-C., Bernard, B., Daniel, H. and Vincent, V., 2008. Origin of groundwater salinity and hydrogeochemical processes in a confined coastal aquifer: Case of the Rhône delta (Southern France). Applied Geochemistry, 23: 2337–2349.

Droubi, A., Cheverry, C., Fritz, B. and Tardy, Y., 1976. Géochimie des eaux et des sels dans les sols des polders du lac Tchad: Application d'un modèle thermodynamique de simulation de l'év aporation. Chemical Geology, 17: 165-177.

Gerakis, A. and Baer, B., 1999. A computer program for soil textural classification. Soil Science Society of America Journal. 63: 807-808.

Gerakis, A. and Baer, B., 2010. T R I A N G L E: A Program For Soil Textural Classification http://nowlin.css.msu.edu/software/triangle_form.html.

Grassi, S., Cortecci, G. and Squarci, P., 2007. Groundwater resource degradation in coastal plains: The example of the Cecina area (Tuscany - Central Italy). Applied geochemistry, 22: 2273-2289.

Hillel, D., 2000. Salinity Management for Sustainable Irrigation: Integrating Science, Environment, and Economics (Environmentally and Socially Sustainable Development. Rural Development). World Bank, 92 pp.

Jemai, S., 1998. Evolution de l'état de la nappe de la nappe de Korba: Etude hydrogéochimique et modélisation numérique. Master Thesis, Institut National Agronomique de Tunis, 180 pp.

Job, J.-O., 1992. Les sols salés de l'oasis d'El Guettar (Sud tunisien). Thèse de Doctorat : Physiol.,biol. des organismes et des populations Thesis, Université de Montpellier 2, Montpellier, France.

Katerji, N., van Hoorn, J.W., Hamdy, A., Karam, F. and Mastrorilli, M., 1996. Effect of salinity on water stress, growth, and yield of maize and sunflower. Agricultural Water Management, 30(3): 237-249.

Katerji, N., van Hoorn, J.W., Hamdy, A. and Mastrorilli, M., 1998. Response of tomatoes, a crop of indeterminate growth, to soil salinity. Agricultural Water Management, 38(1): 59-68.

Katerji, N., van Hoorn, J.W., Hamdy, A. and Mastrorilli, M., 2000. Salt tolerance classification of crops according to soil salinity and to water stress day index. Agricultural Water Management, 43(1): 99-109.

Kijne, J.W., 2003. Water productivity under saline conditions. In: J.W. Kijne, R. Barker and D. Molden (Editors), Water Productivity in Agriculture: Limits and Opportunities for Improvement CABI Publishing, Wallingford, UK, pp. 89-102.

Kim, K., Rajmohan, N., Kim, H.J., Hwang, G.-S. and Cho, M.J., 2004. Assessment of groundwater chemistry in a coastal region (Kunsan, Korea) having complex contaminant sources: a stoichiometric approach. Environmental Geology 46: 763-774.

Koh, D.-C., Ko, K.-S., Kim, Y., Lee, S.-G. and Chang, H.-W., 2007. Effect of agricultural land use on the chemistry of groundwater from basaltic aquifers, Jeju Island, South Korea. Hydrogeology journal, 15: 727–743.

Metternicht, G. and Zinck, A., 2009. Remote Sensing of Soil Salinization: Impact on Land Management. CRC Press. Taylor and Francis, 377 pp.

Mhiri, A., Tarhouni, J., Hachicha, M. and Lebdi, F., 1998. Approche systémique des risques de salinisation par andoréisation anthropique. Etude et Gestion des Sols, 5: 257-268.

Mohamedou, A.O., Aventurier, A., Barbiero, L., Caruba, R. and Valles, V., 1999. Geochemistry of Clay Dunes and Associated Pan in the Senegal Delta, Mauritania. Arid Soil Research and Rehabilitation, 13(3): 265 - 280.

Nezli, I.E., Achour, S. and Djabri, L., 2007. Approche geochimique des processus d'acquisition de la salinite des eaux de la nappe phreatique de la basse vallée de l'oued M'ya (Ouargla). Larhyss Journal, 6: 121-134.

Parkhurst, D., 1995. User's guide to PHREEQC: a computer program for speciation, rreaction-path, advective-transport and inverse geochemical calculations, US Geol Surv Water-Res.

Qadir, M., Sharma, B., R., , Bruggeman, A., Choukr-Allah, R. and Karajeh, F., 2007. Non-conventional water resources and opportunities for water augmentation to achieve food security in water scarce countries. Agricultural Water Management, 87(1): 2-22.

Rhoades, J.D., Chanduvi, F. and Lesch, S., 1999. Soil salinity assessment. Methods and interpretation of electrical conductivity measurements- FAO irrigation and drainage paper 57. FAO-Food and Agriculture Organization of the United Nations, Rome, Italy, 166 pp.

Rhoades, J.D., Kandiah, A. and Mashali, A.M., 1992. The use of saline waters for crop production - FAO irrigation and drainage paper 48. FAO-Food and Agriculture Organization of the United Nations, Rome, Italy.

Richards, L., A.,, 1954. Diagnosis and improvement of saline and alkali soils. Agric. Handbook 60. USDA, Washington D.C, 160 pp.

Salama, R.B., Otto, C.J. and Fitzpatrick, R.W., 1999. Contributions of groundwater conditions to soil and water salinization. Hydrogeology Journal 7: 46–64.

Shahid, S., A., and Abdelfattah, M., A., , 2009. Gypsum Polymorphism in the Desert Environment of Abu Dhabi Emirate. European Journal of Scientific Research, 29(2): 237-248.

Slama, F., Bahri, A., Bouarfa, S., Chaumont, C. and Bouhlila R., 2004. Pratiques d'irrigation et rôle du drainage pour le contrôle de la salinité -cas du périmètre irrigué Kalaât Landelous en Tunisie, Projet européen Inco-Wademed sur la "Modernisation de l'agriculture irriguée dans les pays du Maghreb", Rabat.

Slatni, A., Mailhol, J.C., Zairi, A., Château, G. and Ajmi, T., 2004. Analyse et diagnostic de la pratique de l'irrigation localisée dans les périmètres publics irrigués de la basse vallée de la Medjerda en Tunisie, Projet européen Inco-Wademed sur la "Modernisation de l'agriculture irriguée dans les pays du Maghreb", Rabat.

Sparks, D., L., 2003. Environmental Soil Chemistry. Academic Press, 350 pp.

Ulery, A., L., and Drees, L., Richard, 2008. Methods of Soil Analysis. Part 5: Mineralogical Methods. Soil Science Society of America, Madison, Wisconsin, USA, 544 pp.

Visconti, F., de Paz, J.M. and Rubio, J.L., 2009. Principal component analysis of chemical properties of soil saturation extracts from an irrigated Mediterranean area: Implications for calcite equilibrium in soil solutions. Geoderma, 151(3-4): 407-416.

Visconti, F., De Paz, J.M. and Rubio, J.L., 2010. Calcite and gypsum solubility products in water-saturated salt-affected soil samples at 25°C and at least up to 14 dS m−1. European Journal of Soil Science, 61(2): 255-270.

Chapter 5. Unsaturated modeling of salts movement through sandy soils to estimate solute irrigation return flow [5]

Abstract

HYDRUS1D was used to carry out simulations of flow and solute transport for three salinity profiles. The objective was to estimate the amount of salts loadings towards the groundwater. The model calibration was performed for the wet season under climatic boundary conditions. Results revealed that the irrigation return flux depended on the profile depth and the irrigation amount. The calculated yearly aerial recharge rate ranged from 0.7 to 6.2 % and. Solute fluxes were underestimated and insignificant and the soil profiles were getting concentrated over the simulations. The possible reasons are the temporal distribution of the climatic data input and the flow calibration.

[5]This chapter is based on:
Slama, F., Milnes, E.P. and Bouhlia, R., 2008. Calibrating unsaturated model parameters using electrical resistivity tomography imaging, Redbook N°320. International Association of Hydrological Sciences, Wallingford, pp. 148-153.

Slama, F. et al., 2007. Geochemical modelling of soil and groundwater salinization under irrigation with saline water. In: IAHS (Editor), MODELCARE, Calibration and Reliability in Groundwater Modelling, Copenhagen, Danemark.

1. Introduction

Agricultural activities are loading several chemical substances that are contaminating both soil and groundwater. Diverse contaminants are reaching the groundwater through irrigation return flow mechanisms. The extent of the phenomenon depends on the geological and climatic characteristics of the concerned site (Cardona et al., 2004; Richter and Kreitler, 1991). The quantification of irrigation return flows in terms of water and solute inflows is a relevant question. Indeed, it is important to integrate this component to the solute and water balance of the hydrological system.

Numerical and conceptual models are used to quantify and to predict solute flow of various agricultural chemical substances contaminating the groundwater. Baran et al. (2008) used AGRIFLUX (Banton and Larocque, 1997) to model nitrate movement through a homogeneous loess formation and to identify major processes influencing nitrate concentrations along the soil profiles. Javaux and Vanclooster (2004) simulated long term chloride transport through a layered soil. Rajmohan and Elango (2007) used HYDRUS2D (Simunek et al., 1999) to simulate both nitrate and chloride transport in the vadose zone and to estimate their respective solute fluxes towards groundwater. Araguès et al. (1985) calibrated an irrigation project model to propose the best management scheme that reduces the salt flux in the irrigation return flow.

Hydrogeochemical models (Bouhlila, 1999; Saaltink et al., 2004) are also used to identify processes occurring during contaminant migration through the vadose zone. They simulate multi-component reactive transport in variably saturated flow.
Unsaturated models are, in general, based on the Richards equation for variably saturated flow and the convection-dispersion equation for solute transport (Rajmohan and Elango, 2007). Van Genuchten (1980) developed his model for the unsaturated hydraulic conductivity as a function of soil water retention. However, the Van Genuchten model parameters remain difficult to estimate, mainly in field conditions and for deep soil profiles. Monitoring water content is important in variably saturated modelling. Yet, for deep soil profiles, water content measurements are not always easy to perform. Indirect techniques mainly based on the measure of the soil electrical resistivity were developed to study the water content temporal and spatial variability (Samouëliana et al., 2005).

ERT imaging is an electrical geophysical investigation technique being increasingly experimented for environmental purposes in the last decades. It offers the possibility of mapping the vadose zone at high resolutions. Kemna et al. (2002) found ERT imaging useful to capture the position and shape of the trajectory of a tracer plume. However, they stated that the use of ERT data to quantify transport characteristics in soils is poorly documented. In fact, in situ resistivity depends on a variety of parameters: water content, soil salinity, porosity, temperature and lithology. Daily et al. (1992) studied ground water movement in the vadose zone using ERT imaging.

.

Finally, 1D unsaturated models are useful for estimating solute return fluxes to groundwater. However, they can not predict groundwater concentrations as the former is mostly controlled by the regional flow. Unlike concentrations, those fluxes cannot be measured and cannot be calibrated. Moreover, integrating results of one dimensional simulations to a hydrogeological model is not an easy task. Mainly, because an important database of soil hydrodynamic and quality parameters has to be set up. Tawarakavi et al. (2008) developed a HYDRUS1D package to be used with MODFLOW. The HYDRUS1D package computes the recharge fluxes into groundwater in order to be integrated to MODFLOW. They tested this tool for several case studies.

In this study, we present an attempt to calibrate a model for salt movement through sandy soils under the given climatic and irrigation conditions. Data derived from the experimental study, will be used for the calibration purposes. The objective is to quantify the solute fluxes reaching the groundwater and to identify the patterns of salt fate through the soil profile.

2. Soil and groundwater investigations

The field study carried out along two transects in Korba coastal plain, was described and discussed in the previous chapters. Various techniques were used to analyse both sources and processes related to the soil and groundwater salinization. Results revealed that seawater intrusion and agricultural chemical loadings are the main sources of the groundwater mineralization. The study of the soil profiles chemistry showed that the topsoil solution gets concentrated during the dry season and presents, thereby, high electrical conductivities. The concentration of the topsoil solution under evaporation was controlled by calcite, and then gypsum precipitation. Besides, the survey revealed that

the topsoil solution was considerably diluted during the wet season indicating the leaching process under rainfall.

3. Electrical Resistivity Tomography (ERT) imaging for Water content profiles estimation

ERT imaging was used for determining water content profiles and for the estimation of Van Genuchten soil hydraulic parameters for the PN4, PN5 and PN6 plots located in the transect S1 (Fig.2).

During the drilling, the majority of samples were highly disturbed making it impossible to measure the water content. Hillel (1998) argues that water content should imperatively be measured on undisturbed samples to prevent high uncertainties. Otherwise it is preferable to rely on indirect techniques such as Time Domain Reflectrometry (TDR) (Dalton and Van Genuchten, 1986) and techniques based on soil electrical resistivity measurement (Liu and Yeh, 2004; McCutcheon et al., 2006; Samouëliana et al., 2005). An endeavour to convert ERT imaging measured resistivities to water content is presented herein. We have used the following relationship between resistivity and water content (Montoroi et al., 1997) :

$$R = a\, e^{b/\theta}$$

where R is the electrical resistivity (Ohmm), θ the water content and a and b are constants depending on the soil textural class as described by Montoroi et al. (1997).

Results are shown in Fig. 42. We note that for PN5, the converted water content profile is probably overestimated as the entire profile is almost saturated during the wet saeson. Thus, results have to be adjusted on the basis of a laboratory experiment in order to calibrate the a and b constants.

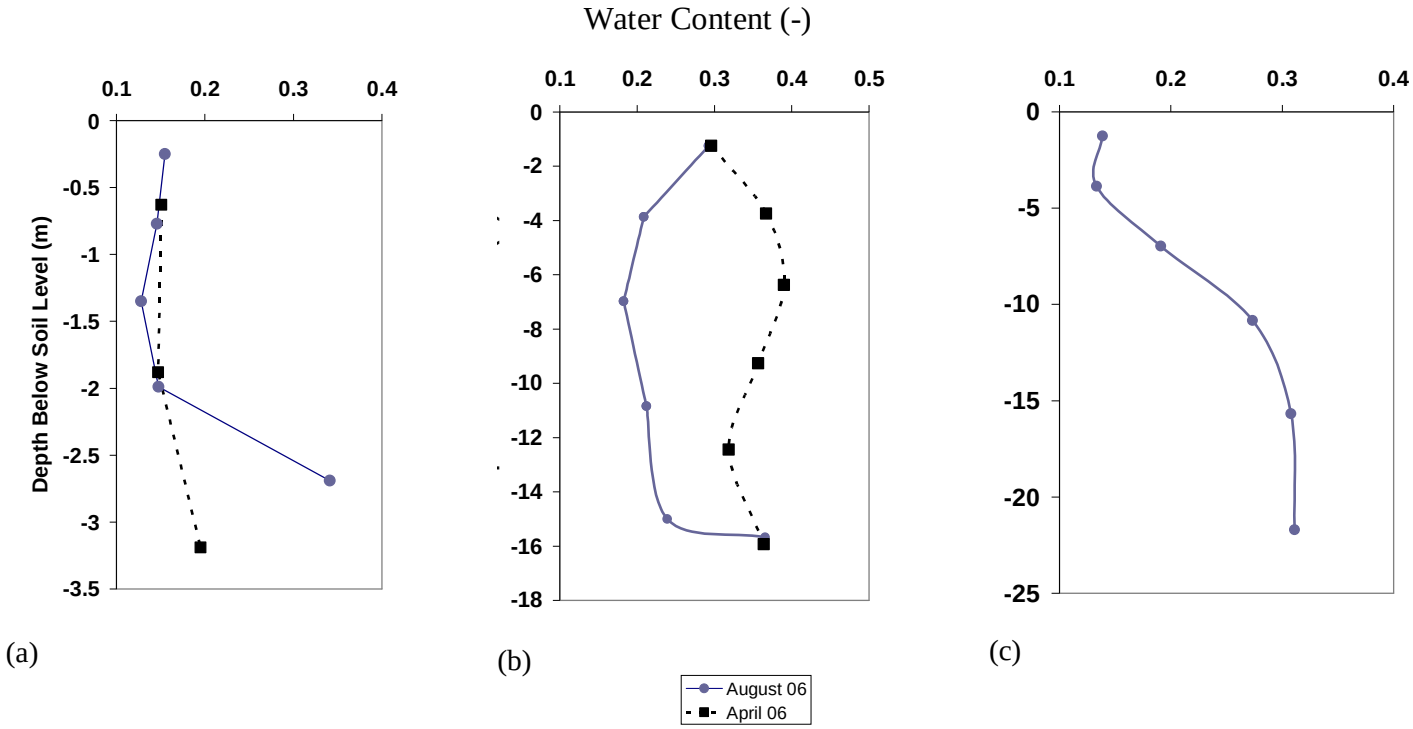

Fig. 42 Water content calculated from resistivity measurements in april 2006 and august 2006 for (a) PN4 (b) PN5 (c) PN6

Besides, simultaneous ERT imaging was combined with a controlled infiltration test for the purpose of calibrating unsaturated soil parameters (Slama et al., 2008) (Appendix C). Thirty-two electrodes were used with a spacing of 1 m leading to an investigation depth of about 5 m. Four ERT profiles were performed during the infiltration test, each with a time-lapse of one hour. Water, with an electrical conductivity of 9.53 mS/cm, was infiltrated into a furrow with a constant flux of 0.75 ls^{-1} during 4 hours. Resistivity difference distributions between the average reference profiles (before infiltration test) and four consecutive ERT profiles, carried out with a time-delay of one hour each, allowed mapping of the soil humidity change through time caused by the infiltration test. The migration of the centre of gravity of the humidity plume was used to estimate the saturated hydraulic conductivity *Ks* and was found to be 2.4 10^{-5} ms^{-1}. Using this hydraulic conductivity value, HYDRUS2D was then used to simulate water flow during the infiltration test and to calibrate the *a* and *n*-parameters on the measured ERT data set using the relationships between water content and resistivity developed by Montoroi et al. (1997).

4. Unsaturated modelling

The modelling study was carried out using HYDRUS1D (Šimùnek et al., 2008). HYDURS1D solves numerically (using Galerkin finite-element schemes) the Richards equation and the convection-dispersion solute transport equation in 1D variably saturated media.

HYDRUS1D was applied to model salt transport in the vadose zone for three profiles corresponding respectively to PN4 (depth=4 m), PN5 (depth=15 m) and PN6 (depth =25 m). In several studies, chloride, considered as a tracer, is used for the modelling of solute movement through the vadose zone (Javaux and Vanclooster, 2004). We will consider Total Dissolved Salts (TDS) as the variable for the solute transport simulations. Indeed, chloride is well correlated to EC (R^2=0.86) (Fig. 43) and thus to TDS. EC was converted into TDS using a multiplication factor of 0.7 (Ben Hamouda et al., 2009).

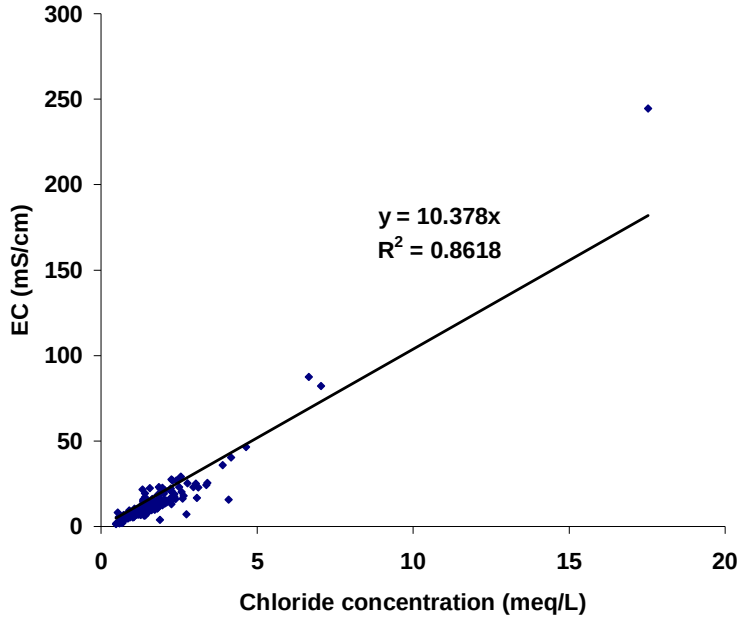

Fig. 43 Chloride concentrations vs. EC

4.1. Model input parameters

4.1.1 Meteorological data

The reference crop evapotranspiration, ET_o, was calculated according to the FAO Penman-Monteith method which is now recommended as the sole standard for the definition and computation of the reference evapotranspiration (Allen et al., 1998). ET_o is defined as the rate of evaptranspiration from "*the reference crop as a hypothetical crop with*

an assumed height of 0.12 m, with a surface resistance of 70 s m-1 and an albedo of 0.23, closely resembling the evaporation from an extensive surface of green grass of uniform height, actively growing and adequately watered" (Allen et al., 1998). The FAO Penman-Monteith equation for calculating daily ET_o (mm day^{-1}) using daily average data is shown in the following equation.

$$ETo = \frac{\frac{0{,}408\Delta}{\gamma}(R_n - G) + \frac{900}{T+273}u_2(e_s - e_a)}{\frac{\Delta}{\gamma} + (1 + 0{,}34u_2)}$$

where *Rn* is the net radiation at the crop surface (MJ m^{-2} day^{-1}); *G* the soil heat flux density (MJ m^{-2} day^{-1}); T the mean daily air temperature at 2 m height (°C); u_2 the wind speed at 2 m height (m s^{-1}); *es* the saturation vapor pressure (kPa); ea the actual vapor pressure (kPa); (*es-ea*) the saturation vapor pressure deficit (kPa); Δ the slope of vapor pressure curve (kPaC^{-1}); and γ the psychrometric constant (kPaC^{-1}).

ET_o was calculated using daily meteorological data (minimum temperature: Tmin, maximum temperature: Tmax, minimum relative humidity: Rhmin, maximum relative humidity Rhmax, wind speed and sunshine hours) from Oued souhil (Nabeul) and using ET_o calculator free software of UCL (based on FAO modified Penman Monthieth equation).

Hydrus1D atmospheric boundary condition requires inputting separately evaporation and transpiration. To split ET_o into potential evaporation and potential transpiration, it is recommended to use the equation proposed by Ritchie (1972):

$$Transpiration = Evapotranspiraion * SCF$$
$$Evaporation = Evapotranspiration * (1 - SCF)$$
$$SCF = 1 - Exp(-0.46 * LAI)$$

where SCF is the Surface Cover Fraction estimates from the Leaf Area Index (LAI). Evapotranspiration, evaporation and transpiration are expressed in mm.

To estimate the LAI, a polynomial function, based on the literature, was generated (Heuvelink, 1995).

4.1.2 Soil layers and properties

Soil profiles were assumed to be layered and were divided into layers corresponding each to a soil material. The choice of layers and the corresponding soil material was based on the grain size analysis (tab). More elaborated geostatistical techniques for handling heterogeneity are cited in the literature (Destouni, 1993; Sudicky et al., 2010). However, the number of parameters to calibrate in the case of unsaturated flow and solute transport problems remains important.

The soil hydraulic properties, according to the Van Genuchten model, were estimated using the Rosetta neural network prediction technique, integrated in HYDRUS1D (Tab.7). This technique requires the percentage of sand, silt and clay.

Tab. 7Van Genuchten parameters for PN4, PN5 and PN6

	Depth (m)	θ_r	θ_s	a	n	Ks (m/day)
PN4	0.9	0.08	0.43	3.60	1.56	2.00
	2.3	0.05	0.38	3.31	2.76	4.28
	2.8	0.07	0.39	2.44	1.33	0.12
	3.4	0.10	0.50	1.94	1.21	0.20
	4	0.08	0.40	2.64	1.26	0.11
	Depth (m)	θ_r	θ_s	a	n	Ks (m/day)
PN5	0.4	0.06	0.38	2.00	2.00	0.10
	1.5	0.05	0.38	2.00	2.00	1.39
	3.8	0.05	0.37	3.17	3.20	3.00
	4.9	0.05	0.38	3.42	2.03	0.50
	6.3	0.05	0.38	3.26	2.97	4.83
	7.8	0.05	0.38	3.62	1.53	0.65
	15	0.05	0.38	3.30	3.09	6.53
	Depth (m)	θ_r	θ_s	a	n	Ks (m/day)
PN6	1	0.05	0.38	3.42	1.43	1.00
	3	0.05	0.38	3.45	2.30	2.50
	4	0.05	0.37	3.15	3.04	5.75
	5	0.05	0.38	3.34	1.44	0.44
	5.5	0.08	0.43	1.38	1.38	0.06
	6.5	0.06	0.37	3.09	3.04	5.67
	9.5	0.06	0.38	3.06	1.48	0.43
	16.5	0.05	0.37	3.14	2.43	2.97
	17	0.05	0.38	3.28	1.43	0.43
	25	0.06	0.37	2.82	2.53	3.25

The molecular diffusion was derived from literature (Hu and Wang, 2003; Rajmohan and Elango, 2007) and was set equal to 0.2 m²/day. Dispersivities were considered according to the mesh size (=0.1 m)

4.1.3 Boundary and Initial conditions

HYDRUS1D offers several possibilities for the top and bottom boundary conditions regarding both flow and solute transport. Atmospheric boundary conditions with surface runoff were considered at the top of the profile. Besides, root water uptake is integrated to the model using Feddes model (Feddes et al., 1976) or the S-shape Model. Daily potential values of evaporation, transpiration and precipitation were added as variable boundary conditions. The code then computes actual transpiration and actual evaporation on the basis of soil saturation conditions. A constant water content was considered as the bottom boundary condition. The top and the bottom solute boundary conditions were assumed as concentration flux ones. The initial conditions were derived from the field study. Indeed, we have used the TDS and the water content, measured in august 2006, as initial solute (Fig. 34) and initial flow conditions (Fig.45) respectively.

4.2. Predictive scenarios

Daily measurements of rainfall, minimum Temperature, maximum Temperature, mean wind speed, mean relative humidity and insolation are available for Kelibia meteorological station located at 20 km north from transect S1. The recorded data covers the period from January 1970 to December 2001. The described time series was daily averaged for all climatic variables. The resulting average year will be considered as the type year to be used in prediction simulations. This method was widely used in building prediction scenarios (Baran et al., 2007). Nevertheless, the averaging technique, used as a procedure of rainfall forecasting is considered basic. Indeed, more elaborated models, as the Autoregressive Moving Average techniques (ARMA) are used to predict and generate rainfall time series (Burlando et al., 1993). One of the problems with using annual mean daily rainfall is that extreme values are not considered. Yet, extreme rainfall values could have an important effect on the leaching process (Hachicha et al., 2003). Evapotranspiration is even more difficult to predict as it is a function of at least four other variables. Interesting studies about analysing temporal trends of reference evapotranspiration are found in the literature (Bandyopadhyay et al., 2009; Liu et al., 2010; Xu et al., 2006). Developing such models needs yet a thorough knowledge of stochastic techniques applied to hydrological sciences.

In the absence of reliable published studies about climate change in the Tunisian context and the lack of an agro-socio-economic analysis integrating forecasts about future water

use by farmers, we have adopted three basic scenarios for carrying out the prediction simulations:

1. The first scenario, **SC1,** assumes that amounts of irrigation water will remain steady. Simulations will be run for a decade considering a yearly tomato crop starting at first April and ending by the 15th July. The distribution of the daily irrigation amounts were derived from a field study in Kalaat Landelous irrigated area (Lower Mejerda valley North East of Tunisia) (Slama et al., 2003; Slama et al., 2004). The total irrigation water amount, in the cited sudy, reached 1000 mm. in the present study we will consider the amount recommended by the FAO for the tomato crop, i.e; 600 mm (FAO, 2010).
2. The second scenario, **SC2**, suggests that irrigation decreases by 30 %, as a consequence of a possible conversion in the cropping system. We have observed that many farmers have already introduced tobacco replacing tomatoes. Indeed, tobacco is a more tolerate crop and requires slightly less irrigation amounts of water. Barley and forage crops are also replacing tomato in areas affected by high groundwater salinity. This scenario can also be associated to a better management of irrigation water quantities.
3. The third scenario, **SC3**, supposes that irrigation is abandoned. Simulations will be run for 20 years under the same climatic conditions.

5. Geochemical modelling

Simulations of geochemical modelling were performed using GEODENS numerical code. GEODENS is a density dependant variably saturated and multi-species geochemical model in porous media (Bouhlila, 1999) which solves the fluid conservation and the multi-species non conservative transport equations using the Finite Element Method.

Simulations were performed for a profile of 15 m (Slama et al., 2007). The soil water chemistry was derived from the groundwater composition measured in Well PN5 in august 2006. The objective was to study the precipitation of minerals under an evaporation cycle of 100 days.

6. Results and discussion

6.1. Unsaturated model calibration (HYDRUS1D)

Field data were used to calibrate the model for the three profiles. We considered 242 days starting from the 1st of September 2006 and ending on 30th of April 2007 as the calibration period. The model parameters will be calibrated using climatic data of the wet season without any irrigation inputs or plant water uptake. The model was run for sensitivity tests, by varying the flow and transport parameters. It was considered sensitive to hydraulic conductivity, dispersivity, molecular diffusion and evapotranspiration. Besides, only parameters of the upper layer had an impact on the results. After the calibration, evapotranspiration was reduced by 10%. The calibration results are shown in Fig. 44. The model, globally, reproduces the leaching process. However, soil salinity at the topsoil was overestimated for the three plots. Reliable measurements of water content would have improved the calibration results. Besides, rainfall is known to present high spatial variability and it was measured at 30 km from the studied plots. Spatial heterogeneity with regard to soil hydrodynamic properties and salinization patterns forms another difficulty for reproducing field data with modelling. Indeed, drip irrigated plots often show vertical and horizontal variability due to salt accumulation under the dripper.

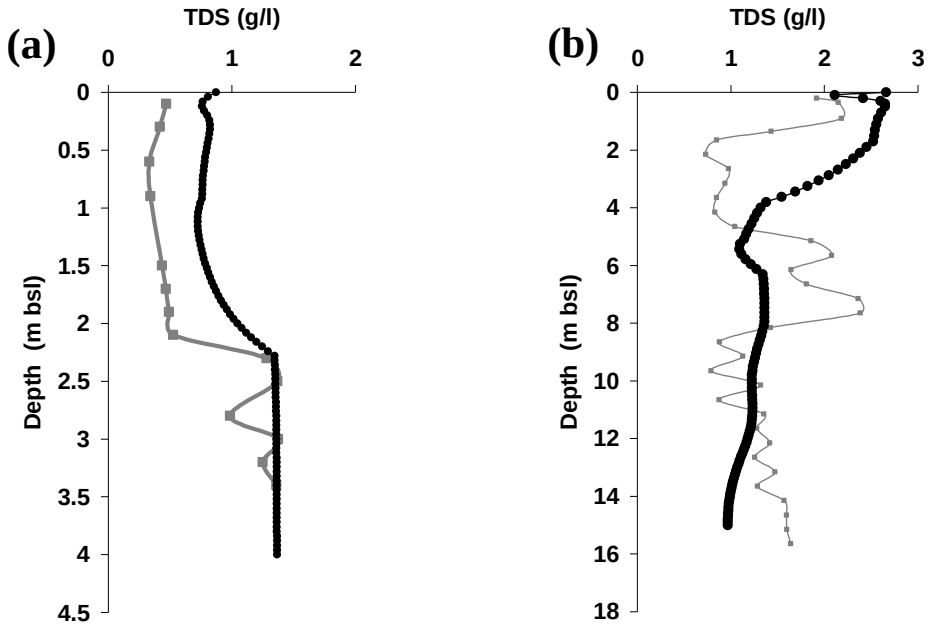

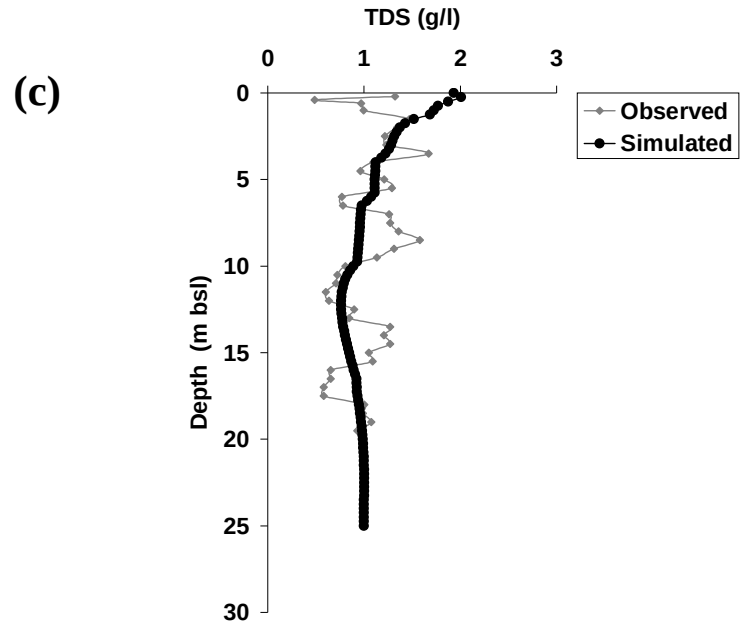

Fig. 44 Depth profiles of observed vs. simulated TDS (g/l) for (a) PN4, (b) PN5 and (c) PN6

6.2. Predictive simulations

Fig. 45 depicts the time evolution of the cumulative bottom solute flux simulated for PN4, PN5 and PN6 respectively according to the three prediction scenarios; SC1, SC2 and SC3. The main outcomes of the prediction study can be summarized as follows:

- The solute flux ranges from 2 10^{-5} to 2 10^{-3} g/m²/year. It decreases with the vadose zone thickness. For PN4, the solute flux is controlled by irrigation. In fact, the outflow is almost concurrent with the beginning of irrigation. The solute fluxes for PN5 and PN6 are controlled by both irrigation and rainfall (Fig. 45). Note that, for PN5, the increase rate of the solute flux is higher under rainfall suggesting a delay in the solute movement along the profile (Fig. 45). This situation can be explained by a piston flow.
- Solute flux considerably decreases with the reduction of irrigation water amounts by 30% (Fig. 45). Moreover, the root water uptake remains the same for both scenarios. This result is important with regard to water resources management. The application of adequate irrigation amounts would, firstly, conserve water by preventing losses through deep percolation and, secondly, reduce amounts of salt loading towards the groundwater.

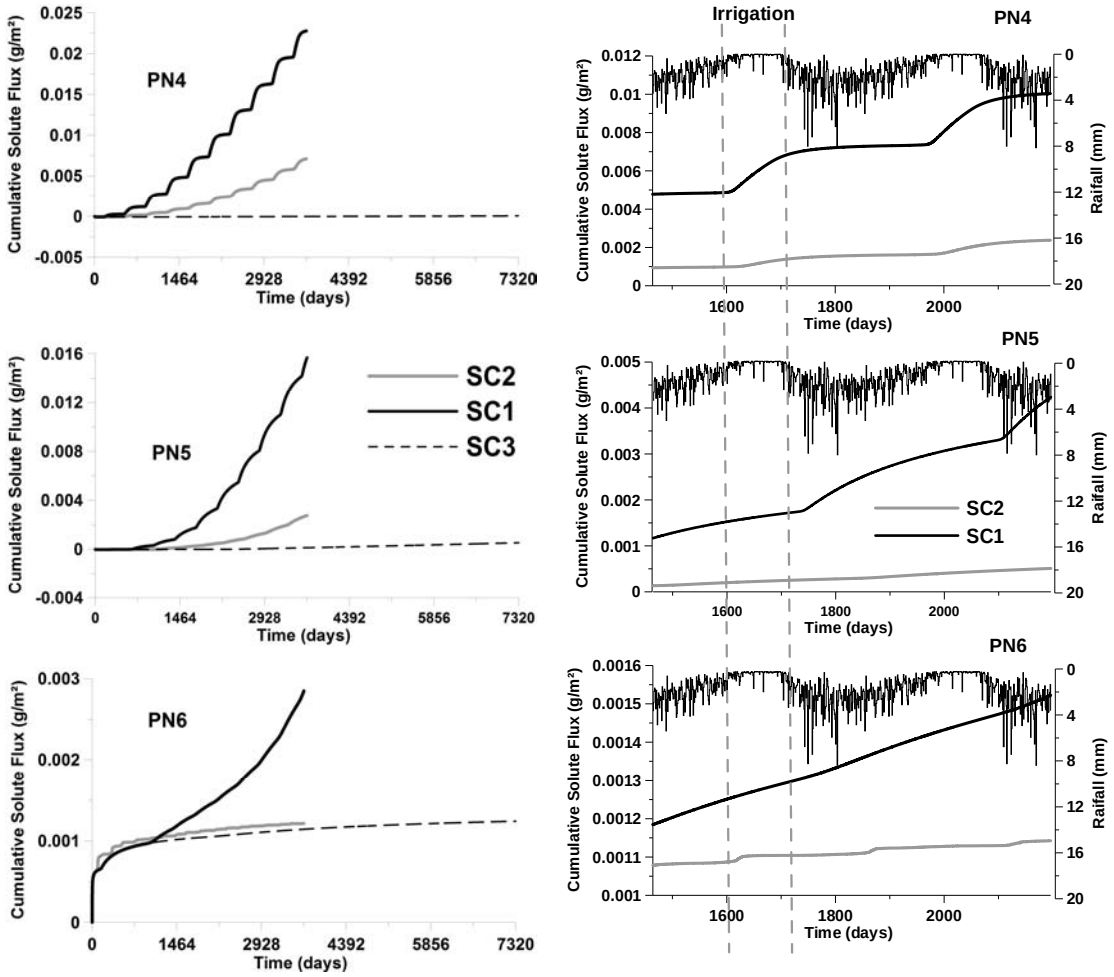

Fig. 45 Time evolution of calculated solute fluxes for PN4, PN5 and PN6 based on SC1, SC2 and SC3 scenarios

- Calculated amounts of loaded salts are insignificant because, for all simulation runs, according to SC1 and SC2, the soil profiles get highly concentrated. Various reasons can explain the salt accumulation. The mean annual daily ETo (derived from measured data in Kelibia station) is higher than that measured from 15/8/2006 to 30/5/2007 in Oued Souhil station (Fig. 48).

  Besides, time distribution of rainfall is considerably different in the two cases (data measured in Oued Souhil and mean annual daily rainfall calculated for Kelibia station). Indeed, rainfall recorded in Oued Souhil is characterized by a high irregularity regarding time and intensity. Note that extreme values reaching 70 mm/day and 30 mm/day were recorded. Moreover, the soil solution was considerably diluted under theses two episodes (Fig. 46). Whereas, the calculated mean annual daily rainfall barely reaches 10 mm/day. It is important to consider a deep analysis of

the climatic data forecast used for predictive scenarios. Indeed, the salt movement and accumulation in the soil are highly sensitive to meteorological data inputs.

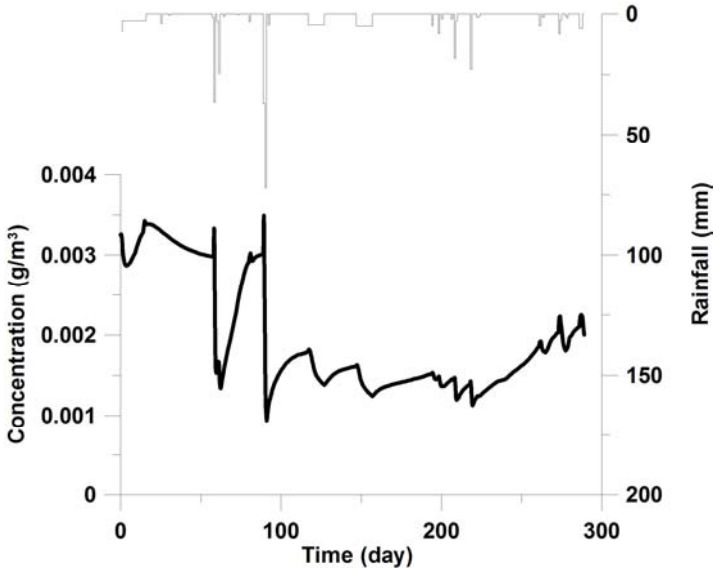

Fig. 46 Simulated concentrations at 0.3 m depth for PN6 under rainfall and ETo measured in Oued Souhil from 15/8/2006 to 31/5/2007

To test this sensitivity, we have run two simulations (from 15/8/2006 to 30/5/2007) for each of the profiles PN6 and PN5. The first simulation was run under rainfall and ETo measured in Oued Souhil from 15/8/2006 to 31/5/2007 whereas the second was run under mean annual daily rainfall and ETo measured in Kelibia. The results show that the soil solution concentration is higher for the simulation computed with mean annual daily values (Fig. 47). Moreover, as the inputs are steady, the concentration will increase for longer simulations following a cumulative process.

Transport and flow parameter calibration and the profile heterogeneity can also influence the simulations result.

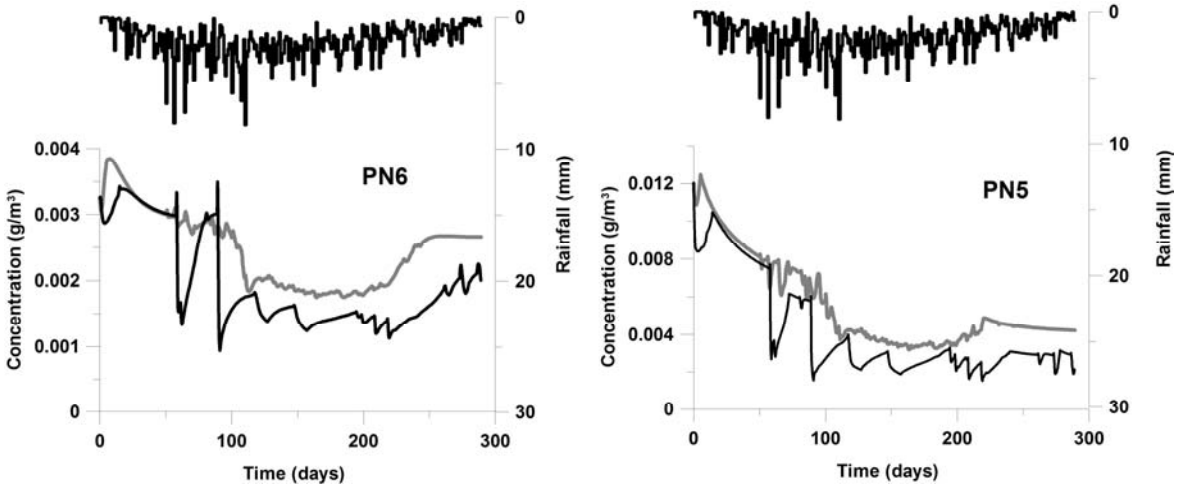

Fig. 47 Simulated concentrations at 0.3 m depth for PN6 and PN5 under rainfall and ETo

measured in Oued Souhil from 15/8/2006 to 31/5/2007 (black line) and mean annual daily rainfall (depicted in this figure) and ETo measured in Kelibia (grey line)

It is important to carry out a better calibration for the flow problem.

Finally, the calculated aerial recharge rates reached 0.7 %, 6.2% and 3.5% of the average annual precipitation for PN4, PN5 and PN6 respectively. These results are underestimated compared to those reported by Ennabli (1980) (8%) and Kerrou et al. (2010) (can reach 20%). For the first scenario SC1, the total infiltration rate with regards to rainfall and irrigation was about, 14.2%, 21.4%, and 10.7% for PN4, PN5 and PN6 respectively.

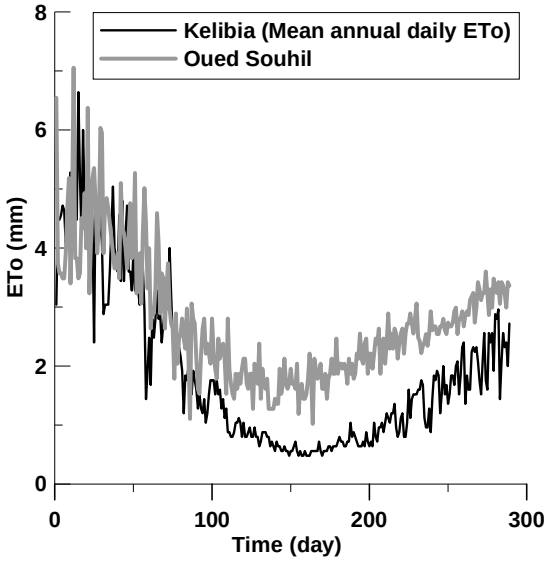

Fig. 48 Measured ETo in Oued Souhil from 15/8/2006 to 31/5/2007 and mean annual daily ETo derived from measured data in Kelibia.

6.3. Geochemical modelling

GEODENS reproduced concentration increase of the dominant ions Ca and Cl in the upper horizons. It also predicted gypsum precipitation after 100 days of evaporation (Fig. 49). The GEODENS version used in this study does not consider carbonate minerals. Further simulations with the new version of GEODENS, extended to carbonate (Bouhlila and Laabidi, 2008) would be useful to confirm calcite precipitation, discussed in the third chapter.

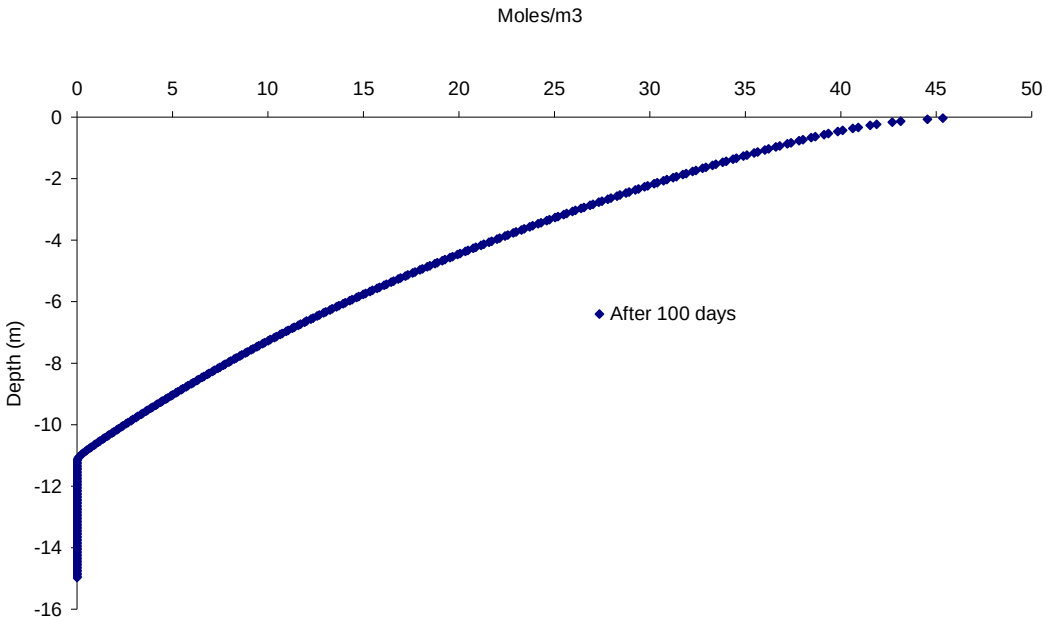

Fig. 49 Amount of Precipitated gypsum (CaSO4,2H2O) in moles/m^3 after 100 days of evaporation

Besides, it would be interesting to test UNSATCHEM (Suarez and Simunek, 1997) (also integrated in HYDRUS1D) in the purpose of modelling major geochemical processes in the vadose zone. UNSATCHEM considers the equilibrium chemical reactions, between major ions, such as complexation, cation exchange and precipitation-dissolution.

7. Conclusion

HYDRUS1D was used to carry out long term simulations of TDS fate in three profiles. Field data were used to define the initial solute and flow conditions, to estimate the soil hydraulic parameters and to calibrate the solute and flow parameters. The model was thereby calibrated for the wet season. However, it is necessary to readjust the model by considering water content status. Yet, this was not possible because of difficulties in performing direct measures of this variable. Furthermore, measured resistivities (using ERT imaging) require laboratory calibration to be converted into water content. An estimation of the Van Genuchten soil hydraulic parameters was also carried out using ERT imaging couple to an infiltration test and unsaturated modelling with HYDRUS2D.

The calibrated model was then used to run prediction simulations based on three scenarios. Results reveal that the solute flux amount and movement depends on the soil profile thickness. The calculated solute fluxes were considered to be insignificant

because of a high salt accumulation in the soil profiles. The handling of the climatic data forecast is probably the main reason for the flux underestimation. The flow problem calibration is also to be improved for a better estimation of the solute fluxes.

Aerial recharge fluxes were also estimated. They ranged between 0.7 and 6.2 % of the average annual precipitation. According to the previous studies in the Korba aquifer, these values are also underestimated.

Simulations also demonstrate that reducing irrigation water amounts would considerably decrease solute irrigation return flux. Indeed, the root water uptake amount was the same for both simulations suggesting that the water excess would have been lost through deep percolation. This result is interesting with regard to irrigation water management and groundwater's quality protection.

References

Allen, R.G., Pereira, L.S., Raes, D. and Smith, M., 1998. Crop Evapotranspiration-Guidelines for Computing Crop Water Requirements-FAO Irrigation and Drainage Paper 56. FAO-Food and Agriculture Organization of the United Nations, Rome, Italy, 293 pp.

Aragüés, R., Tanji, K.K., Quílez, D., Alberto, F., Faci, J., Machín, J. and Arrué, J., L.,1985. Calibration and verification of an irrigation return flow hydrosalinity model Irrigation science, 6(2): 85-94.

Bandyopadhyay, A., Bhadra, A., Raghuwanshi, N., S., and Singh, R., 2009. Temporal Trends in Estimates of Reference Evapotranspiration over India. Journal of Hydrologic Engineering, 14(5): 508-515.

Banton, O. and Larocque, M., 1997. Agriflux 2.0. Notice d'utilisation, www.hydriad.com.

Baran, N., Lepiller, M. and Mouvet, C., 2008. Agricultural diffuse pollution in a chalk aquifer (Trois Fontaines, France): Influence of pesticide properties and hydrodynamic constraints. Journal of Hydrology, 358(1-2): 56-69.

Baran, N., Richert, J. and Mouvet, C., 2007. Field data and modelling of water and nitrate movement through deep unsaturated loess. Journal of Hydrology, 345(1-2): 27-37.

Ben Hamouda, M.F., Leduc, C., Tarhouni, J. and Zouari, K., 2009. Origine de la minéralisation dans l'aquifère plio-quaternaire de la côte orientale du cap Bon (Tunisie). Sècheresse, 20 (1): 78-86.

Bouhlila, R., 1999. Ecoulements, transports et réactions géochimiques couplés dans le milieu poreux, Ecole Nationale d'Ingénieurs de Tunis.

Bouhlila, R. and Laabidi, E., 2008. Impacts of calcite dissolution on seawater intrusion processes in coastal aquifers: Density dependent flow and multi species reactive transport modeling. Calibration and Reliability in Groundwater Modelling Credibility of Modelling. IAHS Publications, 320: 220-225.

Burlando, P., Rosso, R., Cadavid, L.G. and Salas, J.D., 1993. Forecasting of short-term rainfall using ARMA models. Journal of Hydrology, 144(1-4): 193-211.

Cardona, A., Carrillo-Rivera, J., Huizar-Alvarez, R. and Garniel-Castro, E., 2004. Salinization in coastal aquifers of arid zones: an example from Santo Domingo, Baja California Sur, Mexico. Environmental Geology, 45: 350-366.

Daily, W., Ramirez, A., LaBrecque, D. and Nitao, J., 1992. Electrical resistivity tomography of vadose water movement. Water Resources Research, 28: 1429-1442.

Dalton, F., N., and Van Genuchten, M., Th., , 1986. The time-domain reflectometry method for measuring soil water content and salinity. Geoderma, 38: 237-250.

Destouni, G., 1993. Stochastic modelling of solute flux in the unsaturated zone at the field scale. Journal of Hydrology, 143: 45-61.

Ennabli, M., 1980. Etude hydrogéologique des aquifères du nord-est de la Tunisie pour une gestion intégrée des ressources en eau. Doctorat d'Etat Thesis, Ministère de l'agriculture. République Tunisienne.

FAO, 2010. Crop water management.

http://www.fao.org/landandwater/aglw/cropwater/tomato.stm#requirements.

Feddes, R.A., Kowalik, P., Kolinska-Malinka, K. and Zaradny, H., 1976. Simulation of field water uptake by plants using a soil water dependent root extraction function. Journal of Hydrology, 31(1-2): 13-26.

Hachicha, M., Cheverry, C. and Mhiri, A., 2003. Etude comparative de bonification de sols salés sous conditions naturelles et sous irrigation et drainage en milieu semi-aride. Sècheresse, 14: 146-147.

Heuvelink, E., 1995. Growth, development and yield of a tomato crop: periodic destructive measurements in a greenhouse. Scientia Horticulturae, 61(1-2): 77-99.

Hu, Q. and Wang, J.S.Y., 2003. Aqueous-Phase Diffusion in Unsaturated Geologic Media: A Review. Critical Reviews in Environmental Science and Technology, 33(3): 275 - 297.

Javaux, M. and Vanclooster, M., 2004. In Situ Long-Term Chloride Transport through a Layered, Nonsaturated Subsoil. 2. Effect of Layering on Solute Transport Processes. Vadose Zone Journal, 3: 1331–1339

Kemna, A., Kulessa, B. and Vereecken, H., 2002. Imaging and characterisation of subsurface solute transport using electrical resistivity tomography (ERT) and equivalent transport models. Journal of Hydrology, 267(3-4): 125-146.

Liu, Q., Yang, Z., Cui, B. and Tao, S., 2010. The temporal trends of reference evapotranspiration

and its sensitivity to key meteorological variables in the Yellow River Basin, China. Hydrological Processes.

Liu, S. and Yeh, T.-C.J., 2004. An Integrative Approach for Monitoring Water Movement in the Vadose Zone. Vadose Zone Journal 2: 664-676.

McCutcheon, M., C., , Farahani, H., J., , Stednick; J., D., Buchleiter; G., W. and Green, T., R., 2006. Effect of Soil Water on Apparent Soil Electrical Conductivity and Texture Relationships in a Dryland Field. Biosystems Engineering 94(1): 19-32.

Montoroi, J.P., Bellier, G. and Delarivière, J.L., 1997. Détermination de la relation résistivité électrique-teneur en eau au laboratoire. Application aux sols de Tunisie centrale, Colloque GEOFCAN Géophysique des sols et des formations superficielles, Bondy, France.

Rajmohan, N. and Elango, L., 2007. Mobility of major ions and nutrients in the unsaturated zone during paddy cultivation: a field study and solute transport modelling approach. Hydrological Processes, 21(20): 2698-2712.

Richter, B.C. and Kreitler, C.W., 1991. Identification of sources of ground-water salinization using geochemical techniques: , U.S. Environmental Protection Agency, Okalahoma.

Ritchie, J.T., 1972. Model for predicting evaporation from a row crop with incomplete cover. Water Resour. Res., 8(5): 1204-1213.

Saaltink, M.W., Batlle, F., Ayora, C., Carrera, J. and Olivella, S., 2004. RETRASO, a code for modeling reactive transport in saturated and unsaturated porous media. Geologica acta, 2(3): 235-251.

Samouëliana, A., Cousina, I., Tabbagh, A., Bruandd, A. and Richard, G., 2005. Electrical resistivity survey in soil science: a review. Soil and Tillage Research, 83(2): 173-193.

Šimùnek, J., Šejna, M., Saito, H., Sakai, M. and Van Genuchten, M. Th. , 2008. The Hydrus-1D Software Package for Simulating the Movement of Water, Heat, and Multiple Solutes in Variably Saturated Media, Version 4.0, , Department of Environmental Sciences, University of California Riverside, Riverside, California, USA.

Simunek, J., Sejna, M. and Van Genuchten, T., 1999. Simullating water flow, heat and solute transport in two dimensional variably saturated media, US salinity laboratory, agricultural research service, US department of agriculture Riverside, California, USA.

Slama, F., Bahri, A., Bouarfa, S., Chaumont, C. and Bouhlila, R., 2003. Modélisation du fonctionnement des ouvrages de drainage agricole dans le périmètre irrigué de Kalaat Landelous. In: SHF (Editor), "Gestion du risque eau en pays semi-aride" TUNIS.

Slama, F., Bahri, A., Bouarfa, S., Chaumont, C. and Bouhlila R., 2004. Pratiques d'irrigation et rôle du drainage pour le contrôle de la salinité -cas du périmètre irrigué Kalaât Landelous en Tunisie, Projet européen Inco-Wademed sur la "Modernisation de l'agriculture irriguée dans les pays du Maghreb", Rabat.

Slama, F., Labidi, E., Bouhlila, R., Perrochet, P., Renard, P. and Milnes, P.E., 2007. Geochimical modelling of soil and groundwater salinisation under irrigation with saline water. In: IAHS (Editor), MODELCARE, Calibration and Reliability in Groundwater Modelling, Copenhagen, Danemark

Slama, F., Milnes, E.P. and Bouhlia, R., 2008. Calibrating unsaturated model parameters using electrical resistivity tomography imaging, Redbook N°320. International Association of Hydrological Sciences, Wallingford, pp. 148-153.

Suarez, D.L. and Simunek, J., 1997. UNSATCHEM : Unsaturated water and solute transport model with equilibrium and kinetic chemistry, 61. Soil Science Society of America, Madison, WI, ETATS-UNIS.

Sudicky, E., A., , Illman, W., A.,, Goltz, I., K., Adams, J., J., and McLaren, R., G., 2010. Heterogeneity in hydraulic conductivity and its role on the macroscale transport of a solute plume: From measurements to a practical application of stochastic flow and transport theory. Water Resources Research, 46 doi:10.1029/2008WR007558, 2010.

Twarakavi, N.K.C., Simunek, J. and Seo, S., 2008. Evaluating Interactions between Groundwater and Vadose Zone Using the HYDRUS-Based Flow Package for MODFLOW. Vadose Zone Journal, 7(2): 757-768.

Van Genuchten, M.T., 1980. A closed-form equation for predicting the hydraulic conductivity of unsaturated soils. Soil Science, 44: 892-898.

Xu, C.-y., Gong, L., Jianga, T., Chen, D. and V.P., S., 2006. Analysis of spatial distribution and temporal trend of reference evapotranspiration and pan evaporation in Changjiang (Yangtze River) catchment. Journal of Hydrology, 327(1-2): 81-93

Chapter 6. Conclusions and perspectives

1. Summary

Experimental and numerical studies were carried out in Korba coastal plain North-East of Tunisia. The experimental study involved groundwater and soil sampling, piezometric measurements, electrical tomography imaging and an infiltration test, performed along two transects. An important hydrogeochemical database, issued from a three year survey was set up. Various statistical and geochemical techniques were performed to analyse this database. The objective was to identify salinity sources and to study hydrochemical processes occurring within the salinization phenomenon. Besides, variably saturated simulations were carried out in order to attempt to estimate and to predict the quantity of salts loadings that would reach the groundwater.

1.1. Groundwater salinization sources and processes

Results concerning groundwater quality highlighted the complexity and superposition of various processes contributing to groundwater mineralization.

Multivariate statistical analysis (HCA and PCA) allowed identification of major sources of salinity and their area of impact. Indeed, seawater intrusion and agricultural pollution were identified as the main sources of salinization. The former contributes to the groundwater composition along 4000 m and 1500 m from the shoreline in transect S1 transect S2 respectively. The latter controls the groundwater composition in internal areas.

The seawater/freshwater mixing modelling revealed that seawater intrusion is accompanied by three major processes: cation exchange, carbonate weathering and redox processes. Cation exchange processes are actively taking place along the two flow paths, indicating that seawater intrusion is in progress in S1. Using theses reactions as indicators of seawater intrusion, the penetration length can be estimated about 4000 m in transect S1. Besides ionic deviations and saturation indexes (with regard to gypsum, calcite and dolomite), calculations suggested the gypsum dissolution as the source of Ca and SO_4 enrichment recorded in both transects. This result confirms the contamination with agricultural residual substances. Indeed, gypsum potential sources are fertilizers and

the dissolution under rainfall of precipitated gypsum formed at the topsoil under evaporation.

The ERT imaging survey confirmed the presence of a mixing zone at 1200 m of the shoreline.

1.2. Soil salinization processes and trends

Two soil sampling campaigns were carried out using dry drilling in mainly three irrigated plots located in transect S1. Plots were intensively cultivated mainly with tomato crops. Irrigation water was extracted from the brackish groundwater presenting high EC's reaching 9.9 mS/cm. Drip irrigation associated with fertigation is widely used. The experimental data revealed that the soil solution is concentrated during the dry season under irrigation with brackish water and high rates of evapotranspiration. Indeed, ECe reached 17.5 mS/cm. The soil solution showed high to very high risk of salinization and medium to high risk of sodicity hazard. Therefore, crops are affected by the high salinity resulting in poor yields. Nevertheless, rainfall leaches accumulated salts inducing a considerable decrease of ECe in the topsoil (e. g. ECe decreases from 17.53 to 2.73 mS/cm in PNS5). This is mainly possible because of the light textured characteristic of the studied soils and the stormy episodes with daily rainfall amounts reaching up to 70 mm. Yet those processes present a threat for groundwater quality given the high capacity of the vadose zone to transfer contaminants.

Multivariate statistical analysis (PCA in and HCA) identified three major processes occurring in the vadose zone: salinization processes related to concentration and precipitation, N-fertilisers contamination expressed in the high correlation between NO_3, K and SO_4 and finally redox processes.

Besides, the generalized RA applied to all soil samples issued from transect S1 and collected in the dry season showed that calcite followed by gypsum precipitated under evaporation. This result was compliant to seasonal evolution of calculated gypsum and calcite saturation indexes. According to RA, soil solution is following a neutral saline pathway.

The principal result that links different parts of the present study is that the diverse applied techniques revealed the agricultural pollution through its various fingerprints.

1.3. Estimation of irrigation return flow using unsaturated modelling

HYDRUS1D was used to carry out prediction scenarios aiming to analyse and quantify the solute irrigation return flux. The model was first calibrated on the basis of the collected experimental data for the three studied plots. The calibration was performed for the wet season under climatic boundary conditions. Three scenarios were proposed to carry out prediction simulations. The first scenario stipulated that irrigation amounts will remain steady; the second one supposed that these amounts would decrease by 30 % and the third one proposed that irrigation was abandoned. Results revealed that the irrigation return flux depended on the profile depth and the irrigation amount. Indeed the decrease of the irrigation amount considerably reduced the solute flux. As field studies (Slama et al., 2004; Slatni et al., 2004) reported that farmers are over irrigating crops, this result is of interest regarding irrigation water management. Indeed, the root water uptake amount was the same for both simulations suggesting that the water excess would have been lost through deep percolation. Thus, rationalizing the amounts of irrigation water would not only preserve water resources but also reduce groundwater contamination through irrigation return fluxes.

The third scenario was used to estimate the aerial recharge. It ranged from 0.7 to 6.2 %.

The solute fluxes, calculated for the first and second scenario, ranged from $2\ 10^{-5}$ to $2\ 10^{-3}$ g/m²/year. They were underestimated and insignificant as the soil profiles were getting concentrated over the simulations. The possible explanation was that the temporal distribution of the averaged rainfall and the overestimation of the averaged ETo (measured both in Kelibia station). Indeed, considering long term mean daily rainfall generates a smoothed pattern with low maximum values (10 mm/days) excluding thus extreme values known for their efficiency in leaching salts.

2. Perspectives

Further works are to focus on the following axis:

1. It is important to improve the conversion of the resistivity into water content. A laboratory experimentation based on that described by Montoroi et al. (1997) (Montoroi et al., 1997) and adapted from Rhoades ((Rhoades et al., 1999) is under development.
2. Climatic data used as inputs for the unsaturated modelling of solute transport require analysis using statistical techniques in the purpose of generating daily reliable data. Poisson model was already tested for the time series of rainfall and

an Autoregressive Moving Average technique (ARMA) (Burlando et al., 1993) will be performed.

3. It would be interesting to apply PHREEQC (Parkhurst, 1995) or NETPATH (Plummer et al., 1994) in order to model geochemical reactions occurring at the seawater freshwater interface along a flow path (Lambrakis, 2006; Petalas and Lambrakis, 2005). Two dimensional variably saturated flow and solute transport simulations were performed for a vertical section corresponding to transect S1 using FEFLOW (Slama et al., 2007). The Henry problem boundary conditions were reproduced besides the consideration of pumping wells. However, the calculations were heavy to carry out and results were not concluding.
4. It would be of interest to perform an adequate soil sampling at the soil surface, mainly within visible salt crusts, in the purpose of making XRD analysis to identify the kind of precipitated minerals, and to confirm the presence of calcite and gypsum. However, laboratory experiment of irrigation and evaporation remains an easier and clearer way to study the precipitation of minerals under evapotranspiration processes.
5. Soil heterogeneity strongly influences solute transport modelling. Therefore stochastic modelling of heterogeneity can consequently improve the solute transport modelling results (Guarracino and Santos, 2004). However, this subject is poorly documented probably because of the complexity and the important number of variables describing the state of an unsaturated medium. Heterogeneous profiles of the saturated hydraulic conductivity were generated using Sequential Gaussian Simulation performed with SGEMS (Nicolas and Alexandre, 2009). Solute transport modelling using the generated profile will be tested afterwards.

References

Burlando, P., Rosso, R., Cadavid, L.G. and Salas, J.D., 1993. Forecasting of short-term rainfall using ARMA models. Journal of Hydrology, 144(1-4): 193-211.

Guarracino, L. and Santos, J., E., , 2004. Stochastic Modeling of Variably Saturated Transient Flow in Fractal Porous Media. Mathematical Geology, 36(2): 217-238.

Lambrakis, N., 2006. Multicomponent heterovalent chromatography in aquifers. Modelling salinization and freshening phenomena in field conditions. Journal of Hydrology, 323(1-4): 230-243.

Montoroi, J.P., Bellier, G. and Delarivière, J.L., 1997. Détermination de la relation résistivité électrique - teneur en eau au laboratoire. Application aux sols de Tunisie centrale, Colloque GEOFCAN Géophysique des sols et des formations superficielles, Bondy, France.

Nicolas, R. and Alexandre, B., 2009. Applied Geostatistics with SGeMS. A User's Guide. Cambridge university press, 284 pp.

Parkhurst, D., 1995. User's guide to PHREEQC: a computer program for speciation, rreaction-path, advective-transport and inverse geochemical calculations, US Geol Surv Water-Res.

Petalas, C. and Lambrakis, N., 2005. Simulation of intense salinization phenomena in coastal aquifers: the case of the coastal aquifers of Thrace. Journal of Hydrology, 324(1-4): 51-64.

Plummer, L.N., Prestemon, E.C. and Parkhurst, D.L., 1994. An Interactive Code (NETPATH) For Modeling NET Geochemical Reactions Along a Flow PATH Version 2.0. U.S. Geological Survey Water-Resources Investigations Report 94-4169.

Rhoades, J.D., Chanduvi, F. and Lesch, S., 1999. Soil salinity assessment. Methods and interpretation of electrical conductivity measurements- FAO irrigation and drainage paper 57. FAO-Food and Agriculture Organization of the United Nations, Rome, Italy, 166 pp.

Slama, F., Bahri, A., Bouarfa, S., Chaumont, C. and Bouhlila R., 2004. Pratiques d'irrigation et rôle du drainage pour le contrôle de la salinité -cas du périmètre irrigué Kalaât Landelous en Tunisie, Projet européen Inco-Wademed sur la "Modernisation de l'agriculture irriguée dans les pays du Maghreb", Rabat.

Slama, F., Bouhlila, R., Perrochet, P., Renard, P., Trabelsi, E. and Tarhouni, J., 2007. Modelling Groundwater and soil salinisation processes in the irrigated coastal plain of Korba, North of Tunisia. , XXXV IAH Congress: groundwater and ecosystems, Lisbon, Portugal.

Slatni, A., Mailhol, J.C., Zairi, A., Château, G. and Ajmi, T., 2004. Analyse et diagnostic de la pratique de l'irrigation localisée dans les périmètres publics irrigués de la basse vallée de la Medjerda en Tunisie, Projet européen Inco-Wademed sur la "Modernisation de l'agriculture irriguée dans les pays du Maghreb", Rabat.

Appendix A

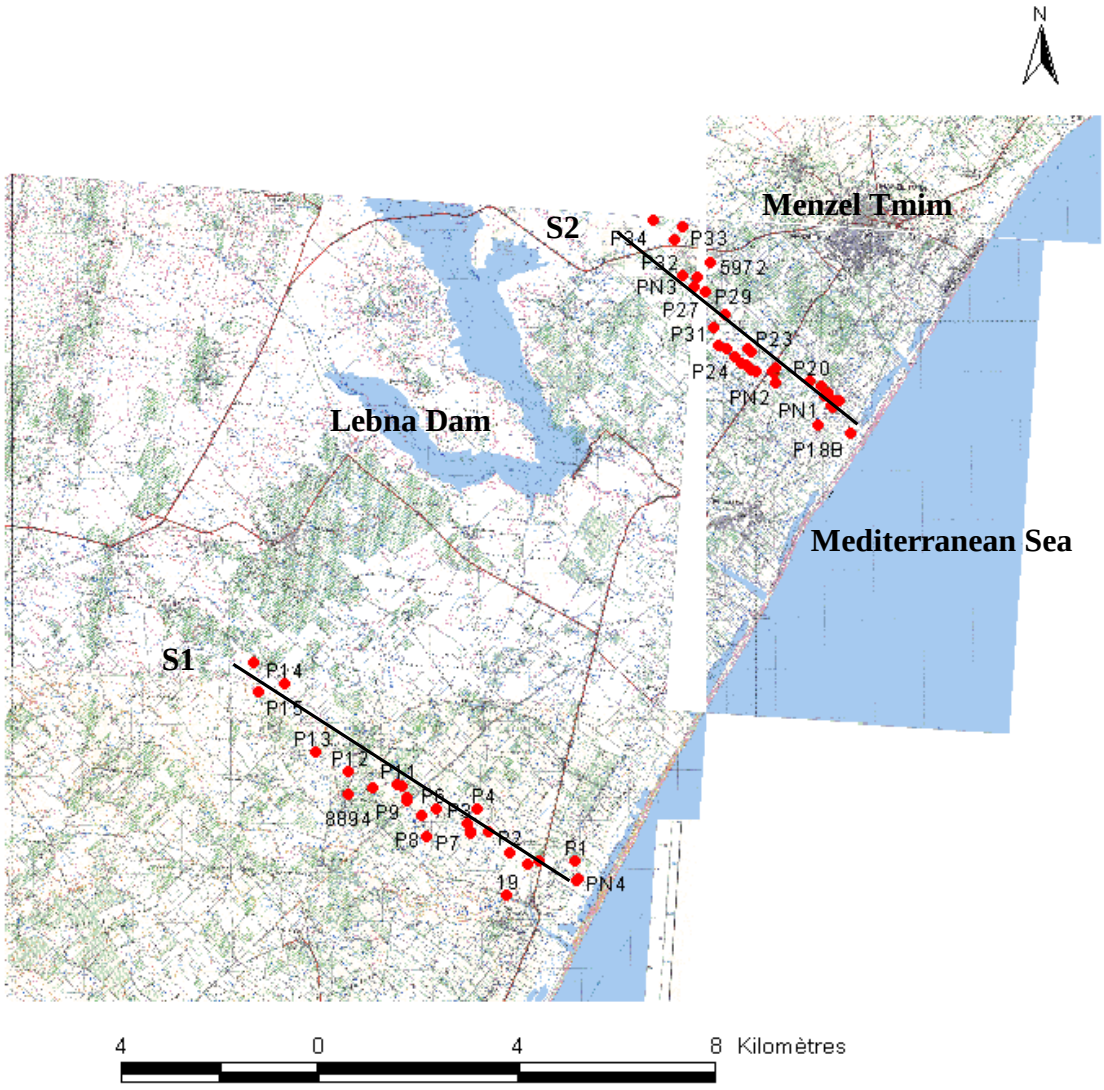

• Observation well

Location Map of Transects S1 and S2

Appendix B

Tab. 1 Statistical summary of concentrations in meq/L, EC in mS/cm, pH and ionic ratios in transects S1 and S2.

					(mS/cm)	(meq/L)														
Transect	Well	NB		pH	EC	Ca	Mg	Na	K	HCO3	CO3	Cl	SO4	NO3	Mg/Ca	Ca/(HCO3+S04)	fsea	Na/Cl	HCO3/Cl	SO4/Cl
S2	PS19	3	Min		3.38	7.54	5.60	28.81	0.14	4.32	0.00	25.40	6.93	0.78	0.74	0.58	2.87	0.92	0.08	0.22
			Max		6.90	14.88	11.60	48.16	0.31	6.08	1.76	51.50	11.75	1.25	0.87	0.94	7.21	1.13	0.24	0.27
			Mean		5.62	11.85	9.52	41.38	0.24	5.15	1.12	41.34	10.08	0.98	0.80	0.77	5.52	1.02	0.14	0.25
			Sd		1.95	3.83	3.40	10.90	0.09	0.88	0.97	13.97	2.73	0.25	0.06	0.18	2.32	0.11	0.08	0.02
	P18	4	Min		5.17	13.57	7.75	33.44	0.13	3.88	0.00	41.37	6.25	1.96	0.50	1.18	5.53	0.81	0.07	0.11
			Max		6.58	16.50	10.00	45.38	0.19	5.00	1.76	54.93	6.52	2.34	0.63	1.62	7.78	0.89	0.12	0.15
			Mean		5.73	15.13	8.58	38.61	0.16	4.41	0.82	45.55	6.35	2.15	0.57	1.42	6.22	0.85	0.10	0.14
			Sd		0.60	1.32	0.98	4.97	0.02	0.54	0.72	6.30	0.12	0.17	0.06	0.20	1.05	0.04	0.02	0.02
	MD2	4	Min	7.3	5.93	13.06	10.24	44.28	0.25	3.92	0.64	46.87	8.35	2.13	0.72	0.93	6.44	0.90	0.08	0.17
			Max		6.79	14.72	10.75	47.06	0.28	5.32	1.52	50.23	8.75	2.47	0.81	1.17	7.00	0.98	0.11	0.18
			Mean		6.57	13.81	10.55	45.48	0.27	4.29	0.98	48.45	8.54	2.28	0.77	1.08	6.71	0.94	0.09	0.18
			Sd		0.43	0.85	0.22	1.16	0.01	0.69	0.38	1.43	0.17	0.18	0.04	0.11	0.24	0.04	0.02	0.01
	MD1	3	Min	7.2	4.27	11.98	7.78	27.70	0.11	4.10	0.72	31.18	6.41	2.19	0.61	1.03	3.84	0.89	0.11	0.19
			Max	7.2	5.28	14.12	9.24	34.96	0.13	4.64	1.28	38.66	7.21	2.55	0.77	1.32	5.08	0.90	0.15	0.21
			Mean	7.2	4.81	12.95	8.53	31.08	0.12	4.39	0.91	34.77	6.73	2.34	0.66	1.17	4.43	0.89	0.13	0.19
S2			Sd		0.51	1.08	0.73	3.65	0.01	0.27	0.32	3.75	0.42	0.19	0.09	0.15	0.62	0.01	0.02	0.01
	PN1	1	Min	7.2	4.94	12.60	6.30	13.29	0.09	2.84	1.28	15.31	6.20	4.73	0.50	1.39	1.20	0.87	0.19	0.40
	PN2	1	Max		3.06	6.71	5.58	18.55	0.09	4.24	1.52	17.60	6.53	2.63	0.83	0.62	1.58	1.05	0.24	0.37
	P18B	1	Mean		3.45	11.57	6.47	19.92	0.13	4.16	1.60	21.72	6.81	3.00	0.56	1.05	2.26	0.92	0.19	0.31
	P17_4	1	Sd		7.93	16.65	12.71	50.76	0.26	3.96	0.88	61.36	8.36	2.13	0.76	1.35	8.85	0.83	0.06	0.14
	P17	3	Min	7.3	5.06	19.02	9.08	32.40	0.09	2.96	1.00	41.29	8.18	3.01	0.45	1.69	5.51	0.73	0.07	0.18
			Max	7.3	5.70	20.77	9.72	34.98	0.11	3.52	1.28	44.47	8.44	3.33	0.48	1.80	6.04	0.83	0.08	0.20
			Mean	7.3	5.46	20.00	9.35	33.86	0.10	3.25	1.11	42.82	8.29	3.14	0.47	1.73	5.77	0.79	0.08	0.19
			Sd		0.35	0.90	0.33	1.32	0.01	0.28	0.15	1.60	0.14	0.17	0.02	0.06	0.27	0.06	0.01	0.01
	P17B	3	Min	7.4	5.28	15.57	8.84	30.21	0.07	3.28	0.00	37.21	7.76	3.18	0.51	1.27	4.84	0.81	0.09	0.20
			Max	7.4	5.33	17.51	9.59	32.19	0.09	4.96	0.80	38.89	7.93	3.57	0.58	1.56	5.12	0.83	0.13	0.21
			Mean	7.4	5.31	16.54	9.15	31.02	0.08	4.19	0.51	37.83	7.87	3.41	0.56	1.38	4.94	0.82	0.11	0.21
			Sd		0.04	0.97	0.39	1.04	0.01	0.85	0.44	0.92	0.10	0.20	0.04	0.16	0.15	0.01	0.02	0.01
	P20	3	Min	7	4.77	14.86	7.46	31.32	0.09	0.76	0.00	35.13	9.02	3.15	0.48	1.10	4.49	0.80	0.02	0.23

			Max	7	5.45	17.68	8.86	34.13	0.12	4.52	1.44	42.40	9.56	3.36	0.59	1.45	5.70	0.89	0.13	0.26
			Mean	7	5.21	15.83	8.29	33.14	0.11	3.16	0.91	38.55	9.36	3.27	0.53	1.28	5.06	0.86	0.09	0.24
			Sd		0.38	1.60	0.74	1.58	0.02	2.08	0.79	3.65	0.30	0.11	0.06	0.18	0.61	0.05	0.06	0.02
	P16	3	Min	7.3	2.54	7.53	5.18	15.81	0.16	4.20	0.00	15.73	6.03	2.35	0.59	0.73	1.27	1.00	0.27	0.38
			Max	7.3	2.81	9.07	5.69	17.56	0.18	5.64	1.36	16.09	6.50	3.19	0.76	0.78	1.33	1.12	0.36	0.40
			Mean	7.3	2.70	8.45	5.46	16.77	0.17	4.88	0.88	15.86	6.22	2.74	0.65	0.76	1.29	1.06	0.31	0.39
S2			Sd		0.14	0.81	0.26	0.88	0.01	0.72	0.76	0.21	0.25	0.42	0.09	0.03	0.03	0.06	0.05	0.01
	KS1	3	Min	7.6	2.68	4.24	6.00	18.02	0.04	5.28	0.84	16.53	5.07	1.78	0.76	0.39	1.40	1.09	0.24	0.26
			Max		3.62	8.18	6.22	25.31	0.12	5.70	1.36	22.36	5.85	2.18	1.41	0.73	2.37	1.13	0.32	0.31
			Mean		3.13	5.95	6.13	21.40	0.07	5.46	1.08	19.13	5.34	1.97	1.11	0.55	1.83	1.12	0.29	0.28
			Sd		0.47	2.02	0.12	3.68	0.04	0.22	0.26	2.97	0.45	0.20	0.33	0.17	0.49	0.02	0.04	0.02
	KS2	2	Min	7.4	2.95	8.13	5.60	19.58	0.09	4.76	0.88	17.07	6.24	2.41	0.47	0.74	1.49	1.15	0.21	0.34
			Max		3.04	11.82	5.88	31.35	0.18	5.04	1.36	24.03	8.06	2.50	0.72	0.90	2.65	1.30	0.28	0.37
			Mean		3.00	9.97	5.74	25.47	0.13	4.90	1.12	20.55	7.15	2.45	0.60	0.82	2.07	1.23	0.24	0.35
			Sd		0.06	2.61	0.20	8.32	0.06	0.20	0.34	4.92	1.29	0.06	0.18	0.12	0.82	0.11	0.05	0.02
	P21BI	3	Min	7.2	2.47	6.56	4.98	15.75	0.05	3.52	0.00	14.79	5.26	2.81	0.59	0.67	1.11	1.05	0.22	0.35
			Max	7.2	2.77	8.60	5.37	16.80	0.06	5.52	1.60	15.94	5.53	3.18	0.76	0.86	1.30	1.09	0.37	0.36
			Mean	7.2	2.65	7.46	5.13	16.40	0.06	4.59	0.77	15.34	5.38	3.02	0.70	0.75	1.20	1.07	0.30	0.35
			Sd		0.16	1.04	0.21	0.57	0.01	1.01	0.80	0.58	0.14	0.19	0.10	0.10	0.10	0.02	0.08	0.00
	P21	1		7.3	2.87	7.21	5.77	16.64	0.10	4.08	1.60	16.75	5.64	2.78	0.80	0.74	1.44	0.99	0.24	0.34
	P23	1			2.31	8.52	5.24	14.64	0.07	4.28	1.52	14.06	5.12	2.46	0.62	0.91	0.99	1.04	0.30	0.36
	P22BI	1			2.25	8.61	4.76	14.11	0.20	4.08	1.84	12.69	5.38	2.21	0.55	0.91	0.76	1.11	0.32	0.42
	P25	2	Min	7.5	1.78	6.86	4.47	10.15	0.06	4.24	0.00	9.86	3.99	1.60	0.65	0.72	0.29	1.03	0.43	0.40
			Max	7.5	1.93	7.38	4.93	10.53	0.06	5.32	1.12	9.90	4.23	1.67	0.67	0.90	0.30	1.06	0.54	0.43
			Mean	7.5	1.86	7.12	4.70	10.34	0.06	4.78	0.56	9.88	4.11	1.64	0.66	0.81	0.30	1.05	0.48	0.42
			Sd		0.10	0.37	0.32	0.27	0.00	0.76	0.79	0.03	0.17	0.05	0.01	0.13	0.00	0.02	0.08	0.02
	P30	3	Min		3.13	8.32	6.74	17.89	0.28	3.44	0.64	19.86	4.26	4.86	0.73	0.90	1.96	0.90	0.17	0.21
S2			Max		3.46	9.82	7.16	20.28	0.99	5.00	1.52	20.50	5.01	5.53	0.81	1.11	2.06	0.99	0.25	0.25
			Mean		3.33	9.12	6.89	19.27	0.53	4.29	1.20	20.24	4.56	5.19	0.76	1.03	2.02	0.95	0.21	0.23
			Sd		0.17	0.76	0.24	1.24	0.40	0.79	0.49	0.33	0.39	0.34	0.05	0.12	0.06	0.05	0.04	0.02
	P31	2	Min		4.62	10.76	10.47	27.73	0.18	4.40	1.36	29.63	8.23	5.56	0.93	0.84	3.58	0.89	0.14	0.26
			Max		4.84	11.20	11.37	28.43	0.19	4.64	1.52	32.09	8.42	6.06	1.06	0.87	3.99	0.94	0.16	0.28
			Mean		4.73	10.98	10.92	28.08	0.18	4.52	1.44	30.86	8.33	5.81	1.00	0.86	3.78	0.91	0.15	0.27
			Sd		0.16	0.31	0.64	0.50	0.01	0.17	0.11	1.74	0.14	0.35	0.09	0.02	0.29	0.04	0.01	0.01
	P29	3	Min		2.75	11.65	4.81	13.80	0.10	4.28	0.00	17.75	3.78	2.99	0.41	1.32	1.60	0.78	0.24	0.21
			Max		3.34	12.43	5.29	16.74	0.11	5.00	0.88	20.90	4.44	3.57	0.43	1.45	2.13	0.80	0.24	0.21
			Mean		3.05	12.04	5.05	15.27	0.11	4.64	0.44	19.32	4.11	3.28	0.42	1.38	1.87	0.79	0.24	0.21
			Sd		0.42	0.55	0.34	2.08	0.01	0.51	0.62	2.23	0.46	0.41	0.01	0.09	0.37	0.02	0.00	0.00

	P27	1		7.4	4.13	14.04	6.79	14.15	0.09	4.16	0.72	18.21	6.79	5.62	0.48	1.28	1.68	0.78	0.23	0.37
	P28	4	Min		2.40	11.13	3.42	10.91	0.09	3.32	0.00	14.99	3.16	2.40	0.31	1.23	1.15	0.73	0.22	0.21
			Max		3.20	14.67	6.91	15.79	0.13	4.36	1.04	18.33	6.73	6.00	0.51	1.72	1.70	0.86	0.25	0.38
			Mean		2.88	13.14	5.69	13.73	0.11	4.01	0.53	17.03	5.49	4.73	0.43	1.43	1.48	0.80	0.23	0.32
			Sd		0.43	1.82	1.97	2.53	0.02	0.60	0.52	1.79	2.02	2.02	0.11	0.26	0.30	0.07	0.01	0.09
	PN3	2	Min		3.05	13.61	6.75	14.49	0.09	4.36	0.00	17.76	6.59	5.78	0.46	1.23	1.61	0.82	0.24	0.36
			Max		3.20	14.67	6.91	15.79	0.13	4.36	0.56	18.33	6.73	6.00	0.51	1.34	1.70	0.86	0.25	0.38
			Mean		3.13	14.14	6.83	15.14	0.11	4.36	0.28	18.05	6.66	5.89	0.48	1.28	1.65	0.84	0.24	0.37
S2			Sd		0.11	0.75	0.11	0.92	0.02	0.00	0.40	0.40	0.09	0.16	0.03	0.08	0.07	0.03	0.01	0.01
	P33	3	Min		1.96	9.37	3.12	9.01	0.07	3.28	0.00	12.31	2.58	2.36	0.29	1.39	0.70	0.73	0.22	0.21
			Max		2.40	11.56	3.42	10.91	0.11	4.16	1.04	14.99	3.16	2.96	0.33	1.82	1.15	0.77	0.34	0.22
			Mean		2.22	10.69	3.28	10.26	0.09	3.59	0.35	13.78	2.94	2.57	0.31	1.64	0.94	0.74	0.26	0.21
			Sd		0.23	1.16	0.15	1.08	0.02	0.50	0.60	1.36	0.31	0.33	0.02	0.22	0.23	0.03	0.06	0.01
	P34	1			3.36	11.07	7.60	17.38	0.05	4.08	0.00	24.42	6.92	1.05	0.69	1.01	2.71	0.71	0.17	0.28
	P23BI	1				5.89	5.85	14.50	0.07	5.08	0.72	15.20	4.97	2.28	0.99	0.59	1.18	0.95	0.33	0.33
	Lebna Dam	1				4.55	4.73	9.87	0.17	2.88	0.48	9.81	3.79	0.08	1.04	0.68	0.29	1.01	0.29	0.39
	5972	1		7.5		9.95	3.36	7.73	0.70	2.88	1.28	12.82	2.62	4.54				0.60	0.22	0.20
S1	PN4	2	Min		4.31	17.04	5.85	21.72	0.11	1.16	0.72	42.21	4.69	1.88	0.34	2.47	5.67	0.51	0.03	0.11
			Max		4.68	20.70	8.60	28.58	0.11	1.64	0.80	42.26	7.23	1.91	0.42	2.69	5.68	0.68	0.04	0.17
			Mean		4.50	18.87	7.23	25.15	0.11	1.40	0.76	42.24	5.96	1.89	0.38	2.58	5.67	0.60	0.03	0.14
			Sd		0.26	2.58	1.95	4.85	0.00	0.34	0.06	0.03	1.80	0.02	0.05	0.16	0.01	0.12	0.01	0.04
	P1	5	Min	7.3	4.45	16.43	6.12	25.69	0.29	2.00	0.00	33.35	5.80	2.73	0.37	1.32	4.20	0.72	0.04	0.10
			Max	7.3	17.19	30.38	29.72	125.31	2.01	4.92	1.12	123.36	18.02	4.24	0.98	2.11	19.15	1.02	0.08	0.17
			Mean	7.3	7.67	21.14	12.14	48.54	0.63	3.33	0.61	57.86	8.29	3.43	0.52	1.94	8.27	0.79	0.06	0.15
			Sd		4.91	5.48	9.26	38.71	0.68	1.25	0.51	34.80	4.80	0.58	0.24	0.30	5.78	0.11	0.01	0.02
	PN5	7	Min	7	8.50	23.22	15.15	50.58	0.40	3.36	0.00	65.94	6.85	1.25	0.56	1.83	9.61	0.69	0.04	0.09
			Max	7	9.98	29.03	17.22	58.33	0.50	5.84	1.28	84.11	7.36	2.73	0.67	2.60	12.63	0.82	0.09	0.11
			Mean	7	9.18	26.92	16.18	54.53	0.44	4.78	0.64	73.42	7.16	1.93	0.60	2.26	10.85	0.75	0.07	0.10
			Sd	0	0.58	2.12	0.83	3.13	0.03	0.73	0.53	6.56	0.17	0.44	0.03	0.25	1.09	0.05	0.01	0.01
	P2	7	Min	7	4.32	15.51	7.71	22.77	0.22	2.96	0.00	31.76	4.98	1.85	0.46	1.42	3.93	0.63	0.08	0.14
			Max	7	5.98	21.46	10.26	29.25	0.43	4.88	1.52	46.26	6.89	3.71	0.58	2.14	6.34	0.72	0.15	0.17
			Mean	7	5.41	19.25	9.40	26.90	0.27	4.08	0.91	39.80	6.33	2.98	0.49	1.86	5.27	0.68	0.11	0.16
			Sd	0	0.54	2.54	0.86	2.60	0.08	0.79	0.71	5.32	0.65	0.76	0.04	0.26	0.88	0.04	0.03	0.01
	P5B	5	Min	7.0	4.88	19.51	8.20	23.40	0.23	2.76	0.32	34.53	6.68	3.83	0.42	1.84	4.39	0.60	0.08	0.18
			Max	7.1	5.93	25.82	11.03	30.80	0.58	3.92	1.12	42.95	8.46	4.98	0.46	2.11	5.79	0.72	0.09	0.20
			Mean	7.0	5.41	21.83	9.60	26.49	0.31	3.42	0.82	40.14	7.65	4.14	0.44	1.98	5.32	0.66	0.08	0.19

		Sd	0.1	0.39	2.38	1.01	2.77	0.15	0.47	0.31	3.38	0.64	0.47	0.02	0.12	0.56	0.05	0.01	0.01
P4	6	Min	7.4	4.74	16.29	9.32	26.30	0.24	2.72	0.00	34.78	5.65	2.82	0.43	1.65	4.43	0.68	0.06	0.16
		Max	7.4	6.22	23.83	10.80	31.27	0.29	4.24	1.52	45.19	7.71	5.83	0.57	2.31	6.16	0.76	0.12	0.18
		Mean	7.4	5.45	21.28	10.14	29.45	0.27	3.69	0.83	40.92	6.97	4.71	0.49	1.99	5.45	0.72	0.09	0.17
		Sd		0.74	4.32	0.75	2.74	0.03	0.84	0.77	5.46	1.15	1.65	0.08	0.33	0.91	0.04	0.03	0.01
P3	6	Min	7.0	3.88	14.65	8.22	23.02	0.20	3.16	0.00	31.22	5.64	2.52	0.45	1.40	3.84	0.62	0.09	0.17
		Max	7.2	4.89	19.35	8.88	24.77	0.24	4.48	1.28	37.31	6.79	3.74	0.56	1.96	4.85	0.74	0.14	0.19
		Mean	7.1	4.59	17.07	8.52	23.47	0.22	3.67	0.83	34.07	6.22	3.02	0.51	1.73	4.32	0.69	0.11	0.18
		Sd	0.2	0.37	2.12	0.29	0.68	0.01	0.61	0.54	2.28	0.38	0.48	0.06	0.23	0.38	0.04	0.02	0.01
P7	6	Min	6.9	3.97	15.95	7.54	19.38	0.20	3.68	0.00	30.10	6.58	3.08	0.37	1.33	3.66	0.63	0.12	0.22
		Max	7.2	4.57	20.86	9.47	22.13	0.29	4.96	1.20	31.60	7.75	4.94	0.59	1.81	3.91	0.70	0.16	0.25
		Mean	7.0	4.29	17.69	8.61	20.42	0.24	4.14	0.57	30.74	7.07	4.00	0.49	1.58	3.76	0.66	0.13	0.23
		Sd	0.2	0.19	1.84	0.82	0.95	0.03	0.55	0.52	0.57	0.42	0.72	0.07	0.19	0.09	0.03	0.02	0.01
P6	6	Min	7.0	3.52	8.21	5.73	18.09	0.18	3.00	0.00	26.99	5.00	2.04	0.63	0.78	3.14	0.61	0.09	0.16
		Max	7.2	5.29	14.07	9.27	27.86	0.88	4.92	1.76	32.61	7.28	3.10	0.73	1.58	4.07	1.03	0.17	0.27
		Mean	7.1	4.05	12.44	8.45	20.36	0.30	3.90	0.71	29.47	5.48	2.53	0.68	1.34	3.55	0.70	0.13	0.19
		Sd	0.1	0.57	1.97	1.23	3.40	0.25	0.67	0.75	1.91	0.81	0.36	0.04	0.27	0.32	0.15	0.03	0.04
P8	6	Min	6.9	5.00	8.21	5.73	25.62	0.13	2.40	0.00	26.99	6.54	2.04	0.28	0.78	3.14	0.61	0.06	0.16
		Max	7.1	5.53	23.50	8.63	28.45	0.88	4.64	1.84	42.76	7.73	4.80	0.70	2.27	5.76	1.03	0.12	0.27
		Mean	7.0	5.33	20.10	7.16	26.70	0.40	3.63	0.48	38.93	7.27	3.88	0.40	1.85	5.12	0.71	0.09	0.19
		Sd	0.2	0.19	5.94	0.98	1.20	0.37	0.81	0.79	5.95	0.46	0.98	0.16	0.54	0.99	0.16	0.02	0.04
P11	5	Min	6.9	4.82	16.81	8.97	24.42	0.43	3.28	0.00	35.50	5.82	1.90	0.42	1.37	4.55	0.61	0.08	0.15
		Max	6.9	5.65	24.24	10.11	27.21	0.48	5.04	1.52	42.84	12.72	2.65	0.55	1.89	5.77	0.71	0.14	0.35
		Mean	6.9	5.30	19.78	9.66	25.86	0.45	4.02	0.91	38.51	7.62	2.42	0.50	1.75	5.05	0.67	0.10	0.20
		Sd		0.30	3.08	0.44	0.99	0.02	0.89	0.68	2.87	2.87	0.31	0.06	0.21	0.48	0.04	0.02	0.08
P9	7	Min	6.8	5.56	9.08	6.54	29.35	0.16	2.80	0.00	41.82	2.59	0.00	0.25	1.43	5.60	0.65	0.06	0.06
		Max	6.9	6.80	28.49	10.26	42.01	0.85	4.80	1.60	49.77	10.50	3.40	0.98	2.14	6.92	0.89	0.10	0.24
		Mean	6.9	6.22	23.09	8.24	34.17	0.29	3.86	0.83	45.81	8.78	2.54	0.43	1.80	6.27	0.75	0.08	0.19
		Sd	0.1	0.50	7.05	1.38	4.38	0.27	0.70	0.53	2.82	3.09	1.27	0.28	0.24	0.47	0.08	0.02	0.07
8894	1				5.61	6.47	14.74	0.58	6.52	0.00	19.84	1.81	1.55	1.15	0.67	1.95	0.74	0.33	0.09
P12	2	Min		4.31	12.56	10.03	21.74	0.17	4.60	0.80	32.15	4.22	1.71	0.79	1.34	4.00	0.61	0.13	0.12
		Max		4.52	12.79	10.17	21.77	0.20	5.12	0.80	35.80	4.40	1.79	0.80	1.42	4.60	0.68	0.16	0.14
		Mean		4.42	12.68	10.10	21.75	0.19	4.86	0.80	33.98	4.31	1.75	0.80	1.39	4.30	0.64	0.14	0.13
		Sd		0.15	0.17	0.10	0.02	0.02	0.37	0.00	2.58	0.13	0.06	0.00	0.06	0.43	0.05	0.02	0.01
P13	2	Min		3.54	9.85	5.78	22.70	0.17	5.44	0.72	25.36	4.61	1.12	0.59	0.92	2.87	0.82	0.19	0.18
		Max		3.74	10.10	6.00	23.39	0.18	5.76	0.80	28.54	5.24	1.44	0.59	0.97	3.40	0.90	0.23	0.18
		Mean		3.64	9.98	5.89	23.05	0.18	5.60	0.76	26.95	4.93	1.28	0.59	0.95	3.13	0.86	0.21	0.18

			Sd		0.14	0.17	0.16	0.49	0.00	0.23	0.06	2.25	0.45	0.23	0.01	0.04	0.37	0.05	0.03	0.00
	P15	2	Min		3.37	8.97	5.11	20.64	0.38	4.16	0.56	24.49	3.29	0.24	0.55	1.11	2.72	0.79	0.15	0.12
			Max		3.86	9.23	5.91	22.02	0.40	5.00	1.28	28.00	3.47	0.35	0.66	1.18	3.31	0.84	0.20	0.13
			Mean		3.62	9.10	5.51	21.33	0.39	4.58	0.92	26.24	3.38	0.30	0.61	1.15	3.02	0.81	0.18	0.13
			Sd		0.35	0.18	0.56	0.97	0.02	0.59	0.51	2.48	0.13	0.08	0.07	0.04	0.41	0.04	0.04	0.01
	P19	1			6.89	17.04	12.21	39.91	0.40	4.76	2.16	54.51	11.60	0.79	0.72	1.04	7.71	0.73	0.09	0.21
	P15B	1			6.12	12.91	10.88	39.98	0.15	3.68	0.96	43.31	10.81	0.66	0.84	0.89	5.85	0.92	0.08	0.25
	P15C	2	Min			4.76	3.37	16.02	0.15	2.52	1.04	12.71	2.43	0.55	0.71	0.67	0.77	0.80	0.07	0.19
			Max			13.10	9.63	29.72	0.29	4.68	1.44	37.27	7.61	1.25	0.73	1.29	4.85	1.26	0.37	0.20
			Mean			8.93	6.50	22.87	0.22	3.60	1.24	24.99	5.02	0.90	0.72	0.98	2.81	1.03	0.22	0.20
			Sd			5.90	4.43	9.69	0.10	1.53	0.28	17.36	3.66	0.50	0.02	0.44	2.89	0.33	0.21	0.01

Appendix C [6]

Calibrating unsaturated model parameters using electrical resistivity tomography imaging

F. SLAMA[1], E. P. MILNES[2] & R. BOUHLILA[1]

1 *Laboratoire de Modélisation en Hydraulique et Environnement, Ecole Nationale d'Ingénieurs de Tunis, BP 37 Le Belvédère 1002, Tunis, Tunisie*
2 *Centre of Hydrogeology CHYN, University of Neuchâtel,. 11, rue Emile-Argand,. CH – 2007 Neuchâtel, Switzerland*
fairouz.slama@unine.ch

Abstract Successive electrical resistivity tomography (ERT) measurements were performed during a controlled infiltration test. Thirty-two electrodes were used with a spacing of 1 m leading to an investigation depth of about 5 m. Four ERT profiles were performed during the infiltration test, each with a time-lapse of one hour. Water, with an electrical conductivity of 9.53 $mScm^{-1}$, was infiltrated into a furrow with a constant flux of 0.75 ls^{-1} during 4 hours. The resistivity difference between the reference and each ERT profiles were computed and mapped to estimate the plume evolution in time. Hydrus2D was used to simulate water flow during the infiltration test and was Van Genuchten's soil hydraulic parameters model were calibrated on the measured ERT data set.

Key words unsaturated model; ERT imaging; infiltration test; Van Genuchten's parameters

INTRODUCTION

Most processes that involve water and soil occur in unsaturated conditions. Unsaturated flow implies variations of the water content in the soil, which is characterised by complex relations between soil variables such as water content, suction and hydraulic conductivity (Hillel, 1998). For the flow in unsaturated media, we adopt the hypothesis stipulating that the air phase is motionless. The movement is then only calculated in the water phase.

The governing equation of the unsaturated flow in a porous media is that established by Richards in 1931. It represents a combination of the generalized Darcy law, in the unsaturated media, and the mass conservation equation. In two dimensions, the equation of Richards is written as follows:

$$c(h)\frac{\partial h}{\partial t} = \frac{\partial}{\partial x}\left[K(h)\frac{\partial h}{\partial x}\right] + \frac{\partial}{\partial z}\left[K(h)\frac{\partial h}{\partial z}\right] \quad (1)$$

[6] Slama, F., Milnes, E.P. and Bouhlia, R., 2008. Calibrating unsaturated model parameters using electrical resistivity tomography imaging, Redbook N°320. International Association of Hydrological Sciences, Wallingford, pp. 148-153.

Where h is the head [L], $c(h)=\frac{\partial\theta}{\partial h}$ is the soil specific retention [L^{-1}], θ is the water content [1] and *K(h)* soil hydraulic conductivity [LT^{-1}]

Based on the statistical pore-size distribution model suggested by Mualem (1976), Van Genuchten (1980) proposed, the following equation for the unsaturated hydraulic conductivity function in terms of soil water retention parameters:

$$\theta(h)=\begin{cases}\theta_r+\dfrac{\theta_s-\theta_r}{\left(1+|\alpha h|^n\right)^m} & h<h_s\\ \theta_s & h\geq h_s\end{cases}\quad,$$

$$K(h)=K_s S_e^{0.5}\left[1-\left(1-S_e^{1/m}\right)^m\right]^2$$

h_s - air-entry value *[L]*
θ_s - saturated water content *[-]*
θ_r - residual water content *[-]*
α, m, n - empirical parameters *[1/L], [-], [-]*
S_e - effective water content *[-]*
K_s - saturated hydraulic conductivity *[L/T]*
K_r - relative hydraulic conductivity *[-]*

(2)

m=1 -1 /n , n >1

The equations (2) contain five independent parameters: θ_s, θ_r, α, n and K_s known as the Van Genuchten's parameters. The pore-connectivity parameter l is generally taken equal to 0.5.

The θ(h) and K(h) relations can be determined in situ or at the laboratory scale. Hillel et al. (1972) proposed an in situ test to estimate those parameters known as internal drainage test. This test is rather difficult to perform and is limited regarding the investigation depth (a maximum of two meters). Thus, this kind of test is not suitable for areas where the unsaturated zone reaches 20 meters. Inverse parameter identification is also being used to determine these relations by finding the minimum of an objective function expressing the quadratic differences between measured and predicted values using an optimization procedure (Beydoun et Lehmann 2006).

In this study, we propose to calibrate Van Genuchten's parameters using simultaneous Electrical Resistivity Tomography (ERT) imaging and an infiltration test. ERT method is known to provide reliable estimations concerning changes in water content (Binley *et al.*, 2002a and Binley *et al.*, 2002b). Moreover, the relationship between soil resistivity and water content has already been proposed in earlier works (Montoroi *et al.*, 1997). This makes it possible to calibrate unsaturated model parameters using observed water content obtained from resistivity measurements.

MATERIALS AND METHODS

Successive ERT measurements were performed at Korba coastal plain in Tunisia (August, 2006), during a controlled infiltration test. The soil is characterised by a layer of consolidated sand lying on a fine sand layer (Fig. 1).

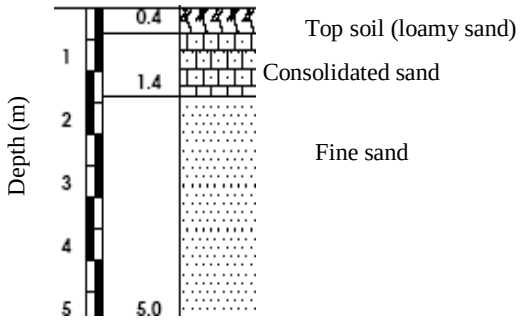

Fig. 1 Soil profile

Thirty two electrodes were used with a Wenner array with an electrode spacing of 1 m leading to an investigation depth of about 5 m. The ERT reference profiles were repeated twice before onset of infiltration, followed by four ERT profiles performed during the infiltration test, each with a time-lapse of one hour. Water, with an electrical conductivity of 9.53 $mScm^{-1}$, was infiltrated into a furrow (5 x 0.4 x 0.1 m^3) with a constant flux of 0.75 ls^{-1} during 4 hours (Fig. 2).

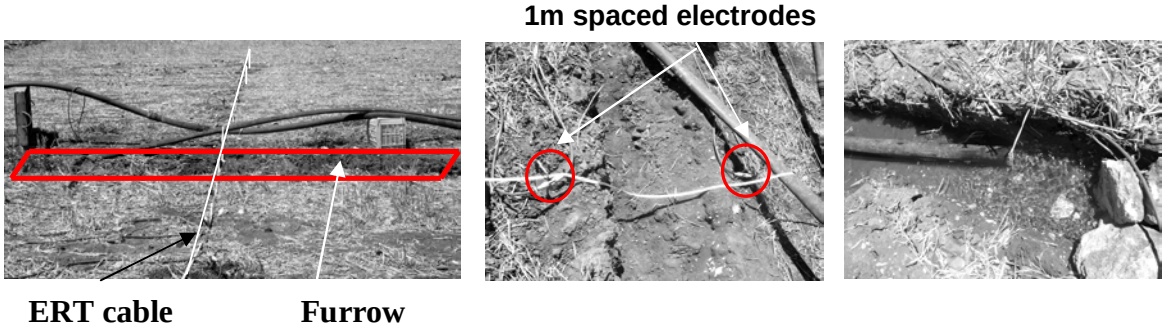

Fig. 2 ERT measurements and infiltration test disposition.

Inversions of the ERT profiles were computed with the Res2Dinv software. The resistivity difference between the reference and each ERT profiles were computed and mapped to estimate the plume evolution in time, i.e., the velocity of the movement of the point of gravity and the expansion of the plume. Two sources of error were considered: measurement errors and errors related to the inversion of the results. For each calculated difference between the reference profile and each profile the total error was estimated. Thereby, all the data within this error range was filtered from the result, yielding a distribution of significant values only (cf. Fig. 4).

Hydrus2D was used to simulate water flow during the infiltration test. Hydrus2D solves numerically Richards' equation for saturated-unsaturated water flow and the convection-dispersion equation for heat and solute transport (Simunek, 1999).

RESULTS AND DISCUSSION

ERT data evaluation

The relative error between the two reference profiles (before infiltration) was about 1.8%, indicating a good reproducibility. The inversed electrical resistivity sections corresponding to the four ERT images are shown in Fig . 3, with inversion errors of approximately 2.5%. We notice that only by visualising a specific iso-contour (90 ohmm), slight differences can be seen (Fig. 3). However, when mapped (Fig. 4) and superimposed (Fig. 5), the resistivity difference between each profile and the average of the reference profiles describes the temporal and spatial expansion of the plume. The plume evolution shown in figure 4 reveals two slightly unexpected features:

a) The plume gravity centre rapidly reaches a depth of 2 meters (in the first section) and then moves on rather slowly.

b) The plume expands like a bulb around the gravity centre.

The reason for the first feature may be the consolidated sand layer acting as a barrier, slowing down the vertical movement. The second feature is due to the filtering of the data. The infiltrated water with an electrical conductivity of 9.53 $mScm^{-1}$ leads to very low resistivities, and the reference section was already characterised by a low resistivity surface layer. The resistivity difference between the very low resistivity zones (due to infiltration) and the low resistivity surface layer lead to values that fall with the error range that were eliminated during data filtering.

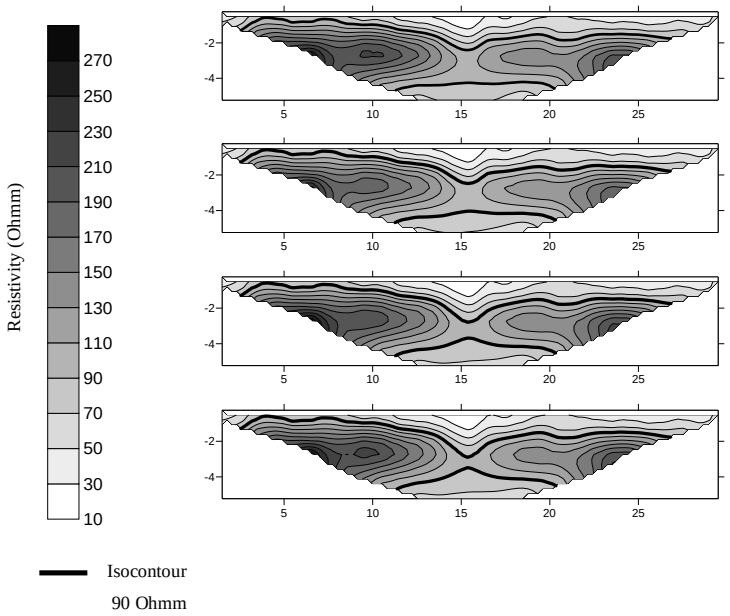

Fig. 3 Pseudosections of the four ERT measurements for four different times: after 1, 2, 3 and 4 hours after onset of infiltration test.

In Fig. 4, the evolution of the isocontour corresponding to a resistivity difference of 40 Ohmm is shown for the four snap-shots in time (after 1, 2, 3 and 4 hours after onset of the infiltration test).

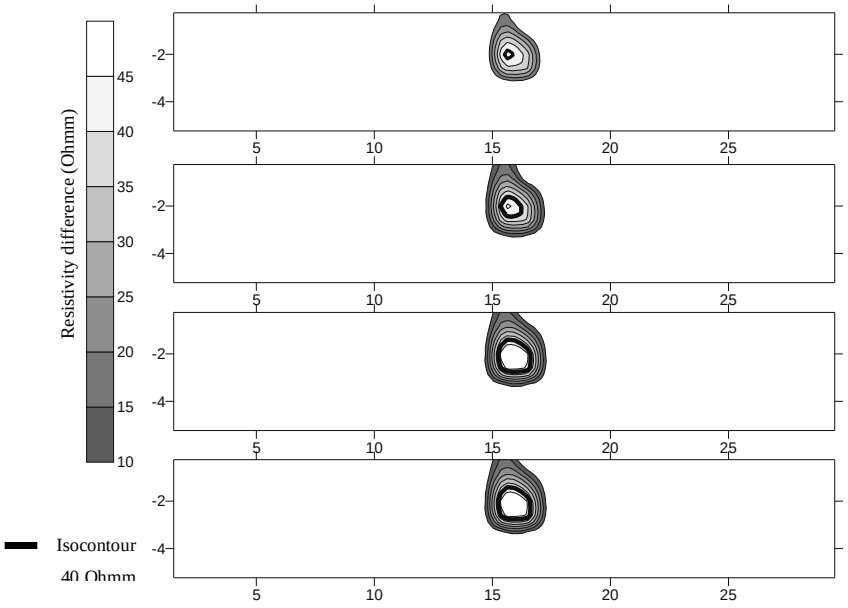

Fig. 4 Mapped resistivity difference between reference and successive profiles

The centre of gravity was calculated for each contour (Fig. 5). In fact we supposed that the movement of the centre of gravity corresponds to that of the wetting front which led to an estimation of the saturated conductivity K_s of 2.4 10^{-5} ms^{-1}. This K_s value lies well within the typical range of sandy soils.

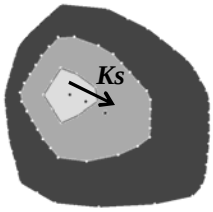

Fig. 5 Superposition of the isocontours 40 Ohmm and migration of the centre of gravitity for the iso-contour 40 Ohmm of three profiles.

Numerical modelling

To model the infiltration test, a two dimensional vertical section (32x5 m) was used. The mesh is composed of 1140 three-noded triangle elements. Boundary conditions are shown in Fig. 6. Initial condition of the water content (0.25) was estimated using the reference ERT profiles.

The simulation time corresponds to the infiltration test duration, i.e., 4 hours and 16 minutes (15360 s). The calibration procedure was based on manual adjustment of the α and n-parameters using the 'observed water content' at the end of the infiltration test. Values of the 'observed water content' were obtained using the following relationship between the soil resistivity and water content (Montoroi *et al*, 1997):

$$R = a\, e^{b/\theta} \quad (3)$$

Where R is the electrical resistivity (Ohmm), θ the water content and *a=24 Ohmm and b= 0.35 are constants.*

Calibration led to values for the α and n - parameters of 10 and 6, respectively which are usual for sandy soils. The water infiltration simulation results with these parameters are shown in Fig.6. At the end of the infiltration test the plume reaches a depth of about 3 m Fig. 6b. This result reproduces well the observation that changes in resistivity only reach a depth of three meters (Fig. 4).

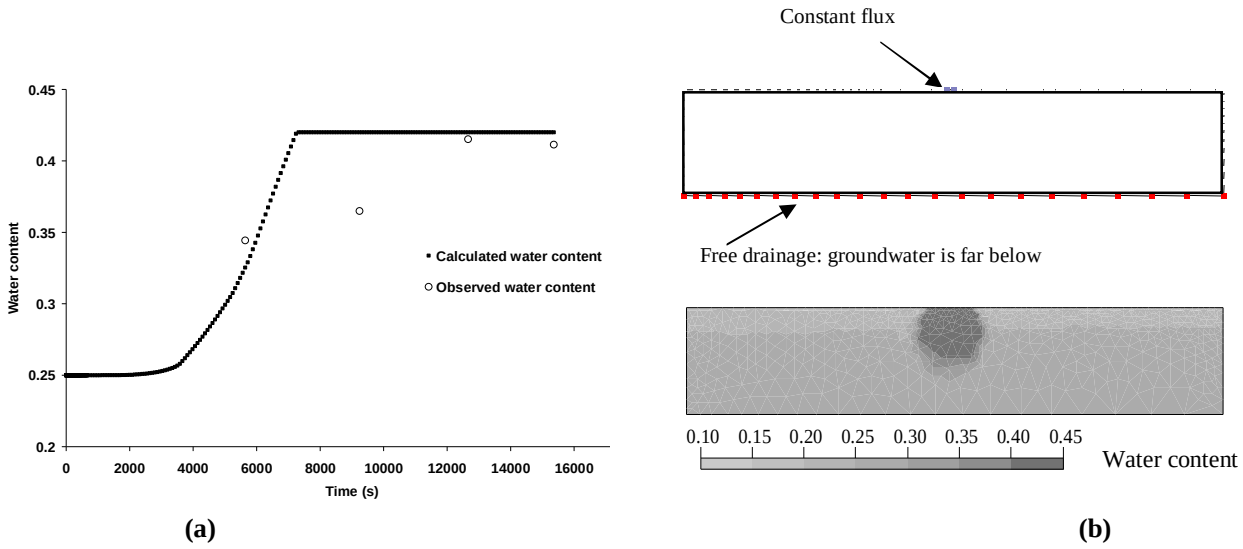

Fig. 6 (a) calculated and observed water content at 2 m depth (b) boundary conditions and water content simulated using hydrus2D after 4h and 16mn.

CONCLUSIONS

Simultaneous ERT imaging was combined with a controlled infiltration test for the purpose of calibrating unsaturated soil parameters. Resistivity difference distributions between the average reference profiles (before infiltration test) and four consecutive ERT profiles, carried out with a time-delay of one hour each, allowed mapping of the soil humidity change through time, caused by the infiltration test. The migration of the centre of gravity of the humidity plume was used to estimate the saturated hydraulic conductivity *Ks* and was found to be 2.4 10^{-5} ms^{-1}.

Using this hydraulic conductivity value, Hydrus2D was then used to simulate water flow during the infiltration test and to calibrate the a and n-parameters on the measured ERT data set using relationships between water content and resistivity developed by Montoroi et al. (1997). Van Genuchten's soil hydraulic parameters model was thereby adjusted leading to a possible combination of soil hydraulic parameters (α=10, n=6). The obtained calibrated parameters can for instance be used to simulate the effects of long-term irrigation cycles on soil salinity evolution.

Acknowledgements This work was entirely funded by The Swiss National Science Foundation (Joint Research Project "Gestion durable des ressources en eaux souterraines côtières - Modélisation physique et probabiliste. Application à la côte orientale du Cap Bon, Tunisie CAPBON").The assistance and support of Prof. Tarhouni Jamila and Trabelsi Emna in the Institut National Agronomique de Tunis are acknowledged.

REFERENCES

Beydoun, H. & Lehmann, F. (2006) Expériences de drainage et estimation de paramètres en milieu poreux non saturé. *C. R. Géoscience*, **338,** 180-187.

Binley, A., Cassiani, G., Middleton, R. & Winship, P., (2002a) Vadose zone flow model parameterisation using cross-borehole radar and resistivity imaging. *Journal of Hydrology*, **267** (3-4), 147-159.

Binley, A., Winship, P., West, L. J., Pokar M., & Middleton, R. (2002b) Seasonal variation of moisture content in unsaturated sandstone inferred from borehole radar and resistivity profiles. *Journal of Hydrology*, **267** (3-4), 160-172.

Hillel, D., Krentos, V., and Stylianou, Y. (1972) Procedure and test of an internal drainage method for measuring soil hydraulic properties in situ. *Soil Science* **114**, 395- 400.

Hillel, D. (1998). Environmental soil physics. Envioronmental sciences, geophysics, agriculture. Academic Press. USA.

Montoroi, J.P., Bellier, G. & Delarivière J. L. (1997) Détermination de la relation résistivité électrique - teneur en eau au laboratoire. Application aux sols de Tunisie centrale. Colloque GEOFCAN Géophysique des sols et des formations superfic ielles11-12 septembre 1997, Bondy, France

Mualem, Y. 1976. A new model for predicting the hydraulic conductivity of unsaturated porous media, *Wat. Resour. Res.* **12**, (3), 513-521.

Simunek, J., Sejna, M. &Van Genuchten, Th. (1999) Simullating water flow, heat and solute transport in two dimensional variably saturated media, U.S salinity laboratory, agricultural research service, U.S department of agriculture Riverside, California.

Van Genuchten, M. Th. (1980). A closed-form equation for predicting the hydraulic conductivity of unsaturated soils. *Soil Science* **44**, 892-898.